TECHNISCHE
UNIVERSITÄT
DARMSTADT

Gradient robust methods for nearly incompressible materials

Vom Fachbereich Mathematik

der Technischen Universität Darmstadt

zur Erlangung des Grades eines

Doktors der Naturwissenschaften

(Dr. rer. nat.)

Dissertation

von

Seshadri Basava, M.Sc.

aus Visakhapatnam, Indien

Erstgutachterin: : Prof. Dr. Winnifried Wollner

Zweitgutachterin : Prof. Dr. Thomas Wick

Darmstadt 2023

Gradient robust methods for nearly incompressible materials

Accepted doctoral thesis by Seshadri Basava

Referent: Prof. Dr. Winnifried Wollner
Koreferent: Prof. Dr. Thomas Wick
Darmstadt, Technische Universität Darmstadt
Veröffentlichungsjahr der Dissertation auf TUprints : 2023

Bitte zitieren Sie dieses Dokument als:
URN: urn:nbn:de:tuda-tuprints-264632
URL:https://tuprints.ulb.tu-darmstadt.de/26463
Dieses Dokument wird bereitgestellt von tuprints,
E-Publishing-Service der TU Darmstadt
http://tuprints.ulb.tu-darmstadt.de
tuprints@ulb.tu-darmstadt.de

To my loving wife,
my sister and my parents
for their love and support

Acknowledgments

First and foremost, I would like to thank my supervisor Prof. Dr.Winnifried Wollner for giving me the opportunity to work at Technische Universität Darmstadt. I would also like to thank him for his endless support, feedback, guidance and invaluable suggestions for the duration of my PhD studies. I thank Prof. Dr.Thomas Wick, Dr.Mirijam Walloth and Dr.Katrin Mang for the fruitful discussions and working as team in Priority Program 1748 (SPP) for three years. I thank Prof. Luca Heltai's for his invaluable discussions on deal.II. The robust-fem code provided by him, set up a very good baseline for our FEValuesInterpolated class.

I would like to extend my gratitude to the German Research Foundation (DFG), for their support within the SPP 1748 and its speaker Prof. Dr.-Ing. habil. Jörg Schröder, for the additional financial support which gave me the opportunity to visit the ECCOMAS Thematic Conference on Modern Finite Element Technologies 2019 at Bad Honnef and Autumn School on Optimal Control and Optimization with PDE'S at Trier University, 2019.

I would like to thank Andreas, for being my goto person and being my "crisis-averter". I thank Christine, Nicolai, Sofiya and Jose for their insights and thoughtful discussions and making it a pleasure to be at work.

Finally, I would like to thank my wife Aiswarya for being my support and rock, my brother-in-law Ashik, whose invaluable advices made every critical decision easier. I owe my deepest gratitude to my parents, my sister and my grandmother for their emotional support and care.

Seshadri Basava
Darmstadt, 2023

Abstract

Mixed finite elements for incompressible Navier-Stokes equations have seen a great success in mathematical fluid dynamics [15, 50, 34, 23, 20], to name a few. However, the dependency on pressure causes numerical instability. Linke [38], proposed a cure for this by introducing the gradient-robust interpolation operator π^{div}.

In this thesis, we extend this operator to nearly incompressible Stokes equation (Chapter 5), linear elasticity (Chapter 6) and phase-field fracture models (Chapter 7). We construct necessary assumptions and conditions needed to choose the suitable finite dimensional subspace of $\mathbf{H}^{\text{div}}(\Omega;\mathbb{R}^d)$, given a stable inf-sup finite element pair solving the linear elasticity problem. We use Raviart-Thomas ($\mathcal{RT}_1$) and Brezzi-Douglas-Marini ($\mathcal{BDM}_2$) elements for $\mathcal{Q}_2 \times \mathcal{DGQ}_1$ and $\mathcal{Q}_2 \times \mathcal{DGP}_1$ finite element pairs respectively.

For computation, we use `C++` based open source finite element libraries `deal.II` [4] and `DOpElib` [24]. We develop the `FEValuesInterpolated` class, which is derived from `FEValues` class of `deal.II`. Our class gives the value of $\pi^{\text{div}}\mathbf{v}_h$, while the latter gives $\mathbf{v}_h$. In case of linear elasticity, under the influence of external thermal force, we show that the gradient-robust method gives a well represented solution with fewer elements, compared to the non-gradient robust techniques for both incompressible and nearly incompressible materials. As an extension of our work [8], we show that, for phase-field fracture models under the effect of external thermal force, a well represented solution of displacement and fracture propagation for gradient-robust methods can be obtained with fewer elements, compared to non-gradient robust techniques.

Zusammenfassung

Gemischte Finite-Elemente-Methoden für die inkompressiblen Navier-Stokes-Gleichungen haben in der mathematischen Fluiddynamik großen Erfolg verzeichnet [15, 50, 34, 23, 20], um nur einige zu nennen. Allerdings führt die Abhängigkeit vom Druck zu numerischer Instabilität. Linke [38], schlug hierfür eine Lösung vor, indem er den gradientenrobusten Interpolationsoperator π^{div} einführte.

In Betrachtung eines stabilen inf-sup Finite-Elemente-Paares für das Elastizitätsproblem, untersuchen wir Annahmen und Bedingungen um einen geeigneten endlich-dimensionalen Unterraum von $\mathbf{H}^{\text{div}}(\Omega;\mathbb{R}^d)$ zu wählen. Hierbei werden Raviart-Thomas ($\mathcal{RT}_1$) bzw. Brezzi-Douglas-Marini ($\mathcal{BDM}_2$) Elemente für die Finite-Elemente-Paare $\mathcal{Q}_2 \times \mathcal{DGQ}_1$ und $\mathcal{Q}_2 \times \mathcal{DGP}_1$ genutzt.

In mehreren numerischen Experimenten zeigen wir die Vorteile dieser Erweiterung. Hierzu, haben wir die `C++` basierten Finite-Elemente-Pakete `deal.II` [4] und `DOpElib` [24] genutzt und die Klasse FEValuesInterpolated entwickelt, welche auf der FEValues Klasse von `deal.II` basiert und es ermöglicht den Wert von $\pi^{\text{div}}\mathbf{v}_h$ berechnen. Im Vergleich zu nicht-gradientenrobusten Techniken zeigen wir für den Fall der linearen Elastizität unter dem Einfluss äußerer thermischer Kräfte, dass die gradientenrobuste Methode eine gut repräsentierte Lösung mit weniger Elementen liefert. Dies können wir sowohl für inkompressibele als auch für nahezu inkompressibele Materialien beobachten. Dieses Verhalten bestätigt sich auch bei der Betrachtung von Rissausbreitungsmodellen unter Einfluss äußerer thermischer Kräfte. Hier kann im Vergleich zu nicht-gradientenrobusten Techniken eine gut repräsentierte Lösung der Verschiebung und Rissausbreitung für gradientenrobuste Methoden mit weniger Elementen erzielt werden.

Contents

Chapter 1

Introduction

The use of nearly incompressible solids and incompressible materials is increasing in many industrial sectors. Techniques like Hydraulic fracturing or Fracking, Ground storage of CO_2 are some of the well known techniques, that use heavy external pressure to introduce fractures in the given material. In cases like these, it's important to study the behavior of the crack propagation under extreme pressure conditions.

Within fracture mechanics, the classical phase-field fracture model [21, 11] is a well-established approach for simulating crack propagation. However, it is still a challenge to give an accurate numerical simulation. Pressurized fracture problems modeled with a phase-field method is currently a highly being research by many groups; see for instance [18, 25, 37, 45, 61], to name a few. In [60], an overview of pressurized and fluid-filled fractures is provided. However, all these above-mentioned works deal with compressible solids, where Poisson's ratio is significantly less than 0.5, i.e., the incompressible limit.

Incompressible solids are however, an important field in solid mechanics [27, 28, 33, 52, 57]. In [43], a robust discretization model using a phase-field method for fractures in solids was proposed. A well-known challenge in phase-field methods is the relationship between the model regularization $\varepsilon > 0$ and the spatial mesh size h. In order to correct this and get an accurate discretizations for small ε around the fracture, an adaptive mesh refinement around the fracture is useful. First studies dates back to [16, 17] investigating residual-type error estimators. A predictor-corrector mesh refinement algorithm which focussed on crack-oriented refinement was developed in [26] and extended to three spatial dimensions in [37]. In [6], anisotropic mesh refinement was studied. Goal-oriented adjoint-based aposteriori error estimation was discussed in [62]. Based on residual-type aposteriori estimators for contact problems [59, 31] a reliable and efficient estimator for singularly-perturbed obstacle problem (with robustness in terms of ε) is given in [59]. Residual-type estimator tests for different fracture phase-field problems with the irreversibility condition is conducted in [41], and for nearly incompressible solids in [42].

In our work [8], as part of the German Priority Program 1748 (DFG SPP 1748), in the project, 'Structure Preserving Adaptive Enriched Galerkin Methods for Pressure-Driven 3D Fracture Phase-Field Models', we first developed a phase-field model from [43] and combined it with pressurized fractures as proposed in [48, 46, 61]. Secondly, we applied the

adaptive spatial mesh refinement based on the residual-type error estimator [41, 58] to our mixed-system phase-field fracture approach. These algorithmic concepts are substantiated with the help of several numerical examples and mesh convergence studies comparing classical primal formulations and our newly developed mixed formulation. Finally, we tested a gradient-robust modification of the discrete mixed formulation.

The aforementioned, gradient-robust methods is heavily inspired by the work of Linke [38] on stationary Stokes equation. He introduced an interpolation operator π^{div} that maps the velocity finite element space to an H^{div} conforming space, and by doing so, he mapped all discretely divergence free functions to divergence free functions. The construction of the interpolation operator depends on the choice of the inf-sup stable finite element spaces used. This proposed method has been implemented to a range of problems and a variety of finite element pairs for the discretization of the Stokes equation, such as non-conforming Crouzeix-Raviart element [40], Taylor-Hood and MINI elements with continuous pressure spaces [35], on rectangular elements [39], for embedded discontinuous Galerkin methods (EDG) [36]. For 3-d polyhedral domains with concave edges, a gradient-robust reconstruction is given in [3]. While the obtained convergence orders are optimal, the price to pay, for these methods is a loss of quasi optimality due to Strang's first lemma. Recently, [32] showed that a more involved construction of the reconstruction operator allows for a quasi-optimal discretization.

In this thesis, we consider the extension of these results to nearly incompressible Stokes and linear elasticity. We have also developed the `FEValuesInterpolated` class in the `C++` open source finite element library `DOpElib` [24]. The class works similar to the `FEValues` class in `deal.II` [4], except, our class takes the interpolated space and the finite element space of velocity/displacement vector and outputs the interpolated vector. To test the correctness of the proposed class `FEValuesInterpolated`, we have run numerical tests in both two and three spatial dimensions.

For linear elasticity, to avoid the locking phenomenon, e.g., [12, Chapter VI.3], typically a mixed form

$$\begin{aligned} -2\mu\,\nabla\cdot\varepsilon(\mathbf{u}) - \nabla p &= \mathbf{f} \quad \text{in } \Omega, \\ \nabla\cdot\mathbf{u} - \frac{1}{\lambda}p &= 0 \quad \text{in } \Omega, \\ \mathbf{u} &= 0 \quad \text{on } \partial\Omega, \end{aligned} \tag{1.0.1}$$

is considered. Here the incompressible case, i.e., $\lambda = \infty$, can easily be included by dropping the term $-\frac{1}{\lambda}p$ in the second line. It is clear conceptually, that the same difficulties as for the Stokes problem will occur in the incompressible limit. However, the treatment of the nearly incompressible case requires additional care. To this end, [22] defined a discretization to be "gradient robust", if the influence of gradient forces $\mathbf{f} = \nabla\phi$ in the discrete solution vanishes sufficiently fast as $\lambda \to \infty$. [22] showed that a standard mixed discretization of (1.0.1) is not gradient robust and provided a gradient robust hybrid discontinuous Galerkin (HDG) scheme. In [9], we showed that mixed methods can be made gradient robust, using the approach proposed by [38] for the mixed discretization of (1.0.1). In addition to this, we use the numerial example with external thermal force

given in [22] and apply the gradient-robust method to phase-field fracture model proposed in [8].

This thesis is structured as follows:
Chapter 2: Preliminaries
We introduce basic notations and definitions of operators, function spaces and their respective norms, necessary inequalities and theorems which are integral to functional analysis.

Chapter 3: Saddle Point Problem
In this chapter, we introduce the saddle point problem. Saddle point problem acts as a base skeleton for both Stokes and elasticity problem which are the two main concerns of this thesis. We discretize the problem and lay a foundation for the necessary and sufficient conditions for the existence and uniqueness of both discrete and the continuous problem.

Chapter 4: Stokes Equation
The stationary Stokes problem is introduced as a saddle point problem. We discuss the pressure dependency of the velocity in the mixed form and show how Linke, proposed a variational crime to solve the issue using Helmholtz Decomposition of the velocity space.

Chapter 5: Conforming Subspaces of H^{div}
We proceed by introducing two H^{div} conforming subspaces namely, Raviart-Thomas and Brezzi-Douglas-Marini finite element spaces. A detailed description of both the spaces is presented along with Piola Transform. Furthermore, we discuss how we constructed the `FEValuesInterpolated` class in `DOpElib` and how it differs from `FEValues` class of `deal.II`. To lay a baseline and to test the class, we present a numerical example given in [38] for 2d domain and a modified version of it for the 3d domain.

Chapter 6: Elasticity Equation
Following up on Linke's work on stationary Stokes equation, we provide assumptions necessary for constructing appropriate H^{div} conforming subspaces for the finite element pair $\mathcal{Q}_2 \times \mathcal{DGP}_1$ and $\mathcal{Q}_2 \times \mathcal{DGQ}_1$. Furthermore, we derive the gradient-robust error estimation for the displacement vector, using the interpolation operator. We confirm the theoretical estimate given in Theorem 6.8, by providing numerical examples. We also achieve faster convergence rate of the displacement vector, compared to the non-interpolated method for the external thermal force example given in [22].

Chapter 7: Phase Field Fractures
In this chapter, we discuss the different formulations of the phase-field fracture model given in [8]. Following [54, 55], three examples with similar setup, are considered and compared using Total crack volume (TCV), Bulk energy E_b and Crack energy E_c. Due to our choice of pressure in these examples, we observed similar results for with and without the interpolation operator. To rectify the situation, we have chosen the external thermal force example used in Chapter 6 and observed similar convergence rates as in the Section 6.3.

Chapter 8: Conclusion
We end the thesis with a recap of the presented results and the challenges within this

thesis.

Some results of the thesis at hand are given in [8, 9].

Chapter 2

Preliminaries

This chapter contains basic notations and preliminaries, that will be used throughout this thesis. In Section 2.1, we define operators and properties related to them. Definitions of function spaces, including a short outline on Hilbert space and Sobolev spaces, dual spaces, respective norms and weak derivatives are given in Section 2.2. Core inequalities needed in functional analysis like Cauchy-Schwarz, Young's Inequality and some basic theorems are discussed in Section 2.3 and Section 2.4. Basic litreature on these topics can be found in [10, 56, 13, 14, 12].

2.1 Operators

Definition 2.1. *We define various operators in this section for vector and scalar valued functions, given any arbitrary dimension $d \in \mathbb{N}$, except for curl. Let $\mathbf{\Omega} \subset \mathbb{R}^d$, be a bounded domain in $\mathbb{R}^d$, we define two vector valued functions $\mathbf{u} = (u_1, u_2, \ldots, u_d) : \mathbf{\Omega} \to \mathbb{R}^d$, $\mathbf{w} = (w_1, w_2, \ldots, w_d) : \mathbf{\Omega} \to \mathbb{R}^d$ and a scalar function $v \colon \mathbf{\Omega} \to \mathbb{R}$.*

***Note**: Throughout this thesis, we use bold letters to denote vector valued variables and spaces, and normal letters for scalar valued variables and spaces.*

1. ***Gradient Operator:***

$$\nabla v \coloneqq \left(\frac{\partial v}{\partial x_1}, \frac{\partial v}{\partial x_2}, \cdots, \frac{\partial v}{\partial x_d} \right)^T,$$
$$(\nabla \mathbf{u})_{ij} \coloneqq \frac{\partial u_i}{\partial x_j}.$$

2. ***Divergence Operator:***

$$\nabla \cdot \mathbf{u} = \sum_{i=1}^{d} \frac{\partial u_i}{\partial x_i}. \tag{2.1.1}$$

3. ***Laplace Operator:***

$$\Delta v := \sum_{i=1}^{d} \frac{\partial^2 v}{\partial x_i^2},$$
$$(\Delta \mathbf{u})_i := \sum_{i=1}^{d} \frac{\partial^2 u_i}{\partial x_i^2}.$$

4. ***Curl Operator:***

$$\nabla \times v := \begin{pmatrix} -\frac{\partial v}{\partial x_2} \\ \frac{\partial v}{\partial x_1} \end{pmatrix} \qquad \text{for } d = 2,$$
$$\nabla \times \mathbf{u} := \frac{\partial u_2}{\partial x_1} - \frac{\partial u_1}{\partial x_2}, \qquad \text{for } d = 2,$$
$$\nabla \times \mathbf{u} := \begin{pmatrix} \frac{\partial u_3}{\partial x_2} & -\frac{\partial u_2}{\partial x_3} \\ \frac{\partial u_1}{\partial x_3} & -\frac{\partial u_3}{\partial x_1} \\ \frac{\partial u_2}{\partial x_1} & -\frac{\partial u_1}{\partial x_2} \end{pmatrix}, \qquad \text{for } d = 3.$$

5. ***Frobenius Inner Product:***

$$\nabla \mathbf{u} : \nabla \mathbf{w} = \sum_{i=1}^{d} \nabla u_i : \nabla w_i = \sum_{ij} \frac{\partial u_i}{\partial x_j} \frac{\partial w_i}{\partial x_j} \tag{2.1.2}$$

Now, we state properties involving the operators defined earlier.

Lemma 2.2. *Let's consider scalar functions ψ, ϕ and vector fields $\mathbf{u}, \mathbf{w}$ which are sufficiently smooth, then we have the following identities.*

(i) $\nabla (\psi\, \phi) = \phi \nabla \psi + \psi \nabla \phi,$

(ii) $\nabla \cdot (\psi\, \mathbf{u}) = \psi \nabla \cdot \mathbf{u} + (\nabla \psi) \cdot \mathbf{u},$

(iii) $\nabla \times (\psi \mathbf{u}) = \psi \nabla \times \mathbf{u} + (\nabla \psi) \times \mathbf{u},$

(iv) $\nabla \cdot (\nabla \times \mathbf{u}) = 0,$

(v) $\Delta \psi = \nabla^2 \psi = \nabla \cdot (\nabla \psi),$

(vi) $\nabla (\nabla \cdot \mathbf{u}) - \nabla \times (\nabla \times \mathbf{u}) = \nabla^2 \mathbf{u},$

(vii) $\nabla \cdot (\phi \nabla \psi) = \phi \nabla^2 \psi + \nabla \phi \cdot \nabla \psi,$

(viii) $\nabla \times (\mathbf{u} \times \mathbf{w}) = \mathbf{u}\, (\nabla \cdot \mathbf{w}) - \mathbf{w}\, (\nabla \cdot \mathbf{u}) + (\mathbf{w} \cdot \nabla)\mathbf{u} - (\mathbf{u} \cdot \nabla)\mathbf{w}.$

Remark 2.3. *The term sufficiently smooth, has to be interpreted as weakly differentiable in the sense of Definition 2.6 and sufficiently smooth should indicate that functions used are differentiable for the applied calculations and considerations.*

2.2 Function Spaces

In this section, we define necessary function spaces and respective norms. We start with the space of continuous functions.

2.2.1 Continuous Functions

Definition 2.4. *We define the space of k times differentiable functions as*

$$C^0(\mathbf{\Omega}) \coloneqq \{v \colon \mathbf{\Omega} \to \mathbb{R} \colon v \text{ is continuous } \}, \tag{2.2.1}$$

$$C^k(\mathbf{\Omega}) \coloneqq \left\{v \colon \mathbf{\Omega} \to \mathbb{R} \colon \partial^\alpha v \in C^0(\mathbf{\Omega}), \forall\, |\alpha| \leq k\right\}, \qquad \alpha \in \mathbb{N}^d, k \in \mathbb{N} \tag{2.2.2}$$

$$C^\infty(\mathbf{\Omega}) \coloneqq \bigcap_{k=0}^{\infty} C^k(\mathbf{\Omega}), \tag{2.2.3}$$

and their extensions with the property that the closure of the support of the functions is a compact subset of $\mathbf{\Omega}$ *by*

$$C_0^k(\mathbf{\Omega}) \coloneqq \left\{v \in C^k(\mathbf{\Omega}) \colon \ \mathit{supp}(v) \subset_{\mathit{compact}} \mathbf{\Omega}\right\}, \tag{2.2.4}$$

$$C_0^\infty(\mathbf{\Omega}) \coloneqq \left\{v \in C^\infty(\mathbf{\Omega}) \colon \ \mathit{supp}(v) \subset_{\mathit{compact}} \mathbf{\Omega}\right\}, \tag{2.2.5}$$

with

$$\mathit{supp}(v) \coloneqq \overline{\{\mathbf{x} \colon v(\mathbf{x}) \neq 0\}}$$

being the support of the function $v \colon \Omega \to \mathbb{R}$.

2.2.2 Lebesgue Space

Definition 2.5. *Let* $p \in [1, \infty)$*; we define the Lebesgue space of order* p *as*

$$L^p(\mathbf{\Omega}) = \left\{ f \colon \mathbf{\Omega} \to \mathbb{R} \text{ measurable } : \int_{\mathbf{\Omega}} |f(\mathbf{x})^p| \, \mathrm{d}\mathbf{x} < \infty \right\},$$

with norm

$$\|f\|_p = \left(\int_{\mathbf{\Omega}} |f^p| \, \mathrm{d}\mathbf{x} \right)^{\frac{1}{p}}. \tag{2.2.6}$$

We use $\|\cdot\|_p$ *for* L^p *norm* $1 < p < \infty$.
For the case of $p = \infty$*, we define* $L^\infty(\Omega)$ *as*

$$L^\infty(\mathbf{\Omega}) \leq \left\{ f \colon \mathbf{\Omega} \to \mathbb{R} \text{ measurable} \colon \int_{\mathbf{\Omega}} |f(x)| \leq C < \infty \text{ a.e. on } \mathbf{\Omega} \right\}. \tag{2.2.7}$$

We define an extension of the above-mentioned spaces,

$$L_0^2(\mathbf{\Omega}) \coloneqq \left\{ q \in L^2(\mathbf{\Omega}) \colon \int_{\mathbf{\Omega}} q(\mathbf{x}) \, \mathrm{d}\mathbf{x} = 0 \right\}.$$

The locally integrable space L^1_{loc} is given as,

$$L^1_{loc} \coloneqq \left\{ q \colon \mathbf{\Omega} \to \mathbb{R} \text{ measurable } : \int_{\mathbf{\Omega}'} |q(\mathbf{x})| \, \mathrm{d}\mathbf{x} < \infty, \forall \, \mathbf{\Omega}' \subset_{compact} \mathbf{\Omega} \right\} \tag{2.2.8}$$

$$\coloneqq \left\{ q \in L^1(\mathbf{\Omega}') \colon \mathbf{\Omega}' \subset_{compact} \mathbf{\Omega} \right\}. \tag{2.2.9}$$

2.2.3 Sobolev Spaces

Before going to Sobolev spaces, we proceed to a more generalization concept of the derivative for functions not assumed differentiable, but only integrable.

Definition 2.6 (Weak derivative)**.** *Let $\boldsymbol{\alpha} = (\alpha_1, \cdots \alpha_n), \alpha_i \in \mathbb{N}$, be a multi-index with $|\boldsymbol{\alpha}| = \alpha_1 + \cdots + \alpha_n$, a given function $f \in L^1_{loc}(\mathbf{\Omega})$ has a weak derivative, $D^{\boldsymbol{\alpha}} f$, provided there exists a function $g \in f^1_{loc}(\mathbf{\Omega})$ such that*

$$\int_{\mathbf{\Omega}} g(x)\phi(x) \, \mathrm{d}x = (-1)^{|\boldsymbol{\alpha}|} \int_{\mathbf{\Omega}} f(x)\phi^{(\boldsymbol{\alpha})}(x) \, \mathrm{d}x \qquad \forall \, \phi \in C_0^\infty(\mathbf{\Omega}) \tag{2.2.10}$$

If such a g exists, we define $D^{\boldsymbol{\alpha}} f = g$.

We use the following example from [14, Chapter 8.2] to show how discontinuous functions can have weak derivative.

Example 2.7. *Take $n = 1, \Omega = [-1, 1]$, and $f(x) = |x|$. We claim that $D^1 f$ exists and is given by*

$$g(x) \coloneqq \begin{cases} -1 & x < 0, \\ 1 & x > 0. \end{cases} \tag{2.2.11}$$

Since the function f is discontinuous at $x = 0$, there is no derivative in the classical sense. However, we can break the interval $[-1, 1]$ into two parts where f is smooth on each interval and integrate by parts using $\phi \in C^\infty(\mathbf{\Omega})$.

$$\begin{aligned}\int_{-1}^{1} f(x)\phi'(x)\,\mathrm{d}x &= \int_{1}^{0} f(x)\phi'(x)\,\mathrm{d}x + \int_{0}^{1} f(x)\phi'(x)\,\mathrm{d}x \\ &= -\int_{-1}^{0}(+1)\phi(x)\,\mathrm{d}x + f\phi|_{-1}^{0} - \int_{0}^{1}(-1)\phi(x)\,\mathrm{d}x + f\phi|_{0}^{1} \\ &= -\int_{-1}^{1} g(x)\phi(x)\,\mathrm{d}x\end{aligned}$$

Remark 2.8.

1. *In order to simplify the notation, the classical and the weak derivates are both denoted by D. From the context it will be clear which one is meant.*

2. *If $f(\mathbf{x})$ has a classical derivative, then it coincides with the corresponding weak derivative.*

3. *Since the Lebesgue integral is not affected by function values on null sets, the notion of a weak derivative works for functions which are not classical differentiable on a set of Lebesgue measure zero.*

4. *The weak derivative is unique up to a set of Lebesgue measure zero.*

Now we proceed to a similar definition of weak divergence.

Definition 2.9 (Weak Divergence)**.** *A vector field $\mathbf{w} \in L^2(\mathbf{\Omega};\mathbb{R}^d)$ is said to have a weak divergence (a divergence in $L^2(\mathbf{\Omega};\mathbb{R}^d)$) if there is a function $s \in L^2(\mathbf{\Omega})$ such that*

$$-\int_{\mathbf{\Omega}} \mathbf{w}\cdot\nabla\phi\,\mathrm{d}\mathbf{x} = \int_{\mathbf{\Omega}} s\,\phi\,\mathrm{d}\mathbf{x}, \qquad \forall\,\phi \in C_0^\infty(\mathbf{\Omega};\mathbb{R}^d). \tag{2.2.12}$$

We, then write $s = \nabla\cdot\mathbf{w}$.

Definition 2.10 (Sobolev Spaces)**.** *Let k be a non-negative integer, and let $f \in L^1_{loc}(\mathbf{\Omega};\mathbb{R}^d)$. Suppose that the weak derivatives $D^{\boldsymbol{\alpha}} f$ exist for all $|\boldsymbol{\alpha}| \le k$. We define the Sobolev space as*

$$W^{k,p}(\mathbf{\Omega};\mathbb{R}^d) \coloneqq \left\{ f \in L^p(\mathbf{\Omega};\mathbb{R}^d) \colon D^{\boldsymbol{\alpha}} f \in L^p(\mathbf{\Omega};\mathbb{R}^d), |\boldsymbol{\alpha}| \le k \right\} \qquad 1 < p < \infty, k \in \mathbb{N}. \tag{2.2.13}$$

Additionally, define the closure of $C_0^\infty(\mathbf{\Omega};\mathbb{R}^d)$ in $W^{k,p}(\mathbf{\Omega};\mathbb{R}^d)$ by

$$W_0^{k,p} \coloneqq \overline{C_0^\infty(\mathbf{\Omega})}^{\|\cdot\|_{W^{k,p}(\mathbf{\Omega})}}, \tag{2.2.14}$$

where the **Sobolev norm** is given as

$$\|f\|_{W^{k,p}(\mathbf{\Omega})} \coloneqq \left(\sum_{|\boldsymbol{\alpha}|\leq k} \|D_w^{\alpha} f\|_{L^p(\mathbf{\Omega})}^p \right)^{\frac{1}{p}}, \tag{2.2.15}$$

for $1 \leq p < \infty$, where for $p = \infty$, we have

$$\|f\|_{W^{k,\infty}(\mathbf{\Omega})} \coloneqq \max_{|\boldsymbol{\alpha}|\leq k} \|D_w^{\alpha} f\|_{L^{\infty}(\mathbf{\Omega})} < \infty. \tag{2.2.16}$$

The space $W^{k,p}(\mathbf{\Omega})$ is a Banach space with the norm $\|\cdot\|_{W^{k,p}}$.

Definition 2.11 (Semi norm)**.** *For a non-negative integer k and $f \in W^{k,p}(\mathbf{\Omega})$, we define the $W^{k,p}$-semi norm as*

$$|f|_{W^{k,p}(\mathbf{\Omega})} \coloneqq \left(\sum_{|\boldsymbol{\alpha}|=k} \|D_w^{\boldsymbol{\alpha}} f\|_{L^p(\mathbf{\Omega})}^p \right)^{\frac{1}{p}}, \tag{2.2.17}$$

in the case $1 \leq p < \infty$, and for $p = \infty$, we define

$$|f|_{W^{k,\infty}(\mathbf{\Omega})} \coloneqq \max_{|\boldsymbol{\alpha}|=k} \|D_w^{\boldsymbol{\alpha}} f\|_{L^{\infty}} . \tag{2.2.18}$$

Remark 2.12.

1. *The space $W^{k,2}(\mathbf{\Omega})$ is a Hilbert space so, we denote it as H_0^k with inner product*

$$(\mathbf{u}, \mathbf{v})_{H_0^1} = \sum_{|\boldsymbol{\alpha}|\leq k} \int_{\Omega} D^{\boldsymbol{\alpha}}\mathbf{u}\, D^{\boldsymbol{\alpha}}\mathbf{v}\, \mathrm{d}\mathbf{x} \tag{2.2.19}$$

   with the norm

$$\|\mathbf{u}\|_{H^k(\Omega)} \coloneqq (\mathbf{u}, \mathbf{u})_{H^k(\Omega)}^{\frac{1}{2}} = \sum_{|\boldsymbol{\alpha}|\leq k} \left(\int_{\Omega} |D^{\boldsymbol{\alpha}}\mathbf{u}|^2 \right)^{\frac{1}{2}} \tag{2.2.20}$$

   and semi norm

$$|\mathbf{u}|_{H^k(\Omega)} \coloneqq \left(\sum_{|\boldsymbol{\alpha}|=k} \int_{\Omega} |D^{\boldsymbol{\alpha}}\mathbf{u}|^2 \, \mathrm{d}\mathbf{x} \right)^{\frac{1}{2}} . \tag{2.2.21}$$

2. *For H^1 we have that $|\mathbf{u}|_{H^1(\mathbf{\Omega})} = \|\nabla \mathbf{u}\|_{L^2(\mathbf{\Omega})}$.*

3. *We also have $H^0(\mathbf{\Omega}) = L^2(\mathbf{\Omega})$.*

4. *The space H_0^1 is repeatedly used in this thesis, so we will briefly discuss:*

$$\mathbf{H}_0^1(\mathbf{\Omega}) = \underbrace{H_0^1(\mathbf{\Omega}) \times H_0^1(\mathbf{\Omega}) \times \cdots H_0^1(\mathbf{\Omega})}_{n \text{ times}} \tag{2.2.22}$$

$$= \left\{ \mathbf{u} \in \mathbf{H}^1(\mathbf{\Omega}) \colon \mathbf{u}|_{\partial\mathbf{\Omega}} = 0 \right\} \tag{2.2.23}$$

$$= \left\{ \mathbf{u} \in \mathbf{L}^2(\mathbf{\Omega}) \colon \nabla\mathbf{u} \in L^2(\mathbf{\Omega}), \mathbf{u}|_{\partial\mathbf{\Omega}} = 0 \right\}. \tag{2.2.24}$$

5. *On H_0^1, the expression*
$$(\mathbf{u}, \mathbf{v}) = \int_{\mathbf{\Omega}} D\mathbf{u}\, D\mathbf{v}\, \mathrm{d}\mathbf{x} \tag{2.2.25}$$
is a scalar product and induces the norm $\|\nabla \mathbf{u}\|_{L^2}$.

6. *On H_0^1, the norm $\|\nabla \mathbf{u}\|_{L^2}$ is equivalent to $\|\mathbf{u}\|_{H^1}$, using the Poincare inequality, see below (2.3.5). Similarly, we have the equivalence for $\|\nabla \mathbf{u}\|_{L^p}$ and $\|\mathbf{u}\|_{W_0^{1,p}}$.*

7. *Using the Poincare inequality, for functions in $H_0^1(\mathbf{\Omega})$, we have $|\cdot|_{H^1}$ is equivalent to $\|\cdot\|_{H^1}$ and from now we use the identity $\|\mathbf{u}\|_{H_0^1} = \|\nabla \mathbf{u}\|_{L^2}$.*

For further details, we refer to [13, Section 1.3]. Before going into the dual space, we introduce the continuous linear operators.

Definition 2.13 (Linear Operator)**.** *Let $\mathbf{V}$ and $\mathbf{W}$ be Hilbert spaces and let $L : \mathbf{V} \to \mathbf{W}$ be a linear mapping from $\mathbf{V}$ to $\mathbf{W}$, we say L is bounded or continuous if there exists a constant c_L such that*
$$\|L\mathbf{v}\|_{\mathbf{W}} \leq c_L \|\mathbf{v}\|_{\mathbf{V}}. \tag{2.2.26}$$
Let $\mathcal{L}(\mathbf{V}, \mathbf{W})$ be the set of all boundend linear functionals/operators, we have $L \in \mathcal{L}(\mathbf{V}, \mathbf{W})$ and the norm is given as
$$\|L\|_{\mathcal{L}(\mathbf{V},\mathbf{W})} \coloneqq \sup_{\substack{\mathbf{v}\in\mathbf{V} \\ \|\mathbf{v}\|\neq 0}} \frac{\|L\mathbf{v}\|_{\mathbf{W}}}{\|\mathbf{v}\|_{\mathbf{V}}}. \tag{2.2.27}$$

Before defining the dual space of Sobolev space, we define dual index q of p as
$$1 = \frac{1}{p} + \frac{1}{q}. \tag{2.2.28}$$

Definition 2.14 (Dual Space)**.** *Given a Banach space X, the set of all bounded linear operators in X is called the dual space of X and is denoted as X'*
$$X' = \{F \colon X \to \mathbb{R} \colon |F(\mathbf{v})| \leq C\|\mathbf{v}\|, \forall\, \mathbf{v} \in X\}.$$
The dual norm is defined as follows from (2.2.27)
$$\|F\|_{X'} \coloneqq \sup_{\substack{\mathbf{v}\in\mathbf{V} \\ \|\mathbf{v}\|\neq 0}} \frac{F\mathbf{v}}{\|\mathbf{v}\|_X} \tag{2.2.29}$$

In particular, it holds $H^{-1}(\mathbf{\Omega}) = (H_0^1(\mathbf{\Omega}))'$.

$$\mathbf{L}^2(\mathbf{\Omega}) = [L^2(\mathbf{\Omega})]^n = \left\{\mathbf{v} \colon \mathbf{\Omega} \to \mathbb{R}^n; v_i \in L^2(\mathbf{\Omega}), \quad \forall\, i = 1, \cdots, n\right\}$$
and
$$\|\mathbf{v}\|_{\mathbf{L}^2(\mathbf{\Omega})} = \left(\sum_{i=1}^{n} \|v_i\|_{L^2(\mathbf{\Omega})}^2\right)^{\frac{1}{2}}$$

2.3 Inequalities

We proceed to defining some very important inequalities that we will be using throughout this thesis.

(i) **Minkowski's Inequality** : For $1 \leq p \leq \infty$, $f, g \in L^p(\Omega)$, we have

$$\|f+g\|_{L^p(\Omega)} \leq \|f\|_{L^p(\boldsymbol{\Omega})} + \|g\|_{L^p(\boldsymbol{\Omega})}\,. \tag{2.3.1}$$

(ii) **Hölder's Inequality** : For $1 \leq p, q \leq \infty$, such that $1/p + 1/q = 1$ and $f \in L^p(\boldsymbol{\Omega})$ and $g \in L^q(\boldsymbol{\Omega})$ then $fg \in L^1(\boldsymbol{\Omega})$ and

$$\|fg\|_1 \leq \|f\|_{L^p(\boldsymbol{\Omega})}\, \|g\|_{L^q(\boldsymbol{\Omega})}\,. \tag{2.3.2}$$

(iii) **Cauchy-Schwarz's inequality** : This is Hölder's inequality with $p = q = 2$, i.e., if $f, g \in L^2(\boldsymbol{\Omega})$ then $fg \in L^1(\boldsymbol{\Omega})$ and

$$\int_{\boldsymbol{\Omega}} |f(\mathbf{x})g(\mathbf{x})|\, \mathrm{d}x \leq \|f\|_{L^2(\boldsymbol{\Omega})}\, \|g\|_{L^2(\boldsymbol{\Omega})}\,. \tag{2.3.3}$$

(iv) **Young's Inequality** : If $a \geq 0, b \geq 0$ are two non-negative numbers and if $p > 1$ and $q < 1$ are real numbers such that $\frac{1}{p} + \frac{1}{q} = 1$, then

$$ab \leq \frac{a^p}{p} + \frac{b^q}{q} = 1. \tag{2.3.4}$$

(v) **Poincaré's Inequality** : Suppose Ω is a bounded domain. Then there exists a constant C (depending on Ω) such that

$$\|\mathbf{u}\|_{W^{1,p}(\Omega)} \leq C\|\nabla \mathbf{u}\|_{L^p(\Omega)} \qquad \forall\, \mathbf{u} \in W_0^{1,p}(\Omega). \tag{2.3.5}$$

Proof. See [14, Proposition 8.13]. □

Lemma 2.15. *Let* $\mathbf{u} \in \mathbf{H}_0^1(\boldsymbol{\Omega})$ *and* $\boldsymbol{\Omega} \subset \mathbb{R}^3$. *Then*

$$\|\nabla \mathbf{u}\|_{L^2}^2 = \|\nabla \cdot \mathbf{u}\|_{L^2}^2 + \|\nabla \times \mathbf{u}\|_{L^2}^2\,.$$

In particular, it holds

$$\|\nabla \mathbf{u}\|_{L^2} \geq \|\nabla \cdot \mathbf{u}\|_{L^2}\,.$$

Proof. Let $\mathbf{v} \in H_0^1(\boldsymbol{\Omega})$. By Lemma 2.2 ((vi)), we have that

$$-\Delta \mathbf{u} = -\nabla(\nabla \cdot \mathbf{u}) + \nabla \times (\nabla \times \mathbf{u})$$

Multiplying with test function ϕ and integrating by parts we get,

$$\int_{\boldsymbol{\Omega}} \nabla \mathbf{u} : \nabla \boldsymbol{\phi}\, \mathrm{d}x = \int_{\boldsymbol{\Omega}} (\nabla \cdot \mathbf{u})(\nabla \cdot \boldsymbol{\phi})\, \mathrm{d}x + \int_{\boldsymbol{\Omega}} (\nabla \times \mathbf{u} \cdot (\nabla \times \boldsymbol{\phi}))\, \mathrm{d}x.$$

Setting $\boldsymbol{\phi} = \mathbf{u}$, the proof is done. □

2.4 Some important theorems

Integration by parts is at the very core in going from a strong formulation to a weak formulation. In this section, we present some basic theorems for the same.

Theorem 2.16. *Let $\mathbf{\Omega} \subset \mathbb{R}^n, n = 2, 3$, be a bounded domain with Lipschitz boundary $\partial\mathbf{\Omega}$ and $\mathbf{u}, \mathbf{v}$ sufficiently smooth. Moreover, we denote the unit outward normal vector as $\hat{\mathbf{n}}$ on $\partial\mathbf{\Omega}$.*

1. Integration by parts :
   Let $\mathbf{u} \in \mathbf{H}^2(\mathbf{\Omega}\colon \mathbb{R}^d)$ and $\mathbf{v} \in \mathbf{H}^1(\mathbf{\Omega}; \mathbb{R}^d)$, then it holds
   $$\int_{\mathbf{\Omega}} (\Delta \mathbf{u})\mathbf{v}\, \mathrm{d}x = \int_{\partial\mathbf{\Omega}} \frac{\partial \mathbf{u}}{\partial \hat{\mathbf{n}}}\mathbf{v}\, \mathrm{d}s - \int_{\mathbf{\Omega}} \nabla \mathbf{u}\colon\ \nabla v\, \mathrm{d}\mathbf{x}. \tag{2.4.1}$$

2. Green's divergence theorem :
   For $\mathbf{u} \in \mathbf{H}^1_0(\mathbf{\Omega}; \mathbb{R}^d)$ and $q \in L^2(\mathbf{\Omega})$, the divergence formula states
   $$\int_{\mathbf{\Omega}} \nabla\cdot\mathbf{u}\, q\, \mathrm{d}x = -\int_{\mathbf{\Omega}} \mathbf{u}\cdot\nabla q\, \mathrm{d}x + \int_{\partial\mathbf{\Omega}} \mathbf{u}\cdot q\, \hat{\mathbf{n}}\, \mathrm{d}s. \tag{2.4.2}$$

Now, we extend the symmetry of weak derivatives.

Theorem 2.17 (Symmetry of weak derivatives)**.** *Let $\mathbf{\Omega} \subset \mathbb{R}^n, \mathbf{u} \in W^{k,p}(\mathbf{\Omega})$ and $\boldsymbol{\alpha}, \boldsymbol{\beta}$ multi-indices with $|\boldsymbol{\alpha}| + |\boldsymbol{\beta}| \leq k$. Then it holds*
$$D^{\boldsymbol{\alpha}}\left(D^{\boldsymbol{\beta}}\mathbf{u}\right) = D^{\boldsymbol{\beta}}\left(D^{\boldsymbol{\alpha}}\mathbf{u}\right). \tag{2.4.3}$$

Proof. Consider a test function $\phi \in C_0^\infty(\mathbf{\Omega})$ and using Definition 2.6, we get
$$\begin{aligned}
\int_{\mathbf{\Omega}} D^{\boldsymbol{\alpha}}\mathbf{u} D^{\boldsymbol{\beta}}\phi\, \mathrm{d}\mathbf{x} &= (-1)^{|\boldsymbol{\alpha}|}\int_{\mathbf{\Omega}} \mathbf{u}\left(D^{\boldsymbol{\alpha}+\boldsymbol{\beta}}\phi\right)\, \mathrm{d}\mathbf{x} \\
&= (-1)^{|\boldsymbol{\alpha}|}\,(-1)^{|\boldsymbol{\alpha}+\boldsymbol{\beta}|}\int_{\mathbf{\Omega}} \left(D^{\boldsymbol{\alpha}+\boldsymbol{\beta}}\mathbf{u}\right)\phi\, \mathrm{d}\mathbf{x} \\
&= (-1)^{|\boldsymbol{\beta}|}\int_{\mathbf{\Omega}} \left(D^{\boldsymbol{\alpha}+\boldsymbol{\beta}}\mathbf{u}\right)\phi\, \mathrm{d}\mathbf{x}.
\end{aligned}$$
From the above equation and definition of weak derivative 2.6, we get $D^{\boldsymbol{\beta}}\left(D^{\boldsymbol{\alpha}}\mathbf{u}\right)$. Now by exchanging the roles of $\boldsymbol{\alpha}$ and $\boldsymbol{\beta}$, we get
$$\begin{aligned}
\int_{\mathbf{\Omega}} D^{\boldsymbol{\beta}}\mathbf{u} D^{\boldsymbol{\alpha}}\phi\, \mathrm{d}\mathbf{x} &= (-1)^{|\boldsymbol{\beta}|}\int_{\mathbf{\Omega}} \mathbf{u}\left(D^{\boldsymbol{\alpha}+\boldsymbol{\beta}}\phi\right)\, \mathrm{d}\mathbf{x} \\
&= (-1)^{|\boldsymbol{\beta}|}\,(-1)^{|\boldsymbol{\alpha}+\boldsymbol{\beta}|}\int_{\mathbf{\Omega}} \left(D^{|\boldsymbol{\alpha}+\boldsymbol{\beta}|}\int_{\mathbf{\Omega}} \mathbf{u}\right)\phi\, \mathrm{d}\mathbf{x} \\
&= (-1)^{|\boldsymbol{\alpha}|}\int_{\mathbf{\Omega}} \left(D^{\boldsymbol{\alpha}+\boldsymbol{\beta}}\mathbf{u}\right)\phi\, \mathrm{d}\mathbf{x},
\end{aligned}$$
i.e., $D^{\boldsymbol{\alpha}}\left(D^{\boldsymbol{\beta}}\mathbf{u}\right) = D^{\boldsymbol{\alpha}+\boldsymbol{\beta}}\mathbf{u}$. □

2.5 Symbols and Abbreviations

The list of used symbols and abbreviations are listed below.

Symbol	Description
1d, 2d, 3d	one, two or three-dimensional
$\mathbb{R}^d$	set of real numbers in d dimensions
$\mathbb{N}$	set of natural numbers
Ω	two/three-dimensional bounded domain
$\partial\Omega$	boundary of the domain
∇	gradient operator
Δ	laplace operator
$\langle\cdot,\cdot\rangle$	dual product
$(\cdot,\cdot)$	inner product
$D\mathbf{u}$	derivative tensor of the vector u
$\|\cdot\|_0$	L^2 norm
$\|\cdot\|_1$	H^1 norm
$a(\cdot,\cdot), b(\cdot,\cdot)$	bilinear forms a, b
L	Lagrangian of the minimization problem
$\mathcal{L}$	linear mapping from vector spaces to $\mathbb{R}$
L, A, B	linear operator between two Hilbert spaces
B'	dual operators
V'	dual space of the space V
$\mathbf{V}$	continuous velocity/displacement space
Q	continuous pressure space
$\mathbf{V}_h$	discrete velocity/displacement space
Q_h	discrete pressure space
$\mathcal{Q}_2$	polynomial space from span$\{1, x, y, xy, x^2, y^2, x^2y, y^2x, x^2y^2\}$
$\mathcal{P}_1$	polynomial space from span$\{1, x, y\}$

Further Definitions, Theorems and Lemmas are described in the later chapters, whenever necessary.

Symbol	Description
π^{div}	interpolation operator
Π_h	Fortin operator
tr()	trace operator
$\mathbb{I}_T$	indicator function on the element T
$\hat{\mathbf{n}}$	unit normal vector
$\mathcal{T}_h$	Triangulation of the domain Ω
T	given element in the triangulation $\mathcal{T}_h$
$\hat{T}$	reference element
$\bar{\mathcal{F}}_h$	set of all edges/faces for a given triangulation
$\mathcal{F}_h$	set of all interior edges/faces for a given triangulation
$F \in \bar{\mathcal{F}}_h$	a given edge/face in the triangulation
$[\phi](\mathbf{x})$	jump at the point x of the function ϕ
Φ	affine Transform
$\mathcal{G}$	Piola Transform
λ, μ	first and second Lamé parameters respectively
α	thermal expansion coefficient
γ	thermal conductivity coefficient
θ	temperature variable
$\mathcal{C}$	crack domain
φ	phase-field variable
κ	regularization of the bulk term
$g(\varphi)$	degradation of the bulk term
G_c	critical energy release rate, material dependent
t	time variable
E_b	bulk energy
E_c	crack energy

Abbreviation	Description
TCV	total crack volume
$\mathcal{RT}_k$	Raviart-Thomas element of order k
$\mathcal{BDM}_k$	Brezzi-Douglas-Marini element of order k
$\mathcal{DGP}_1$	Discontinuous finite elements of order 1 based on Legendre polynomials
$\mathcal{DGQ}_1$	Discontinuous finite elements of order 1 based on tensor product of Lagrangian polynomials
`DOpElib`	Differential equations and optimization environment
`deal.II`	Differential equations' analysis library

Chapter 3

Saddle Point Problem

In this chapter, we lay the foundation for the saddle point problem, which is at the very core, to the type of equations we will be dealing with in this thesis. The necessary and sufficient conditions needed for the existence and uniqueness of the solution in continuous discrete case are discussed in Section 3.2 and 3.3 respectively. For a more detailed description, we refer to [10, 29, 12, 15, 56].

Definition 3.1 (Bilinear form)**.** *The map,* $a(\cdot,\cdot) : \mathbf{V} \times \mathbf{V} \to \mathbb{R}$ *is called a bilinear form if*

$$a(\alpha\mathbf{u}_1 + \beta\mathbf{u}_2, \mathbf{v}) = \alpha a(\mathbf{u}_1, \mathbf{v}) + \beta a(\mathbf{u}_2, \mathbf{v}), \quad \forall\, \mathbf{u}, \mathbf{v} \in \mathbf{V}$$
$$a(\mathbf{u}, \alpha\mathbf{v}_1 + \beta\mathbf{v}_2) = \alpha a(\mathbf{u}, \mathbf{v}_1) + \beta a(\mathbf{u}, \mathbf{v}_2), \quad \forall\, \mathbf{u}, \mathbf{v} \in \mathbf{V}.$$

Definition 3.2 (Symmetric form)**.** *A bilinear form is called symmetric if*

$$a(\mathbf{u}, \mathbf{v}) = a(\mathbf{v}, \mathbf{u}), \quad \forall\, \mathbf{u}, \mathbf{v} \in \mathbf{V}$$

Definition 3.3 (Continuous Bilinear form)**.** *A bilinear form is said to be continuous if there exists a constant* C *such that*

$$a(\mathbf{u}, \mathbf{v}) = C\|\mathbf{u}\|_{\mathbf{V}}\|\mathbf{v}\|_{\mathbf{V}}, \quad \forall\, \mathbf{u}, \mathbf{v} \in \mathbf{V}$$

Consider V and Q, two Hilbert spaces and suppose,

$$a : \mathbf{V} \times \mathbf{V} \to \mathbb{R}, \quad b : \mathbf{V} \times Q \to \mathbb{R}$$

are two continuous bilinear forms.

3.1 Minimization problem

Let $f \in \mathbf{V}'$ and $g \in Q'$, where $\mathbf{V}'$ and Q' are the dual spaces (see Definition 2.14) of $\mathbf{V}$ and Q respectively. Consider the minimization problem over $\mathbf{V}$,

$$J(\mathbf{u}) = \frac{1}{2}a(\mathbf{u}, \mathbf{u}) - \langle \mathbf{f}, \mathbf{u} \rangle_{\mathbf{V}',\mathbf{V}}, \quad \forall\, \mathbf{u} \in \mathbf{V} \tag{3.1.1}$$

subject to the constraint

$$b(\mathbf{u}, q) = \langle \mathbf{g}, q \rangle_{Q',Q}, \quad \forall\, q \in Q. \tag{3.1.2}$$

We define the dual pairing $\langle \cdot, \cdot \rangle$ between elements of the space and its dual space. We drop the spaces from the dual pairing notation whenever it is obvious.

The Lagrangian of the above minimization problem is given as

$$\mathrm{L}(\mathbf{u}, p) = J(\mathbf{u}) + [b(\mathbf{u}, p) - \langle \mathbf{g}, p \rangle] \tag{3.1.3}$$

From the first-order optimality conditions, we have $\partial_u \mathrm{L} = 0$ and $\partial_p \mathrm{L} = 0$. We can rewrite the above problem with the given constraint as: Given $f \in \mathbf{V}'$ and $g \in Q'$, find the pair $(\mathbf{u}, p) \in \mathbf{V} \times Q$ such that

$$\begin{aligned} a(\mathbf{u}, \mathbf{v}) + b(\mathbf{v}, p) &= \langle \mathbf{f}, \mathbf{v} \rangle, \quad \forall\, \mathbf{v} \in \mathbf{V} \\ b(\mathbf{u}, q) &= \langle \mathbf{g}, q \rangle, \quad \forall\, q \in Q \end{aligned} \tag{3.1.4}$$

Definition 3.4 (Saddle Point)**.** *Given spaces, $X \subset \mathbb{R}^d, d = 2, 3, Y \subset \mathbb{R}$ and a linear map $\mathcal{L} : X \times Y \to \mathbb{R}$. A point (x^*, y^*) is called a saddle point of $\mathcal{L}$ in $(X \times Y)$ if*

$$\mathcal{L}(x^*, y) \leq \mathcal{L}(x^*, y^*) \leq \mathcal{L}(x, y^*), \quad \forall x \in X, y \in Y \tag{3.1.5}$$

Remark 3.5.

1. *The p variable acts as a Lagrange multiplier in the minimization problem.*
2. *The first component of the solution i.e., $\mathbf{u}$ solves the minimization problem.*
3. *The solution $(\mathbf{u}, p)$ of the problem (3.1.4) follow the saddle point inequality (3.1.5),*

$$\mathcal{L}(\mathbf{u}, q) \leq \mathcal{L}(\mathbf{u}, p) \leq \mathcal{L}(\mathbf{v}, p), \quad \forall\, \mathbf{v} \in \mathbf{v}, q \in Q$$

4. *The converse of the above statement is not true. Even if the minimization problem has a solution, the existence of the Lagrange multipliers can only be asserted with additional conditions.*

In this thesis, we will be discussing two saddle point problems namely, linearized Navier-Stokes and linear elasticity. In this chapter we will cover the existence and uniqueness of the Saddle point problem (3.1.4). Firstly, let's define some necessary definitions and properties before going into the existence of Saddle point problem. Consider the following problem with $a : \mathbf{U} \times \mathbf{V} \to \mathbb{R}$ and $\mathbf{f} \in \mathbf{U}'$,

$$a(\mathbf{u}, \mathbf{v}) = \langle \mathbf{f}, \mathbf{v} \rangle \quad \forall\, \mathbf{u} \in \mathbf{U}, \mathbf{v} \in \mathbf{V} \tag{3.1.6}$$

Lets define a linear operator $L \colon \mathbf{U} \to \mathbf{V}'$ as

$$\langle L\mathbf{u}, \mathbf{v} \rangle \coloneqq a(\mathbf{u}, \mathbf{v}) \quad \forall\, \mathbf{u} \in \mathbf{U}, \mathbf{v} \in \mathbf{V} \tag{3.1.7}$$

which implies that $\mathbf{u} = L^{-1}\mathbf{f}$.

Definition 3.6 (Isomorphism)**.** *A linear operator L between two normed linear spaces is called an isomorphism if it is bijective and L and L^{-1} are continuous.*

3.2 Existence and Uniqueness

The following theorem shows the necessary and sufficient conditions for isomorphism on L and there in necessary and sufficient conditions for the existence and uniqueness of solution for (3.1.6).

Theorem 3.7. *Let* $\mathbf{U}$ *and* $\mathbf{V}$ *be Hilbert spaces. Then the linear operator* $L : \mathbf{U} \to \mathbf{V}'$ *is an isomorphism if and only if the associated bilinear form* $a : \mathbf{U} \times \mathbf{V} \to \mathbb{R}$ *satisfies the following conditions:*

(i) (Continuity). There exists $C \geq 0$ *such that*

$$|a(\mathbf{u}, \mathbf{v})| \leq C\|\mathbf{u}\|_{\mathbf{U}}\|\mathbf{V}\|_{\mathbf{V}}, \quad \forall\, \mathbf{u}, \mathbf{v} \in \mathbf{V} \tag{3.2.1}$$

(ii) (Inf-sup condition). There exists $\alpha > 0$ *such that*

$$\sup_{\mathbf{v} \in \mathbf{V}} \frac{a(\mathbf{u}, \mathbf{v})}{\|\mathbf{v}\|_{\mathbf{v}}} \geq \alpha\|\mathbf{u}\|_{\mathbf{U}}, \quad \forall\, \mathbf{u} \in \mathbf{U}, \mathbf{v} \in \mathbf{V} \tag{3.2.2}$$

(iii) For every $\mathbf{v} \in \mathbf{V}$*, there exists* $\mathbf{u} \in \mathbf{U}$ *with*

$$a(\mathbf{u}, \mathbf{v}) \neq 0. \tag{3.2.3}$$

Proof. For proof, we refer to [12, Theorem 3.6]. □

In the equation (3.1.4), we can define a linear operator $L : \mathbf{V} \times Q \to \mathbf{V}' \times Q'$ as

$$L(\mathbf{u}, p) := a(\mathbf{u}, \mathbf{v}) + b(\mathbf{v}, p) + b(\mathbf{u}, q), \quad \forall\, \mathbf{u} \in \mathbf{V}, q \in Q \tag{3.2.4}$$

and the equation (3.1.4) can be rewritten as

$$L(\mathbf{u}, p) = \langle \mathbf{f}, \mathbf{v} \rangle + \langle \mathbf{g}, q \rangle, \quad \forall\, \mathbf{u} \in \mathbf{V}, q \in Q \tag{3.2.5}$$

The existence and uniqueness of (3.2.5) can be asserted by using Theorem 3.7. To prove equation (3.2.2), Brezzi [15] has split the conditions in terms of the two bilinear forms. We will outline those properties in the next lemma and theorem. Before that it's convenient to convert the bilinear forms into linear operators and rewrite equation (3.1.4). We define $A : \mathbf{V} \to \mathbf{V}'$, $B : \mathbf{V} \to Q'$ and the adjoint operator $B' : Q \to \mathbf{V}'$ as

$$\begin{aligned} \langle A\mathbf{u}, \mathbf{v} \rangle &:= a(\mathbf{u}, \mathbf{v}), \quad \forall\, \mathbf{u}, \mathbf{v} \in \mathbf{V} \\ \langle B\mathbf{u}, q \rangle &:= b(\mathbf{u}, q), \quad \forall\, \mathbf{u} \in \mathbf{V}, q \in Q \\ \langle B'q, \mathbf{v} \rangle &:= b(\mathbf{v}, q), \quad \forall\, \mathbf{u} \in \mathbf{V}, q \in Q \end{aligned} \tag{3.2.6}$$

Now equation (3.1.4) can be rewritten as: Given $\mathbf{f} \in \mathbf{V}'$ and $\mathbf{g} \in Q'$, find the pair $(\mathbf{u}, p) \in \mathbf{V} \times Q$ such that

$$A\mathbf{u} + B'p = \mathbf{f}, \tag{3.2.7}$$

$$Bu = \mathbf{g}. \tag{3.2.8}$$

We also need to define divergence space (term "divergence" might not make sense now, let's go with it for now, we will explain why in later chapters), orthogonal space and polar set.

Definition 3.8 (Divergence space)**.** *Furthermore, we define the divergence space* $\mathbf{V}^{\text{div}}$ *as*

$$\mathbf{V}^{\text{div}} := \{\mathbf{v} \in \mathbf{V} : b(\mathbf{u}, q) = 0, \quad \forall\, q \in Q\} \tag{3.2.9}$$

Definition 3.9 (Orthogonal Space)**.** *We define the orthogonal space of* V^{div} *as*

$$V^{\text{div},\perp} := \left\{\mathbf{u} \in V : (\mathbf{u}, \mathbf{v}) = 0, \quad \forall\, \mathbf{v} \in V^{\text{div}}\right\} \tag{3.2.10}$$

Definition 3.10 (Polar Set)**.** *If* $\mathbf{V}'$ *is the dual space of* $\mathbf{V}$*, we define the polar set* $\mathbf{V}^0$ *of* $\mathbf{V}$ *as*

$$\mathbf{V}^0 := \{f \in \mathbf{V}' : \langle \mathbf{f}, \mathbf{v}\rangle = 0, \quad \forall\, \mathbf{v} \in \mathbf{V}\}\,. \tag{3.2.11}$$

Lemma 3.11. *The following assertions are equivalent:*

(i) There exists a constant $\beta > 0$ *with*

$$\inf_{q \in Q} \sup_{\mathbf{v} \in \mathbf{V}} \frac{b(\mathbf{v}, q)}{\|\mathbf{v}\|_{\mathbf{V}} \|q\|_Q} \geq \beta. \tag{3.2.12}$$

(ii) The operator $B : \mathbf{V}^{\text{div},\perp} \to Q'$ *is an isomorphism, and*

$$\|B\mathbf{v}\|_{Q'} \geq \beta \|\mathbf{v}\|_{\mathbf{V}}, \quad \forall\, \mathbf{v} \in \mathbf{V}^{\perp}. \tag{3.2.13}$$

(iii) The operator $B' : Q \to \mathbf{V}^0 \subset \mathbf{V}'$ *is an isomorphism, and*

$$\|B'q\|_{\mathbf{V}^0} \geq \beta \|q\|_Q, \quad \forall\, q \in Q. \tag{3.2.14}$$

Proof. For proof, we refer to [12, Lemma 4.2]. □

Now finally, we have the main theorem for saddle point problem. The necessary and sufficient conditions for the existence and uniqueness of the problem is given in the following theorem.

Theorem 3.12 (Brezzi's splitting theorem)**.** *For the saddle point problem (3.1.4), the linear operator* L *in (3.2.5) defines an isomorphism if and only if the following conditions are satisfied:*

(i) The bilinear form $a(\cdot, \cdot)$ *is* $\mathbf{V}^{\text{div}}$*-elliptic, i.e.,*

$$a(\mathbf{v}, \mathbf{v}) \geq \alpha \|\mathbf{v}\|^2, \quad \forall\, \mathbf{v} \in \mathbf{V}^{\text{div}} \tag{3.2.15}$$

where, $\alpha > 0$*.*

(ii) The bilinear form $b(\cdot, \cdot)$ *satisfies the inf-sup condition (3.2.12)*

Proof. For the proof, we refer to [12, Theorem 4.3]. □

3.3 Discretization

Now that we have necessary and sufficient conditions for the well posedness of the saddle point problem, we move on to solving the system using mixed finite elements with discrete subspaces $\mathbf{V}_h \subset \mathbf{V}$ and $Q_h \subset Q$. The notation X_h indicates that the space X_h is discretized uniformly with step size h. We define the discrete problem as: Find $(\mathbf{u}_h, q_h) \in (\mathbf{V}_h \times Q_h)$ such that

$$\begin{aligned} a(\mathbf{u}_h, \mathbf{v}_h) + b(\mathbf{v}_h, p_h) &= \langle \mathbf{f}, \mathbf{v}_h \rangle, \quad \forall\, \mathbf{v}_h \in \mathbf{V}_h, \\ b(\mathbf{u}_h, q_h) &= \langle \mathbf{g}, q_h \rangle, \quad \forall\, q_h \in Q_h \end{aligned} \tag{3.3.1}$$

Next, we would like to find an analogous theorem to 3.12 for the above discrete problem. For that we will define some spaces similar to Definition 3.8.

Definition 3.13 (Discrete divergence space)**.** *We define the discrete divergence space* $\mathbf{V}_h^{\mathrm{div}}$ *as*

$$\mathbf{V}_h^{\mathrm{div}} \coloneqq \{\mathbf{v}_h \in \mathbf{V}_h \colon b(\mathbf{u}_h, q) = 0, \quad \forall\, q \in Q\} \tag{3.3.2}$$

Theorem 3.14. *Suppose the conditions of Theorem 3.12 hold, and suppose* $\mathbf{V}_h$, Q_h *satisfy:*

(i) The bilinear form $a(\cdot,\cdot)$ *is* $\mathbf{V}_h^{\mathrm{div}}$*-elliptic with constant* $\alpha_h > 0$*.*

(ii) The inf-sup condition or Ladyzhenskaja-Babuška-Brezzi condition, there exists a $\beta > 0$ *such that*

$$\inf_{q_h \in Q_h} \sup_{\mathbf{v}_h \in \mathbf{V}_h} \frac{b(\mathbf{v}_h, q_h)}{\|\mathbf{v}_h\| \|q_h\|} \geq \beta_h. \tag{3.3.3}$$

Then the discrete problem (3.3.1) is uniquely solvable, and we have the error estimate

$$\|\mathbf{u} - \mathbf{u}_h\| + \|p - p_h\| \leq c \left(\inf_{\mathbf{v}_h \in \mathbf{V}_h} \|\mathbf{u} - \mathbf{v}_h\| + \inf_{q_h \in Q_h} \|p - q_h\| \right). \tag{3.3.4}$$

Proof. For proof, we refer to [10, Theorem 5.2.2].

□

3.4 Fortin's Criterion

Fortin's Criterion is useful in checking if the discrete space Q_h satisfies the inf-sup condition (3.3.3). It involves an interpolation operator between spaces $\mathbf{V}$ and $\mathbf{V}_h$.

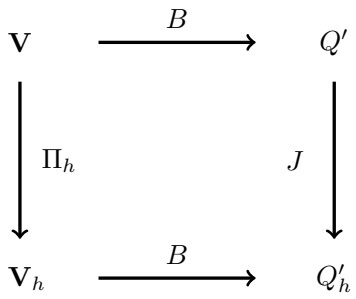

Figure 3.1: Commutative diagram for Fortin operator, Π_h

Figure 3.1 shows a pictorial representation of the Fortin's criterion. The operator J denotes the injection between the spaces Q' and Q'_h.

Theorem 3.15. *Suppose the bilinear form* $b\colon \mathbf{V} \times Q \to \mathbb{R}$ *satisfies the inf-sup condition* (3.2.12). *In addition, for the discrete subspaces* $\mathbf{V}_h$ *and* Q_h, *there exists a bounded linear operator (Fortin operator)* $\Pi_h\colon \mathbf{V} \to \mathbf{V}_h$ *such that*

$$b(\mathbf{v} - \Pi_h \mathbf{v}, q_h) = 0, \quad \forall\, q_h \in Q_h. \tag{3.4.1}$$

If $\|\Pi_h\| \leq c$ *for some constant* c *independent of* h, *then the finite element spaces* $\mathbf{V}_h$ *and* Q_h *satisfy the discrete inf-sup condition* (3.3.3).

Note: The converse of the above theorem is true as well.

Corollary 3.16. *If the finite element spaces* $\mathbf{V}_h$ *and* Q_h *satisfy the inf-sup condition* (3.3.3), *then there exists a bounded linear operator* $\Pi_h\colon \mathbf{V} \to \mathbf{V}_h$ *such that* (3.4.1) *holds.*

In the next chapter, we will apply the saddle point theory to solve the linear Navier-Stokes equation and show the pressure dependency on the velocity error and how can we overcome that using Linke's decomposition [38].

Chapter 4

Stokes Equation

In this chapter we introduce the stationary continuous linear Stokes equation (from [12, 29, 10]) and see the connection with saddle point problem mentioned in the previous chapter. In Section 4.3, we show the invariance property of the velocity vector and discuss the variational crime that would solve the issue.

4.1 Problem Statement

The stationary Stokes equation with homogeneous boundary is given as

$$\begin{aligned} -\nu\Delta\mathbf{u} + \nabla p &= f, \quad \mathbf{u} \in \Omega, \\ \nabla \cdot \mathbf{u} &= 0, \quad \mathbf{u} \in \Omega, \\ \mathbf{u} &= 0, \quad \mathbf{u} \in \partial\Omega, \end{aligned} \tag{4.1.1}$$

where, $\partial\Omega$ is the boundary of the domain Ω and ν is the viscosity. In order to solve the system numerically using finite elements, we reformulate equation (4.1.1) as: Find $(\mathbf{u}, p) \in \left(\mathbf{H}_0^1(\Omega;\mathbb{R}^d) \times L_0^2(\Omega)\right)$, such that

$$\begin{aligned} \nu\left(\nabla\mathbf{u}, \nabla\mathbf{v}\right) - \left(\nabla\cdot\mathbf{v}, p\right) &= \langle f, \mathbf{v}\rangle, \qquad \forall\, \mathbf{v} \in \mathbf{H}^1(\Omega;\mathbb{R}^d), \\ -\left(\nabla\cdot\mathbf{u}, q\right) &= 0, \qquad\qquad \forall\, q \in L_0^2(\Omega). \end{aligned} \tag{4.1.2}$$

We use the notation $\mathbf{H}_0^1(\Omega;\mathbb{R}^d)$, to specify that the set contains vector valued functions. For scalar functions in $\mathbf{L}_0^2(\Omega;\mathbb{R})$, we omit $\mathbb{R}$ and just write $L_0^2(\Omega)$ to distinguish between scalar and vector valued spaces. Now, we can rewrite the above system like the saddle point problem (3.1.4) as: Find $(\mathbf{u}, p) \in \left(\mathbf{H}_0^1(\Omega;\mathbb{R}^d) \times L_0^2(\Omega)\right)$, such that

$$\begin{aligned} a\left(\mathbf{u}, \mathbf{v}\right) + b\left(\mathbf{v}, p\right) &= \langle \mathbf{f}, \mathbf{v}\rangle, \qquad \forall\, \mathbf{v} \in \mathbf{H}^1(\Omega;\mathbb{R}^d), \\ b\left(\mathbf{u}, q\right) &= 0, \qquad\qquad \forall\, q \in L_0^2(\Omega). \end{aligned} \tag{4.1.3}$$

where,

$$\begin{aligned} a(\mathbf{u}, \mathbf{v}) &= \nu\left(\nabla\mathbf{u}, \nabla\mathbf{v}\right), \\ b(\mathbf{v}, q) &= -\left(\nabla\cdot\mathbf{v}, q\right), \end{aligned} \tag{4.1.4}$$

and $g = 0$ with $\mathbf{u}, \mathbf{v} \in \mathbf{V} = \mathbf{H}_0^1(\Omega; \mathbb{R}^d)$ and $q \in Q = L_0^2(\Omega)$. Following the same route from last chapter, we have a similar Theorem to 3.12. We refer to the mentioned text books for more information on existence and uniqueness theorems.

Theorem 4.1. *Let Ω be a bounded domain in $\mathbb{R}^d, d = 2, 3$ with a Lipschitz continuous boundary Γ and let $\mathbf{f} \in \mathbf{H}^{-1}(\Omega; \mathbb{R}^d)$. Then, there exists a unique pair $(\mathbf{u}, p) \in \mathbf{H}_0^1(\Omega; \mathbb{R}^d) \times L_0^2(\Omega)$ that solves (4.1.2).*

For the proof, it is readily obvious that the bilinear forms $a(\cdot, \cdot)$ and $b(\cdot, \cdot)$ satisfy the conditions of Theorem 3.12. Now, we can go into the stability of the solution.

Lemma 4.2. *Let the conditions of Theorem 4.1 are given. Then, the solution $(\mathbf{u}, p)$ of the Stokes problem (4.1.2) depends continuously on the right-hand side, i.e.,*

$$\|\mathbf{u}\|_1 = \|\nabla \mathbf{u}\|_0 \leq \|\mathbf{f}\|_{H^{-1}(\Omega)}, \tag{4.1.5}$$

$$\|p\|_0 = \frac{2}{\beta} \|\mathbf{f}\|_{H^{-1}(\Omega)}. \tag{4.1.6}$$

We use the notation $\|\cdot\|_1$ for H^1 norm (2.2.20) and $\|\cdot\|_0$ for L^2 norm (2.2.6). Before proceeding to the discrete setting of the Stokes problem, we would like to highlight some important properties of the Stokes problem. The following is a Corollary of (3.2.13).

Lemma 4.3. *For each $q \in Q$ there is a unique $\mathbf{v} \in \mathbf{V}^{\mathrm{div},\perp} \subset \mathbf{V}$ such that*

$$\nabla \cdot \mathbf{v} = q \quad \text{and } \|q\|_Q \leq \|\mathbf{v}\|_{\mathbf{V}}, \quad \|\mathbf{v}\|_{\mathbf{V}} \leq C\|q\|_Q, \tag{4.1.7}$$

with $C = \frac{1}{\beta}$, where β is the inf-sup constant in (3.2.12).

For proof, we refer to [29, Corollary 3.44]

4.2 Discretization

Now, we proceed to the discrete setting of the problem. We choose $\mathbf{V}_h \subset \mathbf{V}$ and $Q_h \subset Q$ for the discrete Stokes problem: Find $(\mathbf{u}_h, p_h) \in \mathbf{V}_h \times Q_h$, such that

$$\begin{aligned} a(\mathbf{u}_h, \mathbf{v}_h) + b(\mathbf{v}_h, p_h) &= \langle f, \mathbf{v}_h \rangle, \qquad \forall\, \mathbf{v}_h \in \mathbf{V}_h, \\ b(\mathbf{u}_h, q_h) &= 0, \qquad \forall\, q_h \in Q_h. \end{aligned} \tag{4.2.1}$$

Where, $a(\cdot,\cdot)$ and $b(\cdot,\cdot)$ are defined in (4.1.4). In this thesis, we choose $\mathbf{V}_h/Q_h$ finite element spaces as the inf-sup stable conforming pair $\mathcal{Q}_2/\mathcal{Q}_1$ (Taylor Hood space of order 1). We have a similar theorem to Theorem 3.14.

Theorem 4.4. *Let $(\mathbf{u}, p) \in \mathbf{V} \times Q$ be the unique solution to the Stokes problem (4.1.2). Let the spaces $\mathbf{V}_h$ and Q_h satisfy the inf-sup condition (3.3.3), then the discrete Stokes problem (4.2.1) is uniquely solvable and the velocity solution $\mathbf{u}_h$ follows the following error estimate*

$$\|\mathbf{u} - \mathbf{u}_h\|_1 \leq C \left\{ \inf_{\mathbf{v}_h \in \mathbf{V}_h} \|\mathbf{u} - \mathbf{v}_h\|_1 + \frac{1}{\nu} \inf_{q_h \in Q_h} \|p - q_h\| \right\}. \tag{4.2.2}$$

The central part of this thesis is the velocity error estimate (4.2.2) and how do we make it pressure robust. There are many methods which accomplishes the task and rewrite the estimate as

$$\|\mathbf{u} - \mathbf{u}_h\|_1 \leq C_1 \inf_{\mathbf{v}_h \in \mathbf{V}_h} \|\mathbf{u} - \mathbf{v}_h\|_1. \tag{4.2.3}$$

We will be focussing on a variational crime method proposed by Linke [38]. The problem lies in how the spaces $\mathbf{V}_h^{\text{div}}$ and $\mathbf{V}^{\text{div}}$ are related. Due to the construction ($\mathbf{V}_h \subset \mathbf{V}$), one might expect $\mathbf{V}_h^{\text{div}} \subset \mathbf{V}^{\text{div}}$. If it had been the case we would have gotten the desired estimate (4.2.3). But for most of the inf-sup stable finite element pairs, we have $\mathbf{V}_h^{\text{div}} \not\subset \mathbf{V}^{\text{div}}$ and hence the pressure dependency. What this implies is that we expect all the discretely divergence free functions to be divergence free (in the continuous sense) as well. Linke proposed a variational crime where he introduces an interpolation operator

$$\pi^{\text{div}} \colon \mathbf{V}_h \to H^{\text{div}}(\Omega) = \left\{\mathbf{v} \in \mathbf{L}^2(\Omega; \mathbb{R}^d) \colon \nabla \cdot \mathbf{v} \in L^2(\Omega)\right\} \tag{4.2.4}$$

4.3 Helmholtz decomposition

Before going into Helmholtz decomposition, we would like to define some needed spaces.

$$\mathbf{H}^{-1,\text{div}}(\Omega; \mathbb{R}^d) \coloneqq \left\{\mathbf{f} \in \mathbf{H}^{-1}(\Omega; \mathbb{R}^d) \colon \nabla \cdot \mathbf{f} \in H^{-1}(\Omega)\right\} \tag{4.3.1}$$

Definition 4.5 (H curl)**.**

$$\mathbf{H}^{\text{curl}}(\Omega; \mathbb{R}^d) \coloneqq \left\{\mathbf{v} \in \mathbf{L}^2(\Omega; \mathbb{R}^d) \colon \nabla \times \mathbf{v} \in \mathbf{L}^2(\Omega; \mathbb{R}^d)\right\} \tag{4.3.2}$$

with the natural norm

$$\|\mathbf{v}\|_{\text{curl}}^2 \coloneqq \|\mathbf{v}\|_0^2 + \|\nabla \times \mathbf{v}\|_0^2. \tag{4.3.3}$$

Using the Green's formula, for $\mathbf{v} \in \mathbf{L}^2(\Omega; \mathbb{R}^d)$ and $\phi \in \mathbf{L}^2(\Omega; \mathbb{R}^d)$, we get

$$\int_\Omega \mathbf{v} \cdot (\nabla \times \phi)\, \mathrm{d}x - \int_\Omega \nabla \times \mathbf{v} \cdot \phi \, \mathrm{d}x = \int_{\partial\Omega} (\mathbf{v} \cdot \hat{\mathbf{n}}) \cdot \phi \, \mathrm{d}s. \tag{4.3.4}$$

Definition 4.6 (H_0^{curl})**.**

$$\mathbf{H}_0^{\text{curl}}(\Omega; \mathbb{R}^d) \coloneqq \left\{\mathbf{v} \in \mathbf{H}^{\text{curl}}(\Omega; \mathbb{R}^d) \colon \mathbf{v} \cdot \hat{\mathbf{n}}|_{\partial\Omega} = 0\right\} \tag{4.3.5}$$

Unlike other spaces with subscript zero, we want the trace $(\mathbf{v} \cdot \hat{\mathbf{n}})$ to vanish on the boundary $\partial\Omega$.

Lemma 4.7. *Assume that $\Omega \subset \mathbb{R}^d$ is simply connected. Then every function $\mathbf{f} \in \mathbf{H}^{-1,\text{div}}\left(\Omega; \mathbb{R}^d\right)$ is uniquely decomposable in the form*

$$\mathbf{f} = \nabla\psi + \nabla \times \phi \tag{4.3.6}$$

with $\psi \in H_0^1(\Omega)$ and $\phi \in \mathbf{L}_0^2(\Omega; \mathbb{R}^d)$. Moreover, we have

$$\|\mathbf{f}\|_{\mathbf{H}^{-1,\text{div}}\left(\Omega;\mathbb{R}^d\right)} = \left(\|\psi\|_{1,\Omega}^2 + \|\phi\|_0^2\right)^{\frac{1}{2}}. \tag{4.3.7}$$

For proof, we refer to [12, Lemma 6.1]. We can take the lemma a bit further, if we consider $\mathbf{f} \in \mathbf{L}^2(\Omega;\mathbb{R}^d)$ and not just in $\mathbf{H}^{-1,\mathrm{div}}\left(\Omega;\mathbb{R}^d\right)$, we have the following Lemma.

Lemma 4.8 (Helmholtz decomposition of a vector field in $\mathbf{L}^2(\Omega;\mathbb{R}^d)$)**.** *Let Ω be a bounded Lipschitz domain. Then every $\mathbf{f} \in \mathbf{L}^2(\Omega;\mathbb{R}^d)$ has a unique decomposition*

$$\mathbf{f} = \mathbf{w} + \nabla\psi, \tag{4.3.8}$$

where

$$\mathbf{w} \in \mathbf{H}_0^{\mathrm{div}} = \left\{\mathbf{v} \in \mathbf{H}^{\mathrm{div}}\left(\Omega;\mathbb{R}^d\right) : \nabla\cdot\mathbf{v} = 0 \text{ and } \mathbf{v}\cdot\mathbf{n} = 0 \text{ on } \partial\Omega\right\}, \tag{4.3.9}$$

and $\psi \in L^2(\Omega)$. Similar to (4.3.7), we have

$$\|\mathbf{f}\|_0^2 = \|\mathbf{w}\|_0^2 + \|\nabla\psi\|_0^2. \tag{4.3.10}$$

In addition to this, we have the orthogonality between the components, i.e.,

$$(\mathbf{w}, \nabla\psi) = 0. \tag{4.3.11}$$

For proof, we refer to [56, Lemma 2.5.1].

Definition 4.9 (Helmholtz projection)**.** *The operator $\mathbb{P}\colon L^2(\Omega) \to \mathbf{H}_0^{\mathrm{div}}\left(\Omega;\mathbb{R}^d\right)$ is called the Helmholtz projection and is defined as:*

$$\mathbb{P}(\mathbf{f}) \coloneqq \mathbf{w}. \tag{4.3.12}$$

By the definition (4.3.12), we have that the image $\mathbb{P}(\mathbf{f})$ is invariant under the transformation $\mathbf{f} \to \mathbf{f} + \nabla\phi$, i.e.,

$$\mathbb{P}(\mathbf{f} + \nabla\phi) = \mathbb{P}(\mathbf{f}). \tag{4.3.13}$$

Using the orthogonal properties of the closed sub spaces $\mathbf{V}^{\mathrm{div}}$ and $\mathbf{V}^{\mathrm{div},\perp}$, we have from [29, Remark 3.42],

Remark 4.10. *The space $\mathbf{V}$ can be decomposed uniquely into orthogonal subspaces*

$$\mathbf{V} = \mathbf{V}^{\mathrm{div}} \oplus \mathbf{V}^{\mathrm{div},\perp} \tag{4.3.14}$$

where, the orthogonality is given by the inner product induced by the bilinear form $a(\cdot,\cdot)$.

Using the orthogonal decomposition (4.3.14), we can re-write the continuous Stokes problem (4.1.3) in two parts as, $\forall\,\mathbf{v} \in \mathbf{V}^{\mathrm{div}}$ and $\forall\,\mathbf{v} \in \mathbf{V}^{\mathrm{div},\perp}$ as

$$a(\mathbf{u},\mathbf{v}) = \langle\mathbf{f},\mathbf{v}\rangle, \quad \forall\,\mathbf{v} \in \mathbf{V}^{\mathrm{div}}, \tag{4.3.15}$$

$$b(\mathbf{v},p) = \langle\mathbf{f},\mathbf{v}\rangle, \quad \forall\,\mathbf{v} \in \mathbf{V}^{\mathrm{div},\perp}. \tag{4.3.16}$$

Using the Helmholtz decomposition, (4.3.8) of $\mathbf{f}$, in (4.3.15), to solve for $\mathbf{u}$ we get

$$\begin{aligned}\int_\Omega \nabla\mathbf{u} : \nabla\mathbf{v}\,\mathrm{d}x &= \int_\Omega (\mathbf{f}\cdot\mathbf{v})\,\mathrm{d}x, && \forall\,\mathbf{v}\in\mathbf{V}^{\mathrm{div}},\\ &= \int_\Omega (\mathbf{w}+\nabla\phi)\cdot\mathbf{v}\,\mathrm{d}x, && \forall\,\mathbf{v}\in\mathbf{V}^{\mathrm{div}},\\ &= \int_\Omega \mathbf{w}\cdot\mathbf{v}\,\mathrm{d}x, && \forall\,\mathbf{v}\in\mathbf{V}^{\mathrm{div}},\\ &= \int_\Omega \mathbb{P}\,(\mathbf{f})\cdot\mathbf{v}\,\mathrm{d}x && \forall\,\mathbf{v}\in\mathbf{V}^{\mathrm{div}}.\end{aligned} \tag{4.3.17}$$

We have $\int_\Omega (\nabla\phi\cdot\mathbf{v})\,\mathrm{d}x = 0$, since $\mathbf{v}\in\mathbf{V}^{\mathrm{div}}$ and using Green's divergence theorem (2.4.2), we get

$$\int_\Omega \nabla\phi\cdot\mathbf{v}\,\mathrm{d}x = \underbrace{-\int_\Omega \phi\nabla\cdot\mathbf{v}\,\mathrm{d}x}_{=0 \text{ by def of } \mathbf{V}^{\mathrm{div}}} + \underbrace{\int_{\partial\Omega}\mathbf{v}\cdot\hat{\mathbf{n}}\,\phi\,\mathrm{d}x}_{=0 \text{ by def of } \mathbf{V}=\mathbf{H}^1_0(\Omega;\mathbb{R}^d)} \qquad \forall\,\mathbf{v}\in\mathbf{V}^{\mathrm{div}} \tag{4.3.18}$$

We can infer a couple of things from the above calculations. If we change the external force $\mathbf{f}$ in the Stokes problem to $\mathbf{f}\to\mathbf{f}+\nabla\psi$, we would still have the same solution $\mathbf{u}$, noting from (4.3.13). However, the same is not true for the pressure solution p. Solving (4.3.16), we get

$$\begin{aligned}\int_\Omega (\nabla\cdot\mathbf{v})\cdot p\,\mathrm{d}x &= \int_\Omega \mathbf{f}\cdot\mathbf{v}\,\mathrm{d}x, && \forall\,\mathbf{v}\in\mathbf{V}^{\mathrm{div},\perp},\\ &= \int_\Omega (\mathbf{w}+\nabla\phi)\cdot\mathbf{v}\,\mathrm{d}x, && \forall\,\mathbf{v}\in\mathbf{V}^{\mathrm{div},\perp},\\ &= \int_\Omega (\mathbf{w}\cdot\mathbf{v}+\nabla\phi\cdot\mathbf{v})\,\mathrm{d}x, && \forall\,\mathbf{v}\in\mathbf{V}^{\mathrm{div},\perp},\\ &= \int_\Omega \nabla\phi\cdot\mathbf{v}\,\mathrm{d}x, && \forall\,\mathbf{v}\in\mathbf{V}^{\mathrm{div},\perp},\end{aligned} \tag{4.3.19}$$

Now, under the transformation $\mathbf{f}\to\mathbf{f}+\nabla\psi$, we have $p\to p+\nabla\psi$.

Remark 4.11. *From the above calculations, we can conclude that*

$$(\mathbf{u},p)\to(\mathbf{u},p+\nabla\psi) \;\; \textit{for}\;\; \mathbf{f}\to\mathbf{f}+\nabla\psi. \tag{4.3.20}$$

The invariance property of the velocity in the continuous problem does not carry over to the discrete problem, since $\mathbf{V}_h^{\mathrm{div}}\not\subset\mathbf{V}^{\mathrm{div}}$. In other words, in the discrete case (4.3.17) gives

$$\begin{aligned}\int_\Omega \nabla\mathbf{u}_h : \nabla\mathbf{v}_h\,\mathrm{d}x &= \int_\Omega (\mathbf{f}\cdot\mathbf{v}_h)\,\mathrm{d}x, && \forall\,\mathbf{v}_h\in\mathbf{V}_h^{\mathrm{div}},\\ &= \int_\Omega (\mathbf{w}_h+\nabla\phi)\cdot\mathbf{v}_h\,\mathrm{d}x, && \forall\,\mathbf{v}_h\in\mathbf{V}_h^{\mathrm{div}},\end{aligned} \tag{4.3.21}$$

This will not simplify further because,

$$\int_\Omega \nabla\phi\cdot\mathbf{v}_h\,\mathrm{d}x = \underbrace{-\int_\Omega \phi\nabla\cdot\mathbf{v}_h\,\mathrm{d}x}_{\neq 0 \text{ since } \mathbf{V}_h^{\mathrm{div}}\not\subset\mathbf{V}^{\mathrm{div}}} + \int_{\partial\Omega}\mathbf{v}_h\cdot\hat{\mathbf{n}}\,\phi\,\mathrm{d}x \quad \forall\,\mathbf{v}_h\in\mathbf{V}_h^{\mathrm{div}} \tag{4.3.22}$$

In other words, the discretely divergence free functions $\mathbf{v}_h \in \mathbf{V}_h^{\text{div}}$ are not divergence free. More on this in Chapter 5. To solve this problem, Linke introduced a reconstruction operator (4.2.4) and reformulated the Stokes discrete problem (4.2.1) as

$$\begin{aligned} a(\mathbf{u}_h, \mathbf{v}_h) + b(\mathbf{u}_h, p_h) &= \langle \mathbf{f}, \pi^{\text{div}} \mathbf{v}_h \rangle, \qquad \forall\, \mathbf{v}_h \in \mathbf{V}_h, \\ b(\mathbf{u}_h, q_h) &= 0, \qquad \forall\, q_h \in Q_h. \end{aligned} \tag{4.3.23}$$

The error estimate for the above modified discrete problem is given by

Theorem 4.12. *Let $(\mathbf{u}, p) \in \mathbf{H}^2(\Omega; \mathbb{R}^d) \times H^1(\Omega)$ be the solution of continuous Stokes problem (4.1.4) Then, one obtains for the discrete solution $(\mathbf{u}_h, p_h)$ for (4.3.23) the error estimates*

$$\begin{aligned} \|\mathbf{u} - \mathbf{u}_h\|_1 &\leq C_1 h |\mathbf{u}|_2, \\ \|p - p_h\|_0 &\leq C_2 h (|\mathbf{u}|_2 + |p|_1). \end{aligned} \tag{4.3.24}$$

For varied choices of solution spaces $V_h \times Q_h$, the proof is given accordingly. For Crouzeix-Raviart and Polynomial space of zero order space ($CR \times \mathbb{P}_0$), Crouzeix-Raviart and Tensor product of polynomial space of order zero ($CR \times \mathbb{Q}_0$) and discontinuous pressure spaces the proof is given in [38], [39] and [35]. In the next chapter, we provide more in detail about the interpolation operator π^{div}.

Chapter 5

Conforming Subspaces of H-div

In this chapter, we discuss two subspaces of H^{div}, namely Raviart-Thomas ($\mathcal{RT}$) and Brezzi-Douglas-Marini ($\mathcal{BDM}$). In Section 5.3, we introduce Piola Transform, which preserves the normal components, when transforming a function from any given element $T \in \mathcal{T}_h$ to the reference element $\hat{T}$. Our implementation of the interpolation operator π^{div} in `DOpElib`, is presented in Section 5.4. We conclude the chapter by testing our implementation with the help of numerical examples shown in Section 5.5. For literature on Raviart-Thomas and Brezzi-Douglas-Marini spaces, we refer to [10, 12, 30, 29].

Definition 5.1. *Let $\Omega \subset \mathbb{R}^d$ be a domain. We define the Sobolev space*

$$\mathbf{H}^{\text{div}}(\Omega;\mathbb{R}^d) = \left\{\mathbf{v} \in \mathbf{L}^2(\Omega;\mathbb{R}^d) \colon \nabla\cdot\mathbf{v} \in L^2(\Omega)\right\}, \tag{5.0.1}$$

with the norm

$$\|\mathbf{u}\|_{H^{\text{div}}} \coloneqq \|\mathbf{u}\|_0 + \|\nabla\cdot\mathbf{u}\|_0. \tag{5.0.2}$$

Furthermore, we define

$$\mathbf{H}_0^{\text{div}}(\Omega;\mathbb{R}^d) \coloneqq \left\{\mathbf{v} \in \mathbf{H}^{\text{div}}(\Omega;\mathbb{R}^d) \colon \nabla\cdot\mathbf{v} = 0 \text{ and } \mathbf{v}\cdot\hat{\mathbf{n}} = 0 \text{ on } \partial\Omega\right\} \tag{5.0.3}$$

Since the operator maps the discrete space $\mathbf{V}_h$ into a conforming subset of $\mathbf{H}^{\text{div}}(\Omega;\mathbb{R}^d)$, we define some notation for the finite element triangulation for the discrete space $\mathbf{V}_h$. In this thesis, we used the rectangular mesh for our finite element simulations.

5.1 Notation

1. We will denote by $\mathcal{T}_h, h > 0$ a family of regular finite element triangulations.
2. We denote a rectangle element as $T \in \mathcal{T}_h$.
3. The set of all faces, i.e., the edges of the rectangles for $d = 2$ and cuboid for $d = 3$, will be denoted as $\bar{\mathcal{F}}_h$ and $\mathcal{F}_h$ will denote the set of all interior faces.

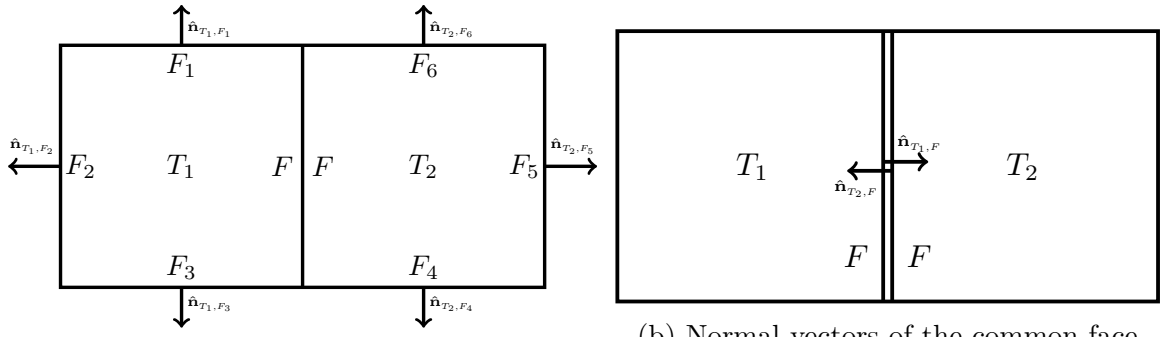

(a) Normal vectors of non-common faces

(b) Normal vectors of the common face

Figure 5.1: Pictorial representation of two elements $T_1, T_2 \in \mathcal{T}_h$.

4. For every face $F \in \bar{\mathcal{F}}_h$, we define a unit face normal vector $\hat{\mathbf{n}}_F$. The orientation of these normal vectors for the interior faces $\mathcal{F} \in \mathcal{F}_h$ are arbitrary but fixed. However, for the exterior faces $F \in \bar{\mathcal{F}}_h \setminus \mathcal{F}_h$, the normal vectors point outward for the domain Ω.

5. Given any element $T \in \mathcal{T}_h$, we denote the set of all faces as $\mathcal{F}_T$, and correspondingly, $\hat{\mathbf{n}}_{T,F}$ will denote the unit normal vector of the simplex T at its face F.

Figure 5.1a summarizes the notation used. Now, let's assume a piecewise polynomial function $\phi \in L^\infty(\Omega)$, then for every interior face $F = T_1 \cap T_2 \in \mathcal{F}_h$, the face jump for all $\mathbf{x} \in F$ is defined as

$$[\phi](\mathbf{x}) := \left(\lim_{\substack{\mathbf{y}\to\mathbf{x} \\ \mathbf{y}\in T_1}} \phi(\mathbf{y}) \cdot \hat{\mathbf{n}}_{T_1,F} + \lim_{\substack{\mathbf{y}\to\mathbf{x} \\ \mathbf{y}\in T_2}} \phi(\mathbf{y}) \cdot \hat{\mathbf{n}}_{T_2,F} \right) \tag{5.1.1}$$

From Figure 5.1b, we get

$$[\phi](\mathbf{x}) = \phi\left(\mathbf{x}^+\right) - \phi\left(\mathbf{x}^-\right), \tag{5.1.2}$$

where $\mathbf{x}^+ \in T_1$ and $\mathbf{x}^- \in T_2$. From Green's divergence theorem (2.4.2), we have $\phi \in H^{\text{div}}$ only if the jump in (5.1.1) equals zero [30, Lemma 4.2.2].

Remark 5.2. *The continuity of the normal component over faces does not imply continuity at vertices, since it's not transferred in tangential direction.*

As a consequence of this remark, part of the construction of H^{div}-conforming finite element spaces consists of defining a polynomial trace space on each face, such that continuity of normal traces can be established by this space. In the next section, we define polynomial spaces needed for the construction of $\mathcal{RT}$ (Raviart-Thomas) and $\mathcal{BDM}$ (Brezzi-Douglas-Marini) spaces, the two H^{div} conforming spaces we use in this thesis.

5.2 Definitions

Definition 5.3. *[$\mathcal{P}_k$] The space of polynomials of degree less than k defined on the domain Ω is denoted as $\mathcal{P}_k(\Omega)$.*

Definition 5.4. *[$\mathcal{Q}_k$] For $d = 2$, we define,*

$$\mathcal{P}_{k_1,k_2}(\Omega) \coloneqq \left\{ p(x_1, x_2) \colon p(x_1, x_2) = \sum_{\substack{i \le k_1 \\ j \le k_2}} a_{ij} x_1^i x_2^j \right\}. \tag{5.2.1}$$

From the above definition, we can define

$$\mathcal{Q}_k(\Omega) \coloneqq \mathcal{P}_{kk}(\Omega) \quad \text{for } d = 2, \tag{5.2.2}$$

Similarly, we can define for a given dimension d,

$$\begin{aligned} \mathcal{Q}_k(\Omega) &\coloneqq \mathcal{P}_{kkk}(\Omega) \quad \text{for } d = 3, \\ \mathcal{Q}_{k_1,\cdots k_d}(\Omega) &\coloneqq \mathcal{P}_{k_1}(\Omega) \otimes \cdots \otimes \mathcal{P}_{k_d}(\Omega) \end{aligned} \tag{5.2.3}$$

Furthermore, we define the vector-valued space,

$$\mathcal{Q}_k^d(\Omega) \coloneqq \underbrace{\mathcal{Q}_k(\Omega) \times \cdots \times \mathcal{Q}_k(\Omega)}_{d \text{ factors}}. \tag{5.2.4}$$

Given a partition $\mathcal{T}_h$ of the domain Ω, we restrict a given polynomial $v_h \in \mathcal{P}_k(\Omega)$ onto the element T as

$$v_h|_T \coloneqq v_h \cdot \mathbb{I}_T \tag{5.2.5}$$

where, $\mathbb{I}_T$ is the indicator function, i.e.,

$$\mathbb{I}_T = \begin{cases} 1 & \text{if } \mathbf{x} \in T, \\ 0 & \text{if } \mathbf{x} \notin T. \end{cases} \tag{5.2.6}$$

We define our spaces on a reference element $\hat{T} = [0, 1]$, which is the standard in the finite element open source libraries `deal.II` and `DOpElib`. Given any element T, we do a Piola transform (will be discussed in detail later) onto the reference element $\hat{T}$ and do our calculations on the reference element. Hence, we define our conforming spaces $\mathcal{RT}$ and $\mathcal{BDM}$ on the reference element.

5.2.1 Raviart-Thomas Finite Element

Definition 5.5 ($\mathcal{RT}_k(T)$ space)**.** *The Raviart-Thomas element of degree $k > 0$ on the reference element $\hat{T} = [0, 1]^d$ consists of the polynomial space*

$$\mathcal{RT}_k(\hat{T}) = \mathcal{Q}_k^d(\hat{T}) + \mathbf{x}\mathcal{Q}_k(\hat{T}). \tag{5.2.7}$$

Its node functionals are

$$\begin{aligned} \mathcal{N}_{1,i,j}(\mathbf{v}_h) &= \int_{F_i} \mathbf{v}_h \cdot \hat{\mathbf{n}}\, \phi_j \,\mathrm{d}s \quad \forall\, \phi_j \in \mathcal{Q}_k(F_i) \quad F_i \subset \partial\hat{T}, \\ \mathcal{N}_{2,i}(\mathbf{v}_h) &= \int_{\hat{T}} \mathbf{v}_h \cdot \mathbf{w} \,\mathrm{d}x \qquad \forall\, \mathbf{w} \in \mathbf{\Psi}_h(\hat{T}), \end{aligned} \tag{5.2.8}$$

where $\Psi_h = \underbrace{\mathcal{Q}_{k-1,k,\cdots k} \times \cdots \times \mathcal{Q}_{k\cdots k,k-1}}_{d \text{ times}}$

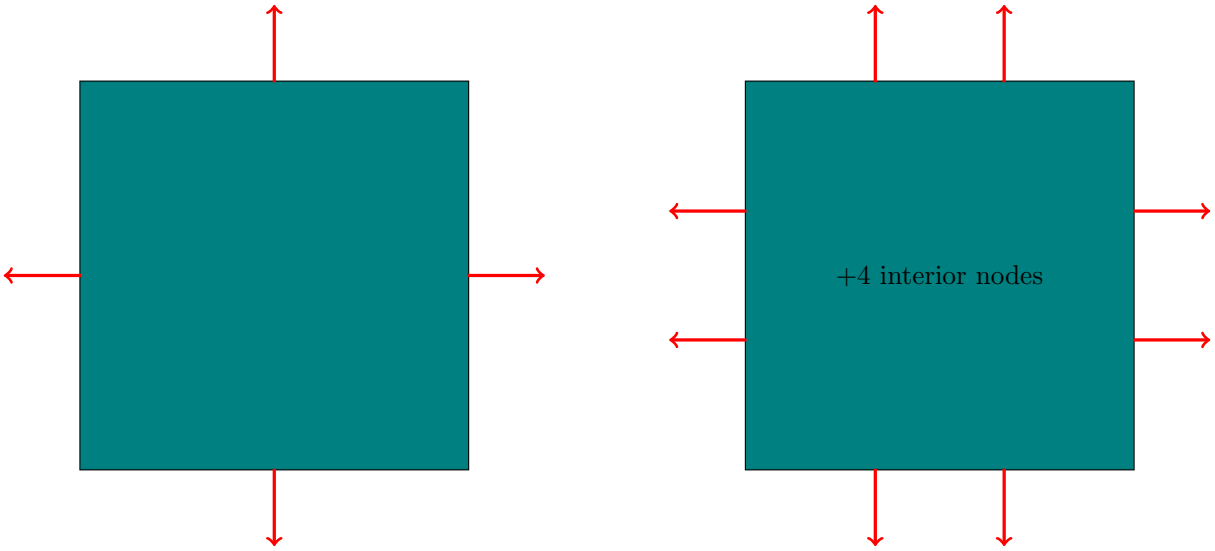

(a) $\mathcal{RT}_0$ element with 4 degree of freedom given by the normal components on the edges.

(b) $\mathcal{RT}_1$ element with 12 degrees of freedom given by normal components and 4 interior nodes.

Figure 5.2: Degrees of freedom for Raviart-Thomas elements, $\mathcal{RT}_0$ and $\mathcal{RT}_1$.

The choice of the node functionals, guarantees the continuity of the normal component. Following lemma, proves the unisolvence of the Raviart-Thomas element.

Lemma 5.6. *For any* $\mathbf{v}_h \in \mathcal{RT}_k(\hat{T})$ *and* $\hat{F}_i \subset \partial\hat{T}$, *if*

$$\begin{aligned} \int_{\hat{F}_i} \mathbf{v}_h \cdot \hat{\mathbf{n}}\, \phi_i \,\mathrm{d}s = 0 \qquad & \forall\, \phi_i \in \mathcal{Q}_k(\hat{F}_i), \\ \int_{\hat{T}} \mathbf{v}_h \cdot \mathbf{w} \,\mathrm{d}x = 0 \qquad & \forall\, \mathbf{w} \in \Psi_h(\hat{T}), \end{aligned} \tag{5.2.9}$$

then, we have $\mathbf{v}_h = 0$.

Proof. For proof, we refer to [10, Proposition 2.4.1]. □

Lemma 5.7. *For Raviart-Thomas elements of order* k, *there holds*

$$\dim \mathcal{RT}_k = 2(k+1)(k+2), \qquad \text{for } d = 2, \tag{5.2.10}$$

and

$$\nabla \cdot \mathcal{RT}_k(\hat{T}) = \mathcal{Q}_k(\hat{T}). \tag{5.2.11}$$

Furthermore, for each $\hat{F} \subset \hat{T}$ *and each* $\mathbf{v}_h \in \mathcal{RT}_k(\hat{T})$ *there holds*

$$\mathbf{v}_h \cdot \hat{\mathbf{n}}|_{\hat{F}} \in \mathcal{Q}_k(\hat{F}). \tag{5.2.12}$$

Proof. For proof, we refer to [30, Lemma 4.2.36]. □

Definition 5.8 (Raviart-Thomas space $\mathcal{RT}_k$)**.** *The global Raviart-Thomas finite element space $\mathcal{RT}_k(\Omega;\mathcal{T}_h)$ on the domain Ω with a given triangulation $\mathcal{T}_h$ is given as*

$$\mathcal{RT}_k(\Omega;\mathcal{T}_h) \coloneqq \left\{\mathbf{v}_h \in \mathbf{H}^{\mathrm{div}}(\Omega;\mathbb{R}^d)\colon \mathbf{v}_h|_{\hat{T}} \in \mathcal{RT}_k(\hat{T}), \hat{T} \in \mathcal{T}_h\right\}. \tag{5.2.13}$$

This space is a finite dimensional subspace of $\mathbf{H}^{\mathrm{div}}(\Omega;\mathbb{R}^d)$.

5.2.2 BDM Finite Element

Now, we define the $\mathcal{BDM}_k$ element.

Definition 5.9 ($\mathcal{BDM}$ space)**.** *The BDM element of degree $k > 0$ on the reference element $\hat{T}$ consists of the polynomial space*

$$\mathcal{BDM}_k = \mathcal{P}_k^2 \otimes \operatorname{span}\left\{(x^{k+1}y), \nabla \times \left(xy^{k+1}\right)\right\}. \tag{5.2.14}$$

Its node functionals are

$$\begin{aligned} \mathcal{N}_{1,i,j}(\mathbf{v}_h) &= \int_{\hat{F}_i} \mathbf{v}_h \cdot \hat{\mathbf{n}}\, \phi_j \,\mathrm{d}s \quad \forall\, \phi_j \in \mathcal{P}_k\left(\hat{F}_i\right) \quad \hat{F}_i \subset \partial\hat{T}, \\ \mathcal{N}_{2,i}(\mathbf{v}_h) &= \int_{\hat{T}} \mathbf{v}_h \cdot \mathbf{w} \,\mathrm{d}x \qquad \forall\, \mathbf{w} \in \mathcal{P}_{k-2}^d(\hat{T}). \end{aligned} \tag{5.2.15}$$

Similar to the Raviart-Thomas element, the choice of the node functionals assert the continuity of the normal component. The following lemma provides the unisolvence of the Brezzi-Douglas-Marini element.

Lemma 5.10. *For $k \geq 1$, any $\mathbf{v}_h \in \mathcal{BDM}_k(\hat{T})$ and $\hat{F}_i \subset \partial\hat{T}$, if*

$$\begin{aligned} \int_{\hat{F}_i} \mathbf{v}_h \cdot \hat{\mathbf{n}}\, \phi_i \,\mathrm{d}s = 0 \qquad \forall\, \phi_i \in \mathcal{P}_k(\hat{F}_i), \\ \int_{\hat{T}} \mathbf{v}_h \cdot \mathbf{w} \,\mathrm{d}x = 0 \qquad \forall\, \mathbf{w} \in \mathcal{P}_{k-2}^d(\hat{T}), \end{aligned} \tag{5.2.16}$$

then, we have $\mathbf{v}_h = 0$.

Proof. For proof, we refer to [10, Proposition 2.4.2]. □

Lemma 5.11. *Given any BDM element of order $k \geq 1$, there holds*

$$\dim \mathcal{BDM}_k = (k+1)(k+2) + 2, \quad \text{for } d = 2, \tag{5.2.17}$$

and

$$\nabla\cdot\, \mathcal{BDM}_k(\hat{T}) = \mathcal{P}_{k-1}(\hat{T}). \tag{5.2.18}$$

Furthermore, for each $F \subset \hat{T}$ and each $\mathbf{v}_h \in \mathcal{BDM}_k(\hat{T})$ there holds

$$\mathbf{v}_h \cdot \hat{\mathbf{n}}|_{\hat{F}} \in \mathcal{P}_k(\hat{F}). \tag{5.2.19}$$

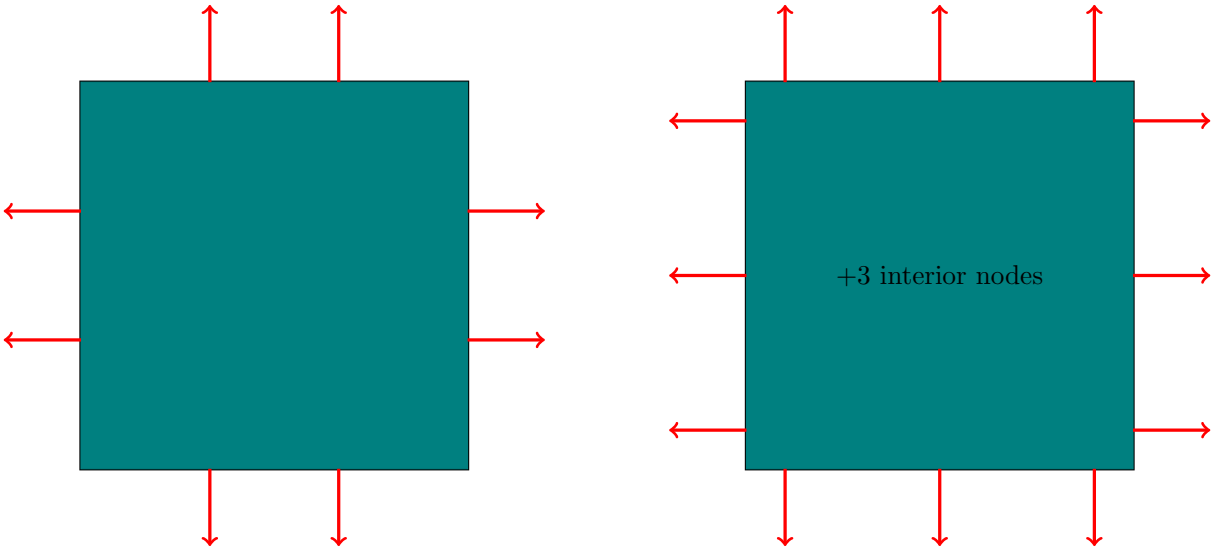

(a) $\mathcal{BDM}_1$ element with 8 degrees of freedom given by the normal components on the edges.

(b) $\mathcal{BDM}_2$ element with 12 degrees of freedom given by normal components and 3 interior nodes.

Figure 5.3: Degrees of freedom for Brezzi-Douglas-Marini elements, $\mathcal{BDM}_1$ and $\mathcal{BDM}_2$.

Proof. For proof, we refer to [30, Lemma 4.2.40]. □

Definition 5.12 (Brezzi-Douglas-Marini finite element space $\mathcal{RT}_k$)**.** *The global Brezzi-Douglas-Marini finite element space $\mathcal{BDM}_k(\Omega;\mathcal{T}_h)$ on the domain Ω with a given triangulation $\mathcal{T}_h$ is given as*

$$\mathcal{BDM}_k(\Omega;\mathcal{T}_h) \coloneqq \left\{\mathbf{v}_h \in \mathbf{H}^{\mathrm{div}}(\Omega;\mathbb{R}^d)\colon \mathbf{v}_h|_{\hat{T}} \in \mathcal{BDM}_k(\hat{T}), \hat{T} \in \mathcal{T}_h\right\}. \tag{5.2.20}$$

This space is a finite dimensional subspace of $\mathbf{H}^{\mathrm{div}}(\Omega;\mathbb{R}^d)$. The standard affine mapping from a given element $T \in \mathcal{T}_h$ onto the reference element $\hat{T}$ does not preserve the normal components and hence, we need a special transformation called Piola Transform.

5.3 Piola Transform

In finite elements, we regularly undergo coordinate changes because, we use a standard reference element. So an affine mapping for the elements comes in handy. An affine mapping Φ (at least C^1) is a mapping from $\mathbb{R}^d$ into $\mathbb{R}^d$. Formally, we define

Definition 5.13. *Given a triangulation $\mathcal{T}_h$ of the domain Ω and an element $T \in \mathcal{T}_h$, we define the mapping $\Phi\colon \hat{T} \to T$ as*

$$T = \Phi(\hat{T}). \tag{5.3.1}$$

We define Jacobi matrix, Jacobi determinant and the face Jacobian as

$$\begin{aligned} D\Phi(\hat{x}) &= (\partial_j \Phi_i)\,, && \forall\, \hat{x} \in \hat{T}, \\ \mathrm{J}(\hat{x}) &= \det D\Phi(\hat{x}), && \forall\, \hat{x} \in \hat{T}, \\ \mathrm{J}_n(\hat{x}) &= \mathrm{J}(\hat{x}) |D\Phi^{-T}(\hat{x})\hat{\mathbf{n}}|, && \forall\, \hat{x} \in \partial\hat{T}. \end{aligned} \tag{5.3.2}$$

The mapping Φ is globally invertible on any element $T \in \mathcal{T}_h$. Moreover, the Jacobian matrix $D\Phi(\hat{x})$ is invertible for any $\hat{x} \in \hat{T}$. And, given any $\mathbf{v}_h \in T$ and $\hat{\mathbf{v}}_h \in \hat{T}$ with $\mathbf{v}_h = \Phi(\hat{\mathbf{v}}_h)$, we have the usual properties like

$$\begin{aligned} \int_T \Phi(\hat{\mathbf{v}}_h)\,\mathrm{d}x &= \int_{\hat{T}} \hat{\mathbf{v}}_h \mathrm{J}\,\mathrm{d}\hat{x}, \\ \int_{\partial T} \Phi(\hat{\mathbf{v}}_h)\,\mathrm{d}s &= \int_{\partial\hat{T}} \hat{\mathbf{v}}_h \mathrm{J}_{\hat{\mathbf{n}}}\,\mathrm{d}\hat{s}. \end{aligned} \tag{5.3.3}$$

Lemma 5.14. *The mapping Φ is an isomorphism from $\mathbf{L}^2(\hat{T};\mathbb{R}^d)$ onto $\mathbf{L}^2(T;\mathbb{R}^d)$ and $\mathbf{H}^1(\hat{T};\mathbb{R}^d)$ onto $\mathbf{H}^1(T;\mathbb{R}^d)$.*

Proof. For proof, we refer to [10, Lemma 2.1.5]. □

The main flaw with such a mapping is that it does not preserve normal components, which is essential for our work here. In order to overcome this problem, we use the Piola Transform.

Definition 5.15 (Piola Transform)**.** *Given a vector field $\mathbf{v}_h \in \mathbf{L}^2(\hat{T};\mathbb{R}^d)$, and the affine mapping $\Phi\colon \hat{T} \to T$, we define the Piola transform $\mathcal{G}\colon \mathbf{L}^2(\hat{T};\mathbb{R}^d) \to \mathbf{L}^2(T;\mathbb{R}^d)$ as*

$$\mathcal{G}(\hat{\mathbf{v}}_h)(\hat{x}) \coloneqq \frac{1}{\mathrm{J}(\hat{x})} D\Phi(\hat{x})\hat{\mathbf{v}}_h(\hat{x}), \qquad \text{where } x = \Phi(\hat{x}). \tag{5.3.4}$$

Furthermore, we have

$$\begin{aligned} \nabla \mathbf{v}_h(x) &= \frac{1}{\mathrm{J}(\hat{x})} D\Phi \left[\hat{\nabla}\hat{\mathbf{v}}_h(\hat{x})\right] D\Phi^{-1}, \\ \nabla\cdot \mathbf{v}_h(x) &= \frac{1}{\mathrm{J}(\hat{x})} \hat{\nabla}\cdot \hat{\mathbf{v}}_h(\hat{x}). \end{aligned} \tag{5.3.5}$$

Now, combining the properties of the Piola transform, we can assert the following lemma,

Lemma 5.16. *The mapping $\mathcal{G}$ is an isomorphism from $\mathbf{H}^{\mathrm{div}}(\hat{T};\mathbb{R}^d)$ onto $\mathbf{H}^{\mathrm{div}}(T;\mathbb{R}^d)$.*

Proof. For proof, we refer to [10, Lemma 2.1.7]. □

Now that we have the Piola transform which maps the conforming H^{div} subspaces from the reference element $\hat{T}$ to $T \in \mathcal{T}_h$, and preserves normal components, we would like to show how to construct these spaces numerically using the open source library `DOpElib`.

5.4 Implementation in DOpElib

DOpElib(Differential equations and optimization environment) [24], is an open source library based on deal.II-a general purpose object-oriented finite element library [4]. Throughout this thesis, all the numerical simulations are carried out using DOpElib. We have also implemented a new class called FEValuesInterpolated, in the DOpElib library. This class will take the functions $\mathbf{v}_h \in \mathbf{V}_h$ and interpolates them onto an H^{div} conforming space you choose. In other words, FEValuesInterpolated is the numerical implementation of the interpolation operator π^{div} in (4.2.4).

Before going into the actual implementation, it's easier if we start with an example. Consider the following integral

$$\int_\Omega \mathbf{f}\cdot \mathbf{v}_h \,\mathrm{d}x, \quad \forall\, \mathbf{v}_h \in \mathbf{V}_h. \tag{5.4.1}$$

The above equation (5.4.1) is the standard right-hand side of the discrete Stokes equation (4.2.1) or discrete saddle point problem (3.3.1). We use the inf-sup stable conforming Taylor-Hood finite element $\mathcal{Q}_2\backslash\mathcal{Q}_1$ for our numerical simulations, so we have $\mathbf{V}_h = \mathcal{Q}_2$ in (5.4.1). The integral (5.4.1) contributes to the right-hand side matrix or load matrix, $\mathbb{F}$ in the finite element system. Let $\mathbb{F}_i$ be the i^{th} element of the matrix $\mathbb{F}$ corresponding to the i^{th} shape function ϕ_i of $\mathcal{Q}_2$. Now, we have

$$\begin{aligned}
\mathbb{F}_i = \int_\Omega \mathbf{f}\cdot \boldsymbol{\phi}_i \,\mathrm{d}x &= \sum_{T\in\mathcal{T}_h} \int_T \mathbf{f}(\mathbf{x})\cdot \boldsymbol{\phi}_i(\mathbf{x}) \,\mathrm{d}\mathbf{x}, \\
&= \sum_{T\in\mathcal{T}_h} \int_{\hat{T}} \hat{\mathbf{f}}(\hat{x})\cdot \hat{\boldsymbol{\phi}}_i(\hat{x}) \,\mathrm{J}\,\mathrm{d}\hat{x}, \\
&= \sum_{T\in\mathcal{T}_h} \left\{ \sum_{q=1}^{n_q} \hat{\mathbf{f}}(\hat{\mathbf{x}}_q)\cdot \hat{\boldsymbol{\phi}}(\hat{\mathbf{x}}_q) \,\mathrm{J}\cdot w(\hat{\mathbf{x}}_q) \right\}
\end{aligned} \tag{5.4.2}$$

So, we expanded the integral over the domain into the sum of integrals over the triangulation $\mathcal{T}_h$. Then, we transform the element T to the reference element $\hat{T}$ using the affine transformation (we don't need H^{div} conforming here) Φ. Next, we use a quadrature formula to solve the integral numerically, q is the index that runs over all the quadrature points of our choosing and n_q is the number of quadrature points used. n_q depends on the order of the quadrature used. $w(\hat{x}_q)$ are the weights of the quadrature used. Note that we have also dropped the $(\hat{\mathbf{x}})$ in front of the Jacobian J, for convenience. We will specify $\mathrm{J}(\mathbf{x})$ if needed, else we will assume its on the reference element.

In DOpElib, we use the inbuilt class FEValues which gives transformed values $\hat{\boldsymbol{\phi}}(\hat{\mathbf{x}}_q)$. After which, we sum the values over the quadrature for each element $T \in \mathcal{T}_h$ for all $\mathbb{F}_i$. We cannot use the FEValues class for the modified Stokes problem (4.3.23), because FEValues class does not preserve normal components for functions in $\mathcal{Q}_2$ space. Before going into the details of the Interpolated class, we want to introduce canonical interpolation, which gives us an idea on how to interpolate functions onto any given finite element space.

Definition 5.17 (Canonical Interpolation)**.** *Given an element $T \in \mathcal{T}_h$ and a finite element defined by its shape function space $\mathcal{S}_T$ and node functionals $\mathcal{N}_i$ for $i = 1, \dots, n$, where $n = \dim \mathcal{S}$ (which is also the dimension of the finite element space). Let ψ_i be the nodal basis of $\mathcal{S}_T$, i.e.,*

$$\mathcal{N}_i(\psi) = \delta_{ij} \quad i, j = 1, \dots, n. \tag{5.4.3}$$

Then, the operator $\pi : C^\infty(T; \mathbb{R}^d) \to \mathcal{S}_T$ for any $\phi \in C^\infty(T)$ is defined as

$$\pi(\phi) = \sum_{i=1}^{n} \mathcal{N}_i(\phi)\psi_i. \tag{5.4.4}$$

Now let's consider the i^{th} element of the matrix $\mathbb{F}$ in (4.3.23)

$$\begin{aligned} \mathbb{F}_i = \int_\Omega \mathbf{f} \cdot \pi^{\text{div}} \boldsymbol{\phi}_i \, \mathrm{d}\mathbf{x} &= \sum_{T \in \mathcal{T}_h} \int_T \mathbf{f}(\mathbf{x}) \cdot \pi^{\text{div}} \phi_i \, \mathrm{d}\mathbf{x}, \\ &= \sum_{T \in \mathcal{T}_h} \int_T \mathbf{f}(\mathbf{x}) \cdot \left(\sum_{=1}^{n} \mathcal{N}_j(\phi_i)\psi_j(\mathbf{x}) \right) \mathrm{d}\mathbf{x}, \\ &= \sum_{T \in \mathcal{T}_h} \int_{\hat{T}} \hat{\mathbf{f}}(\hat{\mathbf{x}}) \cdot \left(\sum_{j=1}^{n} \hat{\mathcal{N}}_j(\hat{\phi}_i)\hat{\psi}_j(\hat{\mathbf{x}}) \right) J \, \mathrm{d}\hat{\mathbf{x}}, \end{aligned} \tag{5.4.5}$$

where n is the dimension of the conforming $H^{\text{div}}(\Omega)$ space,$\mathcal{M}$ we are using and ψ_j for $j = 1, \dots n$ are the shape functions of $\mathcal{M}$. Now since ψ_i is in $\mathcal{M}$ we have to use Piola transform and not the affine transform Φ. Then, we get

$$\hat{\psi}_j(\hat{x}) = \frac{1}{J^{-1}(\mathbf{x})} D\Phi^{-1}(\mathbf{x})\psi_j(\mathbf{x}). \tag{5.4.6}$$

Substituting this back in the equation, we get

$$\int_\Omega \mathbf{f} \cdot \pi^{\text{div}} \phi_i \, \mathrm{d}\mathbf{x} = \sum_{T \in \mathcal{T}_h} \sum_{q=1}^{n_q} \left\{ \hat{\mathbf{f}}(\hat{\mathbf{x}}_q) \cdot \left(\sum_{j=1}^{n} \hat{\mathcal{N}}_j \left(\hat{\phi}_i \right) \left(\frac{1}{J^{-1}(\mathbf{x}_q)} D\Phi^{-1}(\mathbf{x}_q)\psi(\mathbf{x}_q) \right) \right) J \cdot w(\hat{\mathbf{x}}_q). \right\} \tag{5.4.7}$$

Similar to (5.4.2), our class `FEValuesInterpolated` provides the user with the entire information:

$$\texttt{FEValuesInterpolated.value(i,q)} = \left(\sum_{j=1}^{n} \hat{\mathcal{N}}_j \left(\hat{\phi}_i \right) \left(\frac{1}{J^{-1}(\mathbf{x}_q)} D\Phi^{-1}(\mathbf{x}_q)\psi(\mathbf{x}_q) \right) \right). \tag{5.4.8}$$

The user can then, sum it up over all quadrature points to finish the computation. As mentioned earlier, we have used only interpolated onto two spaces, i.e., Raviart-Thomas and BDM spaces. However, the class `FEValuesInterpolated` works for any H^{div} conforming space with nodal functions $\mathcal{N}$ (specified for $\mathcal{RT}$ in Lemma 5.6 and for $\mathcal{BDM}$ in Lemma 5.10) in the `deal.II` library. We have also incorporated gradient of the interpolation as well, i.e.,

$$\texttt{FEValuesInterpolated.gradient(i,q)} = \nabla \pi^{\text{div}} \phi_i(\mathbf{x}_q). \tag{5.4.9}$$

You could in theory calculate the divergence of the interpolation $\nabla \cdot \pi^{\text{div}} \phi$ as well, by calculating the gradient and adding the trace from the obtained gradient tensor.

5.5 Numerical Results

In this section, we will solve the Stokes problem (4.1.1) and compare it with the velocity error with and without using interpolation operator π^{div}. The choice of the H^{div} space depends on the finite element space Q_h chosen for the pressure. For the finite element pair $\mathcal{Q}_2 \times \mathcal{DGQ}_1$, we choose $\mathcal{RT}_1$ and for the pair $\mathcal{Q}_2 \times \mathcal{DGP}_1$, we choose $\mathcal{BDM}_2$. Where, $\mathcal{DGQ}_1$ and $\mathcal{DGP}_1$ are discontinuous Galerkin polynomial spaces.

Example 5.18. *Consider the stationary Stokes problem (4.1.1), where the solution is taken from [38, Section 5] as*

$$\begin{aligned} \mathbf{u}_1(x,y) &= 200x^2(1-x)^2y(1-y)(1-2y), \\ \mathbf{u}_2(x,y) &= -200y^2(1-y)^2x(1-x)(1-2x), \\ p(x,y) &= -\left(10(x-\frac{1}{2})^3y^2 + (1-x)^3(y-\frac{1}{2})^3 + \frac{1}{8}\right). \end{aligned} \tag{5.5.1}$$

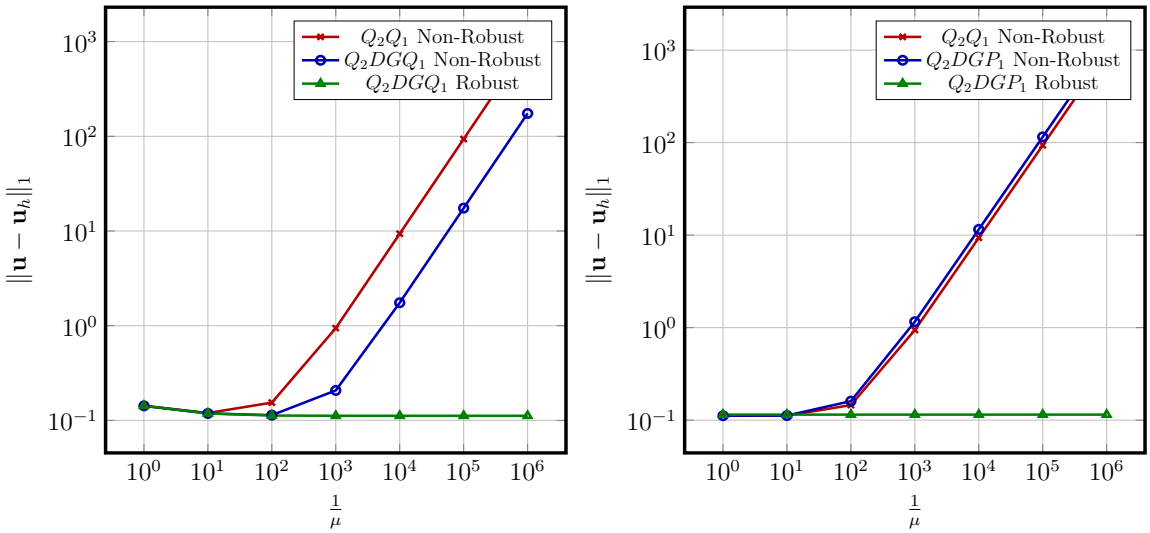

(a) Interpolation w.r.t. RT space $\mathcal{RT}_1$ (b) Interpolation w.r.t. BDM space $\mathcal{BDM}_2$

Figure 5.4: Velocity error in H^1 norm $\|\mathbf{u}-\mathbf{u}_h\|_1$ vs viscosity ν in 2D.

Example 5.19. *3D example for the Stokes problem where the exact solution is given as*

$$\begin{aligned} \mathbf{u}_1(x,y,z) &= 4x^2yz(1-x)^2(1-y)(1-z)(z-y) \\ \mathbf{u}_2(x,y,z) &= -2xy^2z(1-x)(1-y)^2(1-z)(1-2x) \\ \mathbf{u}_3(x,y,z) &= 2xyz^2(1-x)(1-y)(1-z)^2(1-2x) \\ p(x,y,z) &= -\left(10(x-\frac{1}{2})^3y^2(1-z)^2 + (1-x)^3(y-\frac{1}{2})^3 + (z-\frac{1}{2})^3(x-1)^2\right) \end{aligned} \tag{5.5.2}$$

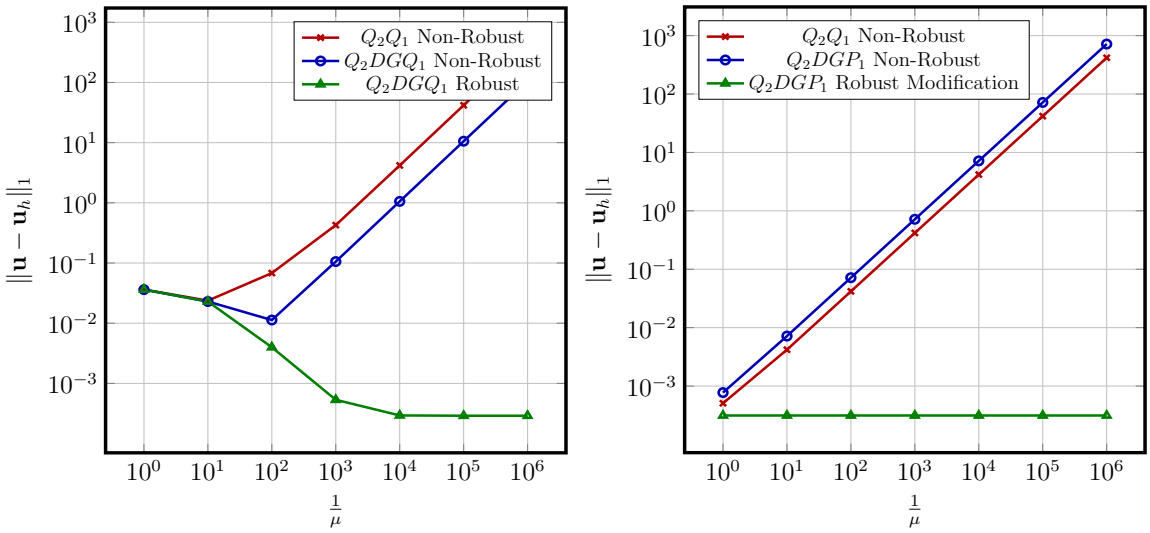

(a) Interpolation w.r.t. RT space $\mathcal{RT}_1$ (b) Interpolation w.r.t. BDM space $\mathcal{BDM}_2$

Figure 5.5: Velocity error in H^1 norm $\|\mathbf{u}-\mathbf{u}_h\|_1$ vs viscosity ν in 3D.

The velocity error estimate for the discrete Stokes problem (4.2.1) is given as (4.2.2). From Figure 5.4 and 5.5, we can see that, for the non-robust method, velocity error depends linearly on the viscosity, which comes from the pressure term $\frac{1}{\nu}\|p-p_h\|_0$ and hence shows the pressure dependency of the velocity component. Whereas, with the modified Stokes equation (4.3.23), we get a constant velocity error is given as

$$\|\mathbf{u}-\mathbf{u}_h\|_1 \leq C_1 \inf_{\mathbf{v}_h \in \mathbf{V}_h} \|\mathbf{u}-\mathbf{v}_h\|_1$$

similar to (4.2.3), which confirms that the velocity is indeed pressure independent. In the next chapter, we extend Linke's approach to linear elasticity.

Chapter 6

Elasticity Equation

In this chapter, we consider the nearly incompressible linear elasticity, e.g.,

$$\begin{aligned} -2\mu\nabla\cdot\varepsilon(\mathbf{u}) - \lambda\nabla(\nabla\cdot\mathbf{u}) &= \mathbf{f} \quad \text{in } \Omega, \\ u &= 0 \quad \text{on } \partial\Omega, \end{aligned}$$

where $\varepsilon(\mathbf{u})$ denotes the symmetric gradient, and $\mu, \lambda > 0$ are the Lamé parameters. To avoid the locking phenomenon, e.g., [12, Chapter VI.3], typically a mixed form

$$\begin{aligned} -2\mu\,\nabla\cdot\varepsilon(\mathbf{u}) - \nabla p &= \mathbf{f} \quad \text{in } \Omega, \\ \nabla\cdot\mathbf{u} - \frac{1}{\lambda}p &= 0 \quad \text{in } \Omega, \\ \mathbf{u} &= 0 \quad \text{on } \partial\Omega, \end{aligned} \tag{6.0.1}$$

The rest of the chapter is structured as follows. In Section 6.1, we introduce the notion of gradient robustness and discuss the discretization of (6.0.1). Next, in Section 6.2, we show that the proposed discretization is indeed gradient robust and provide error estimates. We conclude the paper with a series of examples highlighting the derived results in Section 6.3.

6.1 Gradient Robustness and Discretization

6.1.1 Gradient Robustness

We use the spaces, $\mathbf{V} = \mathbf{H}^1(\Omega;\mathbb{R}^d)$ and $Q = L^2_0(\Omega)$. We note that the elasticity problem (6.0.1) in the weak form is a saddle point problem (3.1.4) with

$$a(\mathbf{u},\mathbf{v}) = 2\mu\,(\varepsilon(\mathbf{u}),\varepsilon(\mathbf{v}))\,, \tag{6.1.1}$$

$$b(q,\mathbf{v}) = (q,\nabla\cdot\mathbf{v})\,. \tag{6.1.2}$$

Using the spaces $\mathbf{V}^{\mathrm{div}}$ (3.2.9) and $\mathbf{V}^{\mathrm{div},\perp}$ (3.2.10), any function $\mathbf{v}\in\mathbf{V}$ is uniquely written as $\mathbf{u} = \mathbf{u}^0 + \mathbf{u}^\perp \in \mathbf{V}^{\mathrm{div}} \oplus \mathbf{V}^{\mathrm{div},\perp}$.

Using Helmholtz decomposition (Lemma 4.8), $\mathbf{f}\in L^2(\Omega;\mathbb{R}^d)$ can be uniquely decomposed as

$$\mathbf{f} = \nabla\phi + \mathbf{w}, \tag{6.1.3}$$

where $\phi \in H^1(\Omega)/\mathbb{R}$ is irrotational, $\mathbf{w}$ is divergence free and both are orthogonal with respect to the $L^2(\Omega)$-scalar product, i.e.,

$$(\mathbf{w}, \nabla \phi) = 0. \tag{6.1.4}$$

With these definitions, the decay of the influence of gradient forces, i.e., $\mathbf{w} = 0$, onto the solutions $\mathbf{u}$ of (6.0.1) can be quantified as the following result from [22, Theorem 1] shows:

Lemma 6.1. *If $\mathbf{f} \in H^{-1}(\Omega)$ is a gradient, i.e., $\mathbf{f} = \nabla\phi$, for some $\phi \in L^2(\Omega)$. Then for the solution $\mathbf{u} = \mathbf{u}^0 + \mathbf{u}^\perp$ of (6.0.1) it holds $\mathbf{u}^0 = 0$ and*

$$\|\mathbf{u}\|_1 = \|\mathbf{u}^\perp\|_1 \leq \frac{c}{\mu + \lambda}\|\phi\|_0.$$

In particular, $\|\mathbf{u}\|_1 = O(\lambda^{-1})$ as $\lambda \to \infty$.

Since this bound need not hold for arbitrary, inf-sup stable, discretizations, [22, Definition 2] introduced the following notion:

Definition 6.2. *A discretization of (6.0.1) is called* gradient robust, *if for any fixed $\mathbf{f} = \nabla\phi$ with $\phi \in L^2(\Omega)$, $\mu > 0$ and any discretization parameter h there is a constant c_h such that the approximate solution $\mathbf{u}_h \in \mathbf{V}_h^\perp$ and satisfies*

$$\|\mathbf{u}_h\|_1 \leq \frac{c_h}{\lambda}\|\phi\|_0.$$

6.1.2 Abstract Discretization

Similar to Stokes equation, we select subspaces $\mathbf{V}_h \subset \mathbf{V}$ and $Q_h \subset Q$ such that there is a positive constant β satisfying the inf-sup condition

$$\inf_{q_h \in Q_h} \sup_{\mathbf{v}_h \in \mathbf{V}_h} \frac{(q_h, \nabla \cdot \mathbf{v}_h)}{\|q_h\|_0 \|\mathbf{v}_h\|_1} \geq \beta. \tag{6.1.5}$$

Now, the standard, in general not gradient robust, weak formulation is given as follows: Find $(\mathbf{u}_h, p_h) \in \mathbf{V}_h \times Q_h$ such that

$$\begin{aligned} a(\mathbf{u}_h, \mathbf{v}_h) + b(p_h, \mathbf{v}_h) &= (\mathbf{f}, \mathbf{v}_h) \quad && \forall \mathbf{v}_h \in \mathbf{V}_h, \\ b(q_h, \mathbf{u}_h) - \frac{1}{\lambda}(p_h, q_h) &= 0 && \forall q_h \in Q_h. \end{aligned} \tag{6.1.6}$$

Under the well known inf-sup condition (6.1.5) on $\mathbf{V}_h$ and Q_h, the system (6.1.6) is uniquely solvable [10, Theorem 5.5.2]. Following [10, Proposition 5.5.3] the displacement error is thus bounded as follows:

$$\|\mathbf{u} - \mathbf{u}_h\|_1 \leq \frac{c}{\beta} \inf_{\mathbf{v}_h \in \mathbf{V}_h} \|\mathbf{u} - \mathbf{v}_h\|_1 + \frac{1}{\mu}\left(\frac{1}{\lambda} + 1\right) \inf_{q_h \in Q_h} \|p - q_h\|_0. \tag{6.1.7}$$

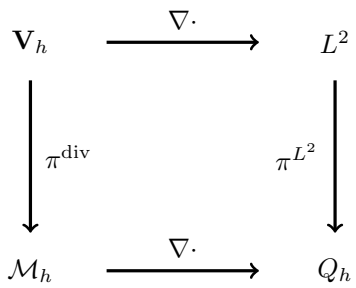

Figure 6.1: Commutative diagram for the reconstruction operator $\boldsymbol{\pi}^{\mathrm{div}}$

Following [38], we assume that there exists a reconstruction operator

$$\boldsymbol{\pi}^{\mathrm{div}} \colon \mathbf{V}_h \to H^{\mathrm{div}}(\Omega;\mathbb{R}^d) = \left\{ \mathbf{v} \in L^2(\Omega;\mathbb{R}^d) \,:\, \nabla\cdot\mathbf{v} \in L^2(\Omega) \right\},$$

to be specified later in Section 6.1.3, mapping discretely divergence free functions to divergence free functions. Then the modified problem is given as:

$$\begin{aligned} a(\mathbf{u}_h,\mathbf{v}_h) + b(p_h,\mathbf{v}_h) &= (\mathbf{f},\boldsymbol{\pi}^{\mathrm{div}}\mathbf{v}_h) \quad && \forall \mathbf{v}_h \in \mathbf{V}_h, \\ b(q_h,\mathbf{u}_h) - \frac{1}{\lambda}(p_h,q_h) &= 0 && \forall q_h \in Q_h. \end{aligned} \tag{6.1.8}$$

Clearly, by construction, the modified problem (6.1.8) admits a solution under the same conditions as (6.1.6), since only the right hand side has been modified. In Theorem 6.7, we will see that the discretization (6.1.8) is gradient robust, under appropriate assumptions on $\boldsymbol{\pi}^{\mathrm{div}}$. Further, in Theorem 6.8, we show the gradient robust displacement error estimate

$$\|\mathbf{u}-\mathbf{u}_h\|_1 \leq ch^k \left(1+\sqrt{\frac{\mu}{\lambda}}\right) \|\mathbf{u}\|_{k+1} + c\frac{h^k}{\lambda}\|p\|_k, \tag{6.1.9}$$

where $\|\cdot\|_k$ denotes the norm on $H^k(\Omega)$ or $H^k(\Omega;\mathbb{R}^d)$; of course assuming sufficient regularity of $\mathbf{u}$ and p and approximation order of $\mathbf{V}_h$ and Q_h. While the introduction of a variational crime in (6.1.8) means that instead of a quasi-best approximation error we only provide an estimate of optimal convergence order the estimate (6.1.9) is clearly better than (6.1.7) in view of the asymptotics as $\lambda \to \infty$ and $\mu \to 0$.

6.1.3 Reconstruction Operator and Assumptions

The construction of the reconstruction operator $\boldsymbol{\pi}^{\mathrm{div}}$ proposed by [38] is based on the choice of a suitable subspace $\mathcal{M}_h \subset H^{\mathrm{div}}(\Omega\mathbb{R}^d)$ satisfying the commuting diagram in Figure 6.1 where π^{L^2} denotes the L^2-projection onto Q_h. The commuting diagram is equivalently expressed by the equation

$$b(q_h,\boldsymbol{\pi}^{\mathrm{div}}\mathbf{v}_h) = b(q_h,\mathbf{v}_h) \qquad \forall \mathbf{v}_h \in \mathbf{V}_h, q_h \in Q_h, \tag{6.1.10}$$

holds assuming that $\nabla \cdot \mathcal{M}_h \subseteq Q_h$. Further, we define

$$\mathbf{V}_h^0 = \{\mathbf{v}_h \in \mathbf{V}_h \,:\, b(q_h, \mathbf{v}_h) = 0 \;\forall q_h \in Q_h\}, \tag{6.1.11}$$

$$H_0^{\mathrm{div}}(\Omega;\mathbb{R}^d) = \{\mathbf{v} \in H^{\mathrm{div}}(\Omega;\mathbb{R}^d) \,:\, \nabla \cdot v = 0\}. \tag{6.1.12}$$

Then clearly, by (6.1.10) we have that the restriction of $\boldsymbol{\pi}^{\mathrm{div}}$ to discretely divergence free functions maps into divergence free functions, i.e.,

$$\boldsymbol{\pi}^{\mathrm{div}} \colon \mathbf{V}_h^0 \to H_0^{\mathrm{div}}(\Omega;\mathbb{R}^d) \tag{6.1.13}$$

and further for any $\mathbf{v}_h \in \mathbf{V}_h$ it holds

$$\boldsymbol{\pi}^{\mathrm{div}}\mathbf{v}_h \cdot \mathbf{n} = 0 \quad \text{on } \partial\Omega \tag{6.1.14}$$

where, $\mathbf{n}$ is the unit outward normal vector. Analogously to the continuous setting, we can define the orthogonal complement $\mathbf{V}_h^\perp$ by

$$\mathbf{V}_h^\perp = \left\{\mathbf{u}_h \in \mathbf{V}_h : a(\mathbf{u}_h, \mathbf{v}_h) = 0, \forall\, \mathbf{v}_h \in \mathbf{V}_h^0\right\},$$

and the corresponding discrete decomposition $\mathbf{u}_h = \mathbf{u}_h^0 + \mathbf{u}_h^\perp \in \mathbf{V}_h^0 \oplus \mathbf{V}_h^\perp$. Before we continue, let us make some, generic assumptions on the considered spaces $\mathbf{V}_h$ and Q_h defined on a shape regular family $\mathcal{T}_h$ of decompositions of Ω.

Assumption 1. *Following [39, Assumptions A1,A2, and A3], we assume, that for some $k \geq 2$ and $i = 0, 1$ the finite element space $\mathbf{V}_h$ is equipped with an interpolation operator $I_h \colon H^{k+1}(\Omega;\mathbb{R}^d) \to \mathbf{V}_h$ satisfying*

$$h_T^i \|I_h\mathbf{v} - \mathbf{v}\|_{i,T} \leq c h_T^{k+1} \|\mathbf{v}\|_{k+1,T} \qquad \forall \mathbf{v} \in H^{k+1}(\Omega;\mathbb{R}^d), T \in \mathcal{T}_h$$

where $\|\cdot\|_{i,T}$ denotes the respective norm on the element T, and h_T is the element diameter. For the space Q_h, we assume that the L^2-projection $\pi^{L^2} \colon H^k(\Omega) \to Q_h$ satisfies

$$h_T^i \|\pi^{L^2} q - q\|_{i,T} \leq c h_T^k \|q\|_{k,T} \qquad \forall q \in H^k(\Omega), T \in \mathcal{T}_h.$$

Further, it is assumed that $\mathbf{V}_h$ and Q_h satisfy the inf-sup inequality (6.1.5). Finally, we assume that there exists a subspace $\widetilde{\mathbf{Q}}_h \subset L^2(\Omega;\mathbb{R}^d)$ such that the respective L^2-projection $\widetilde{\boldsymbol{\pi}}^{L^2}$ satisfies

$$h_T^i \|\widetilde{\boldsymbol{\pi}}^{L^2}\mathbf{q} - \mathbf{q}\|_{i,T} \leq c h_T^{k-1} \|\mathbf{q}\|_{k-1,T} \qquad \forall \mathbf{q} \in H^k(\Omega;\mathbb{R}^d), T \in \mathcal{T}_h.$$

Further requirements on $\widetilde{\mathbf{Q}}_h$ will be made in Assumption 2.

With these preparations, we can now state the additional assumptions on the reconstruction operator.

Assumption 2. *Following [39, Assumption A4], we first assume, that the reconstruction operator satisfies the following orthogonality relation*

$$\left(\mathbf{v}_h - \boldsymbol{\pi}^{\mathrm{div}}\mathbf{v}_h, \mathbf{q}\right) = 0 \qquad \forall \mathbf{v}_h \in \mathbf{V}_h, \mathbf{q} \in \widetilde{\mathbf{Q}}_h, \tag{6.1.15}$$

where $\widetilde{\mathbf{Q}}_h \subset L^2(\Omega;\mathbb{R}^d)$ is given in Assumption 1. Second, we assume the following local approximation property to hold

$$\|\boldsymbol{\pi}^{\mathrm{div}}\mathbf{v}_h - \mathbf{v}_h\|_{0,T} \leq c h_T^m |\mathbf{v}_h|_{m,T} \qquad \forall\, \mathbf{v}_h \in \mathbf{V}_h, T \in \mathcal{T}_h, m = 0, 1. \tag{6.1.16}$$

Before concluding the assumption, let us note that the assumptions can indeed be satisfied. To this end, we give an example which we will also use for the numerical results in Section 6.3.

Example 6.3. *Let us assume that the domain can be decomposed into a family $\mathcal{T}_h$ of shape regular rectangular ($d = 2$) or brick ($d = 3$) elements. For the space $\mathbf{V}_h = \mathbf{V}_h^k$, we consider, parametric, piecewise $\mathcal{Q}_k$ and globally continuous finite elements with $k \geq 2$. For the discretization of $Q_h = Q_h^{k-1}$, we select the space of discontinuous piecewise P_{k-1} functions. Indeed theses pairs satisfy the inf-sup condition (6.1.5), see, e.g., [10, Sec. 8.6.3 & 8.7.2] for $k = 2$, for arbitrary k [23, Sec. 3.2] or [44] for mapped pressure spaces. Moreover, [39, Sec. 4.2.1] showed, that the choice $\mathcal{M}_h = \mathcal{BDM}_k$ as space of Brezzi-Douglas-Marini elements yield the desired commuting diagram property (6.1.10) together with the canonical interpolation $\boldsymbol{\pi}^{\text{div}}$. Further, they showed [39, Lemma 2.1], that the restriction of $\boldsymbol{\pi}^{\text{div}}$ to discretely divergence free functions maps into divergence free functions, i.e.,*

$$\boldsymbol{\pi}^{\text{div}} \colon \{\mathbf{v}_h \in \mathbf{V}_h \,:\, b(q_h, \mathbf{v}_h)\ \forall q_h \in Q_h\} \to \{\mathbf{v} \in H^{\text{div}}(\Omega; \mathbb{R}^d) \,:\, \nabla \cdot v = 0\}$$

and further for any $\mathbf{v}_h \in \mathbf{V}_h$ it holds

$$\boldsymbol{\pi}^{\text{div}} \mathbf{v}_h \cdot \mathbf{n} = 0 \quad \text{on } \partial\Omega.$$

Further, [39, Section 4.2.1] shows the validity of Assumption 2 where $\widetilde{\mathbf{Q}}_h$ is the space of discontinuous piecewise P_{k-2}^d functions.

Remark 6.4. *Infact, [39] showed that (6.1.10) follow from a set of assumed orthogonality properties and surjectivity of divergence and normal traces from which suitable choices of $\mathcal{M}_h$ and constructions of $\boldsymbol{\pi}^{\text{div}}$ can be obtained.*

6.2 Error Analysis

This section is taken from our previously published work [9]. We proceed with the error analysis of the modified weak form (6.1.8). We split the analysis in two parts for incompressible materials ($\lambda = \infty$) and nearly incompressible materials ($\lambda \neq \infty$).

6.2.1 Incompressible Materials

We proceed to the error analysis of incompressible materials, where $\lambda = \infty$ and the term involving $\frac{1}{\lambda}$ is dropped in (6.1.8). The analysis follows, at large, the arguments in [40] with some minor adjustments to the elasticity case.

Theorem 6.5. *Let Assumptions 1 and 2 be satisfied and $\lambda = \infty$. Then the solution $(\mathbf{u}, p) \in H^{k+1}(\Omega; \mathbb{R}^d) \times H^k(\Omega)$ of the continuous problem (6.0.1) and the solution $(\mathbf{u}_h, p_h) \in \mathbf{V}_h \times Q_h$ of (6.1.8) satisfy the error estimate*

$$\|\mathbf{u} - \mathbf{u}_h\|_1^2 \leq c \sum_{T \in \mathcal{T}_h} h_T^{2k} |\mathbf{u}|_{k+1,T}^2 \leq c h^{2k} \|\mathbf{u}\|_{k+1},$$

where $|\cdot|_k$ *denotes the* H^k*-semi-norm, where* $k \geq 2$ *is given by Assumption 1.*

Before proving the above theorem, we would like to prove an important lemma which is need to prove the theorem.

Lemma 6.6. *Let Assumptions 1 and 2 be satisfied and* $\lambda = \infty$*. Then for any functions* $\mathbf{u} \in H^{k+1}(\Omega;\mathbb{R}^d)$ *and* $\mathbf{w}_h \in \mathbf{V}_h$ *it is*

$$\left|(\nabla\cdot\varepsilon(\mathbf{u}),\boldsymbol{\pi}^{\mathrm{div}}\mathbf{w}_h)+(\varepsilon(\mathbf{u}),\varepsilon(\mathbf{w}_h))\right| \leq c\sum_{T\in\mathcal{T}_h} h_T^k|\mathbf{u}|_{k+1,T}\|\mathbf{w}_h\|_{1,T}, \tag{6.2.1}$$

where $|\cdot|_{k,T}$ *denotes the* H^k*-semi-norm on* T*, where* $k \geq 2$ *is given by Assumption 1.*

Proof. We add and subtract $(\nabla\cdot\varepsilon(\mathbf{u}),\mathbf{w}_h)$ on the left to obtain

$$\begin{aligned}(\nabla\cdot\varepsilon(\mathbf{u}),\boldsymbol{\pi}^{\mathrm{div}}\mathbf{w}_h)+(\varepsilon(\mathbf{u}),\varepsilon(\mathbf{w}_h)) &= (\nabla\cdot\varepsilon(\mathbf{u}),\boldsymbol{\pi}^{\mathrm{div}}\mathbf{w}_h-\mathbf{w}_h)\\ &\quad+(\varepsilon(\mathbf{u}),\varepsilon(\mathbf{w}_h))+(\nabla\cdot\varepsilon(\mathbf{u}),\mathbf{w}_h).\end{aligned} \tag{6.2.2}$$

Since $\nabla\cdot\varepsilon(\mathbf{u}) \in L^2(\Omega;\mathbb{R}^d)$, we can apply the projection $\widetilde{\boldsymbol{\pi}}^{L^2}$, from Assumption 1, to get $\widetilde{\boldsymbol{\pi}}^{L^2}\nabla\cdot\varepsilon(\mathbf{u}) \in \widetilde{\mathbf{Q}}_h$. By the assumed orthogonality in (6.1.15), we have

$$\left(\widetilde{\boldsymbol{\pi}}^{L^2}\nabla\cdot\varepsilon(\mathbf{u}),\boldsymbol{\pi}^{\mathrm{div}}\mathbf{w}_h-\mathbf{w}_h\right)=0, \qquad \forall\ \mathbf{w}_h\in\mathbf{V}_h.$$

Using Assumption 1 and (6.1.16), we obtain, for the first summand on the right of (6.2.2),

$$\begin{aligned}\left(\nabla\cdot\varepsilon(\mathbf{u}),\boldsymbol{\pi}^{\mathrm{div}}\mathbf{w}_h-\mathbf{w}_h\right) &= \left(\nabla\cdot\varepsilon(\mathbf{u})-\widetilde{\boldsymbol{\pi}}^{L^2}\nabla\cdot\varepsilon(\mathbf{u}),\boldsymbol{\pi}^{\mathrm{div}}\mathbf{w}_h-\mathbf{w}_h\right)\\ &\leq \sum_{T\in\mathcal{T}_h}\|\nabla\cdot\varepsilon(\mathbf{u})-\widetilde{\boldsymbol{\pi}}^{L^2}\nabla\cdot\varepsilon(\mathbf{u})\|_{0,T}\|\boldsymbol{\pi}^{\mathrm{div}}\mathbf{w}_h-\mathbf{w}_h\|_{0,T}\\ &\leq \sum_{T\in\mathcal{T}_h} ch_T^{k-1}|\nabla\cdot\varepsilon(\mathbf{u})|_{k-1,T}h_T\|\mathbf{w}_h\|_{1,T}\\ &\leq \sum_{T\in\mathcal{T}_h} ch_T^{k}|\mathbf{u}|_{k+1,T}\|\mathbf{w}_h\|_{1,T}.\end{aligned} \tag{6.2.3}$$

For the last two summands of (6.2.2), we apply Gauss divergence theorem to get

$$(\nabla\cdot\varepsilon(\mathbf{u}),\mathbf{w}_h)+(\varepsilon(\mathbf{u}),\varepsilon(\mathbf{w}_h))=\int_{\partial\Omega}\varepsilon(\mathbf{u})\cdot\mathbf{n}\ \mathbf{w}_h\,\mathrm{d}s=0 \tag{6.2.4}$$

since $\mathbf{w}_h = 0$ on $\partial\Omega$. Combining (6.2.2) with the bounds (6.2.3) and (6.2.4) the assertion is shown. □

Now, we continue to prove Theorem 6.5

Proof. (of Theorem 6.5) Let $\mathbf{u}_h$ be the solution of (6.1.8), with $\lambda = \infty$, and let $\mathbf{v}_h \in \mathbf{V}_h^0$ be arbitrary. Defining $\mathbf{w}_h = \mathbf{u}_h - \mathbf{v}_h \in \mathbf{V}_h^0$ and applying the triangle inequality gives

$$\|\mathbf{u}-\mathbf{u}_h\|_1 = \|\mathbf{u}-\mathbf{w}_h-\mathbf{v}_h\|_1 \leq \|\mathbf{u}-\mathbf{v}_h\|_1+\|\mathbf{w}_h\|_1. \tag{6.2.5}$$

In view of the interpolation estimate in Assumption 1, we are left to estimate $\|\mathbf{w}_h\|_1$. From Korn's inequality, we have

$$c\|\mathbf{w}_h\|_1^2 \leq \|\varepsilon(\mathbf{w}_h)\|_0^2.$$

From this, we conclude

$$\begin{aligned} 2\mu c\|\mathbf{w}_h\|_1^2 &\leq a(\mathbf{w}_h, \mathbf{w}_h) \\ &= a(\mathbf{u}_h - \mathbf{v}_h, \mathbf{w}_h) \\ &= a(\mathbf{u}_h - \mathbf{v}_h + \mathbf{u} - \mathbf{u}, \mathbf{w}_h) \\ &\leq |a(\mathbf{u} - \mathbf{v}_h, \mathbf{w}_h)| + |a(\mathbf{u}_h - \mathbf{u}, \mathbf{w}_h)|. \end{aligned} \tag{6.2.6}$$

For the first summand on the right of (6.2.6) we use Cauchy-Schwartz inequality to get

$$|a(\mathbf{u} - \mathbf{v}_h, \mathbf{w}_h)| \leq 2\mu\|\varepsilon(\mathbf{u} - \mathbf{v}_h)\|_0\|\varepsilon(\mathbf{w}_h)\|_0 \leq 2\mu\|\mathbf{u} - \mathbf{v}_h\|_1\|\mathbf{w}_h\|_1. \tag{6.2.7}$$

Before we come to the bound of the second summand in (6.2.6), we make some preliminary calculations. Since $\mathbf{u}_h$ is the solution of (6.1.8), choosing $\mathbf{v}_h = \mathbf{w}_h \in \mathbf{V}_h^0$ gives

$$a(\mathbf{u}_h, \mathbf{w}_h) = a(\mathbf{u}_h, \mathbf{w}_h) + b(p_h, \mathbf{w}_h) = (\mathbf{f}, \boldsymbol{\pi}^{\mathrm{div}}\mathbf{w}_h). \tag{6.2.8}$$

Further, since $\mathbf{u}$ is the solution to the equation (6.0.1) multiplication with $\boldsymbol{\pi}^{\mathrm{div}}\mathbf{w}_h$ and integration yields

$$-2\mu \int_\Omega \nabla \cdot \varepsilon(\mathbf{u})\boldsymbol{\pi}^{\mathrm{div}}\mathbf{w}_h \,\mathrm{d}x - \int_\Omega \nabla p \; \boldsymbol{\pi}^{\mathrm{div}}\mathbf{w}_h \,\mathrm{d}x = \int_\Omega \mathbf{f}\boldsymbol{\pi}^{\mathrm{div}}\mathbf{w}_h \,\mathrm{d}x$$

by the compatibility of the reconstruction with the kernel of the divergence, i.e., (6.1.13) and (6.1.14), this gives

$$-2\mu(\nabla \cdot \varepsilon(\mathbf{u}), \boldsymbol{\pi}^{\mathrm{div}}\mathbf{w}_h) = (\mathbf{f}, \boldsymbol{\pi}^{\mathrm{div}}\mathbf{w}_h)$$

Combining this with (6.2.8), we get

$$a(\mathbf{u}_h, \mathbf{w}_h) = -2\mu(\nabla \cdot \varepsilon(\mathbf{u}), \boldsymbol{\pi}^{\mathrm{div}}\mathbf{w}_h). \tag{6.2.9}$$

Now, we can bound the second summand on the right of (6.2.6), using (6.2.9) we get

$$\begin{aligned} |a(\mathbf{u}_h - \mathbf{u}, \mathbf{w}_h)| &= \Big|-2\mu(\nabla \cdot \varepsilon(\mathbf{u}), \boldsymbol{\pi}^{\mathrm{div}}\mathbf{w}_h) - 2\mu(\varepsilon(\mathbf{u}), \varepsilon(\mathbf{w}_h))\Big| \\ &\leq 2\mu\Big|(\nabla \cdot \varepsilon(\mathbf{u}), \boldsymbol{\pi}^{\mathrm{div}}\mathbf{w}_h) + (\varepsilon(\mathbf{u}), \varepsilon(\mathbf{w}_h))\Big|. \end{aligned}$$

By the previously shown lemma, i.e., (6.2.1), we can bound the right hand side to get

$$\begin{aligned} |a(\mathbf{u}_h - \mathbf{u}, \mathbf{w}_h)| &\leq 2\mu c \sum_{T\in\mathcal{T}_h} \left(h_T^k |\mathbf{u}|_{k+1,T}\|\mathbf{w}_h\|_{1,T}\right) \\ &\leq 2\mu c \left(\sum_{T\in\mathcal{T}_h} h_T^{2k}|\mathbf{u}|_{k+1,T}^2\right)^{\frac{1}{2}} \|\mathbf{w}_h\|_1. \end{aligned} \tag{6.2.10}$$

Now combining (6.2.6) with the two bounds (6.2.7) and (6.2.10), we get

$$\|\mathbf{w}_h\|_1 \leq c\|\mathbf{u}-\mathbf{v}_h\|_1 + c\left(\sum_{T\in\mathcal{T}_h} h_T^{2k}|\mathbf{u}|_{k+1,T}^2\right)^{\frac{1}{2}}.$$

Substituting this in (6.2.22) yields

$$\|\mathbf{u}-\mathbf{u}_h\|_1 \leq c\|\mathbf{u}-\mathbf{v}_h\|_1 + c\left(\sum_{T\in\mathcal{T}_h} h_T^{2k}|\mathbf{u}|_{k+1,T}^2\right)^{\frac{1}{2}}. \tag{6.2.11}$$

To bound the best approximation error on $\mathbf{V}_h^0$ in this inequality, we proceed using inf-sup condition as in [23, Chapter 2, (1.16)] and the assumed interpolation estimate on $\mathbf{V}_h$ in Assumption 1, to get the estimate

$$\inf_{\mathbf{v}_h\in\mathbf{V}_h^0}\|\mathbf{u}-\mathbf{v}_h\|_1 \leq c\inf_{\mathbf{v}_h\in\mathbf{V}_h}\|\mathbf{u}-\mathbf{v}_h\|_1 \leq c\left(\sum_{T\in\mathcal{T}_h} h_T^{2k}|\mathbf{u}|_{k+1,T}^2\right)^{\frac{1}{2}}.$$

Using this in (6.2.11) gives the desired estimate. □

6.2.2 Nearly Incompressible Materials

For the nearly incompressible case, i.e., ($\lambda \neq \infty$), we start by assuming a gradient force $\mathbf{f} = \nabla\phi$, for some $\phi \in L^2(\Omega)$. From Lemma 6.1, we have that the solution of (6.0.1) for such an $\mathbf{f}$ is $\mathbf{u} = \mathbf{u}^\perp$. The following result shows, that our mixed discretization (6.1.8) is gradient robust in the sense of Definition 6.2.

Theorem 6.7. *Let Assumptions 1 and 2 be satisfied. If the right hand side $\mathbf{f} \in H^{-1}(\Omega;\mathbb{R}^d)$ of equation (6.1.8) is a gradient field, i.e., $\mathbf{f} = \nabla\phi$, for some $\phi \in L^2(\Omega)$, then the solution $(\mathbf{u}_h, p_h) \in \mathbf{V}_h \times Q_h$ of (6.1.8) with $\lambda \neq \infty$ satisfies $\mathbf{u}_h \in \mathbf{V}_h^\perp$ and the gradient robust bound*

$$\|\mathbf{u}_h\|_1 \leq c\frac{1}{\lambda+\mu}\|\phi\|_0. \tag{6.2.12}$$

with a constant c independent of h.

Proof. Consider $\mathbf{v}_h = \mathbf{u}_h$ in equation (6.1.8) with $\mathbf{f} = \nabla\phi$. Then integration by parts for the right hand side, using the zero trace from (6.1.14), we get

$$a(\mathbf{u}_h,\mathbf{u}_h) + b(p_h,\mathbf{u}_h) = -(\phi, \nabla\cdot\boldsymbol{\pi}^{\mathrm{div}}\mathbf{u}_h). \tag{6.2.13}$$

Since $\nabla\cdot\boldsymbol{\pi}^{\mathrm{div}}\mathbf{u}_h \in Q_h$ we can rewrite the right hand side as

$$(\phi, \nabla\cdot\boldsymbol{\pi}^{\mathrm{div}}\mathbf{u}_h) = (\pi^{L^2}\phi, \nabla\cdot\boldsymbol{\pi}^{\mathrm{div}}\mathbf{u}_h). \tag{6.2.14}$$

Since $\pi^{L^2}\nabla\cdot\mathbf{u}_h \in Q_h$, we can use it to test the second line in (6.1.8) giving

$$\begin{aligned}(\pi^{L^2}\nabla\cdot\mathbf{u}_h, \pi^{L^2}\nabla\cdot\mathbf{u}_h) &= (\pi^{L^2}\nabla\cdot\mathbf{u}_h, \nabla\cdot\mathbf{u}_h)\\ &= \frac{1}{\lambda}(p_h, \pi^{L^2}\nabla\cdot\mathbf{u}_h)\\ &= \frac{1}{\lambda}(p_h, \nabla\cdot\mathbf{u}_h)\\ &= \frac{1}{\lambda}b(p_h, \mathbf{u}_h).\end{aligned} \tag{6.2.15}$$

Substituting (6.2.14) and (6.2.15) in (6.2.13), we get

$$a(\mathbf{u}_h, \mathbf{u}_h) + \lambda(\pi^{L^2}\nabla\cdot\mathbf{u}_h, \pi^{L^2}\nabla\cdot\mathbf{u}_h) = -(\pi^{L^2}\phi, \nabla\cdot\boldsymbol{\pi}^{\mathrm{div}}\mathbf{u}_h). \tag{6.2.16}$$

Now $\pi^{L^2}\phi \in Q_h$ and $\mathbf{u}_h \in \mathbf{V}_h$ hence, by (6.1.10), it holds

$$(\pi^{L^2}\phi, \nabla\cdot\boldsymbol{\pi}^{\mathrm{div}}\mathbf{u}_h) = (\pi^{L^2}\phi, \nabla\cdot\mathbf{u}_h).$$

Filling this into (6.2.16) gives

$$2\mu\left(\varepsilon(\mathbf{u}_h), \varepsilon(\mathbf{u}_h)\right) + \lambda\left(\pi^{L^2}\nabla\cdot\mathbf{u}_h, \pi^{L^2}\nabla\cdot\mathbf{u}_h\right) = -\left(\pi^{L^2}\phi, \pi^{L^2}\nabla\cdot\mathbf{u}_h\right). \tag{6.2.17}$$

Using Cauchy-Schwartz inequality, we get

$$2\mu\|\varepsilon(\mathbf{u}_h)\|_0^2 + \lambda\|\pi^{L^2}\nabla\cdot\mathbf{u}_h\|_0^2 \le \|\pi^{L^2}\phi\|_0\|\pi^{L^2}\nabla\cdot\mathbf{u}_h\|_0 \le \|\phi\|_0\|\pi^{L^2}\nabla\cdot\mathbf{u}_h\|_0. \tag{6.2.18}$$

Now, to estimate the H^1-norm of $\mathbf{u}_h$, we notice that by the choice of $\mathbf{f}$ and (6.1.13), testing the first equation in (6.1.8) with a function $\mathbf{v}_h \in \mathbf{V}_h^0$ yields

$$a(\mathbf{u}_h, \mathbf{v_h}) = -b(p_h, \mathbf{v}_h) - (\phi, \nabla\cdot\boldsymbol{\pi}^{\mathrm{div}}\mathbf{v}_h) = 0$$

and thus $\mathbf{u}_h \in \mathbf{V}_h^{\perp}$. Hence by, e.g., [29, Lemma 3.58] it holds

$$\|\mathbf{u}_h\|_1 \le c\|\pi^{L^2}\nabla\cdot\mathbf{u}_h\|_0 \tag{6.2.19}$$

with a constant c depending on the inf-sup constant β from (6.1.5), since $\pi^{L^2}\nabla\cdot\mathbf{u}_h \in Q_h$.

Using Korn's inequality, (6.2.18), and (6.2.19), we get

$$\begin{aligned}(\mu+\lambda)\|\mathbf{u}_h\|_1^2 &\le c\mu\|\varepsilon(\mathbf{u}_h)\|_0^2 + \lambda c\|\pi^{L^2}\nabla\cdot\mathbf{u}_h\|_1^2\\ &\le c\|\phi\|_0\|\mathbf{u}_h\|_1,\end{aligned} \tag{6.2.20}$$

and thus the assertion is shown. □

Theorem 6.8. *Let Assumptions 1 and 2 be satisfied. Then the solutions $(\mathbf{u}, p) \in \mathbf{V}\times Q$, of the problem (6.0.1) and $(\mathbf{u}_h, p_h) \in \mathbf{V}_h \times Q_h$ of (6.1.8) satisfy the error estimate*

$$\|\mathbf{u}-\mathbf{u}_h\|_1 \le c\,h^k\left(1+\sqrt{\frac{\mu}{\lambda}}\right)\|\mathbf{u}\|_{k+1} + c\frac{h^k}{\lambda}\|p\|_k, \tag{6.2.21}$$

provided the regularity $(\mathbf{u}, p) \in H^{k+1}(\Omega;\mathbb{R}^d)\times H^k(\Omega)$ is given, where $k \ge 2$ is given by Assumption 1.

Proof. As in the proof of Theorem 6.5, we could split the error

$$\|\mathbf{u}-\mathbf{u}_h\|_1 = \|\mathbf{u}-\mathbf{w}_h-\mathbf{v}_h\|_1 \le \|\mathbf{u}-\mathbf{v}_h\|_1 + \|\mathbf{w}_h\|_1, \tag{6.2.22}$$

where $\mathbf{w}_h = \mathbf{u}_h - \mathbf{v}_h$, with arbitrary $\mathbf{v}_h \in \mathbf{V}_h$ and $q_h \in Q_h$. However, as it will turn out to be useful, we will select $q_h = \pi^{L^2} p$ and $\mathbf{v}_h$ as a particular Fortin operator applied to $\mathbf{u}$, i.e., satisfying the following equation

$$\begin{aligned} (\varepsilon(\mathbf{v}_h),\varepsilon(\boldsymbol{\varphi}_h)) + b(\tilde{p}_h,\boldsymbol{\varphi}_h) &= (\varepsilon(\mathbf{u}),\varepsilon(\boldsymbol{\varphi}_h)) && \forall \boldsymbol{\varphi}_h \in \mathbf{V}_h, \\ b(s_h,\mathbf{v}_h) &= b(s_h,\mathbf{u}) && \forall s_h \in Q_h. \end{aligned} \tag{6.2.23}$$

Clearly, the solution to the continuous counterpart is $(\mathbf{v},\tilde{p}) = (\mathbf{u},0)$. Since the above equation is uniquely solvable, see, e.g. [10, Theorem 4.2.3], we have the orthogonality $b(\pi^{L^2}p - p_h, \mathbf{u}-\mathbf{v}_h) = 0$ and the approximation error satisfies, e.g., [10, Theorem 5.2.2].

$$\|\mathbf{u}-\mathbf{v}_h\|_1 + \|\tilde{p}-\tilde{p}_h\|_0 \le c \inf_{\boldsymbol{\varphi}_h\in\mathbf{V}_h} \|\mathbf{u}-\boldsymbol{\varphi}_h\|_1 + c \inf_{s_h\in Q_h} \|0-s_h\|_0, \tag{6.2.24}$$

which gives

$$\|\mathbf{u}-\mathbf{v}_h\|_1 \le c \inf_{\boldsymbol{\varphi}_h\in\mathbf{V}_h} \|\mathbf{u}-\boldsymbol{\varphi}_h\|_1 \tag{6.2.25}$$

Due to the interpolation estimates in Assumption 1, we are left with bounding $\mathbf{w}_h = \mathbf{u}_h - \mathbf{v}_h \in \mathbf{V}_h$ and $r_h = p_h - q_h \in Q_h$. We split $\mathbf{w}_h = \mathbf{w}_h^0 + \mathbf{w}_h^\perp \in \mathbf{V}_h^0 \oplus \mathbf{V}_h^\perp$. By definition of the bilinear forms a and b, i.e., (6.1.1) and (6.1.2), and the first line in (6.1.8) and (6.0.1), the remainder $\mathbf{w}_h$ and r_h satisfy, for any discrete function $\boldsymbol{\varphi}_h \in \mathbf{V}_h$,

$$\begin{aligned} a(\mathbf{w}_h,\boldsymbol{\varphi}_h) + b(r_h,\boldsymbol{\varphi}_h) &= a(\mathbf{u}_h-\mathbf{v}_h,\boldsymbol{\varphi}_h) + b(p_h-q_h,\boldsymbol{\varphi}_h) \\ &= (\mathbf{f},\boldsymbol{\pi}^{\mathrm{div}}\boldsymbol{\varphi}_h - \boldsymbol{\varphi}_h) + a(\mathbf{u}-\mathbf{v}_h,\boldsymbol{\varphi}_h) + b(p-q_h,\boldsymbol{\varphi}_h). \end{aligned} \tag{6.2.26}$$

Analogously, from the second line in (6.1.8) and (6.0.1), we get for arbitrary $s_h \in Q_h$

$$\begin{aligned} b(s_h,\mathbf{w}_h) - \frac{1}{\lambda}(r_h,s_h) &= b(s_h,\mathbf{u}_h-\mathbf{v}_h) - \frac{1}{\lambda}(p_h-q_h,s_h) \\ &= b(s_h,\mathbf{u}_h) - \frac{1}{\lambda}(p_h,s_h) - \Big(b(s_h,\mathbf{v}_h) - \frac{1}{\lambda}(q_h,s_h)\Big) \\ &= b(s_h,\mathbf{u}-\mathbf{v}_h) - \frac{1}{\lambda}(p-q_h,s_h). \end{aligned} \tag{6.2.27}$$

Testing (6.2.26) and (6.2.27) with $\varphi_h = \mathbf{w_h}$ and $s_h = r_h$ we get

$$\begin{aligned} c\mu\|\mathbf{w}_h\|_1^2 + \frac{1}{\lambda}\|r_h\|_0^2 &\le a(\mathbf{w}_h,\mathbf{w}_h) + \frac{1}{\lambda}(r_h,r_h) \\ &= a(\mathbf{w}_h,\mathbf{w}_h) + b(r_h,\mathbf{w}_h) - b(r_h,\mathbf{w}_h) + \frac{1}{\lambda}(r_h,r_h) \\ &= (\mathbf{f},\boldsymbol{\pi}^{\mathrm{div}}\mathbf{w}_h - \mathbf{w}_h) + a(\mathbf{u}-\mathbf{v}_h,\mathbf{w}_h) \\ &\quad + b(p-q_h,\mathbf{w}_h) - b(r_h,\mathbf{u}-\mathbf{v}_h) + \frac{1}{\lambda}(p-q_h,r_h). \end{aligned} \tag{6.2.28}$$

Using (6.2.1) and (6.0.1), we obtain a bound on $(\mathbf{f}, \boldsymbol{\pi}^{\text{div}}\mathbf{w}_h - \mathbf{w}_h)$ as follows

$$\begin{aligned}(\mathbf{f}, \boldsymbol{\pi}^{\text{div}}\mathbf{w}_h - \mathbf{w}_h) &= -2\mu(\nabla\cdot\varepsilon(\mathbf{u}), \boldsymbol{\pi}^{\text{div}}\mathbf{w}_h - \mathbf{w}_h) - (\nabla p, \boldsymbol{\pi}^{\text{div}}\mathbf{w}_h - \mathbf{w}_h)\\ &= -2\mu(\nabla\cdot\varepsilon(\mathbf{u}), \boldsymbol{\pi}^{\text{div}}\mathbf{w}_h) - 2\mu\left(\varepsilon(\mathbf{u}), \varepsilon(\mathbf{w}_h)\right) + b(p, \boldsymbol{\pi}^{\text{div}}\mathbf{w}_h - \mathbf{w}_h)\\ &\leq c\mu \sum_{T\in\mathcal{T}_h} h_T^k |\mathbf{u}|_{k+1,T}\|\mathbf{w}_h\|_{1,T} + b(p, \boldsymbol{\pi}^{\text{div}}\mathbf{w}_h - \mathbf{w}_h)\\ &\leq 2\mu c\left(\sum_{T\in\mathcal{T}_h} h_T^{2k}|\mathbf{u}|_{k+1,T}^2\right)^{\frac{1}{2}}\|\mathbf{w}_h\|_1 + b(p, \boldsymbol{\pi}^{\text{div}}\mathbf{w}_h - \mathbf{w}_h).\end{aligned}$$

Substituting this in (6.2.28), we get

$$\begin{aligned}c\mu\|\mathbf{w}_h\|_1^2 + \frac{1}{\lambda}\|r_h\|_0^2 \leq 2\mu c&\left(\sum_{T\in\mathcal{T}_h} h_T^{2k}|\mathbf{u}|_{k+1,T}^2\right)^{\frac{1}{2}}\|\mathbf{w}_h\|_1\\ &+ \Big(b(p, \boldsymbol{\pi}^{\text{div}}\mathbf{w}_h - \mathbf{w}_h) + b(p-q_h, \mathbf{w}_h) - b(r_h, \mathbf{u}-\mathbf{v}_h)\Big)\\ &+ \Big(a(\mathbf{u}-\mathbf{v}_h, \mathbf{w}_h) + \frac{1}{\lambda}(p-q_h, r_h)\Big).\end{aligned} \tag{6.2.29}$$

The last line can be estimated as

$$a(\mathbf{u}-\mathbf{v}_h, \mathbf{w}_h) + \frac{1}{\lambda}(p-q_h, r_h) \leq \frac{c\mu}{2}\|\mathbf{u}-\mathbf{v}_h\|_1^2 + \frac{c\mu}{2}\|\mathbf{w}_h\|_1^2 + \frac{1}{2\lambda}\|p-q_h\|_0^2 + \frac{1}{2\lambda}\|r_h\|_0^2.$$

From (6.1.10), we have that $b(q_h, \boldsymbol{\pi}^{\text{div}}\mathbf{w}_h - \mathbf{w}_h) = 0$. Hence the second line in (6.2.29) becomes

$$\begin{aligned}b(p, \boldsymbol{\pi}^{\text{div}}\mathbf{w}_h - \mathbf{w}_h) + b(p-q_h, \mathbf{w}_h) - b(r_h, \mathbf{u}-\mathbf{v}_h)&\\ = b(p-q_h, \boldsymbol{\pi}^{\text{div}}\mathbf{w}_h - \mathbf{w}_h) + b(p-q_h, \mathbf{w}_h) - b(r_h, \mathbf{u}-\mathbf{v}_h)&\\ = b(\pi^{L^2}p - q_h, \boldsymbol{\pi}^{\text{div}}\mathbf{w}_h) - b(p_h - q_h, \mathbf{u}-\mathbf{v}_h)&\\ = b(\pi^{L^2}p - q_h, \mathbf{w}_h) - b(p_h - q_h, \mathbf{u}-\mathbf{v}_h)&\end{aligned}$$

where we used the properties of the L^2 projection π^{L^2}, the commutative diagram (6.1.10) and $\nabla\cdot\mathcal{M}_h \subset Q_h$. Now, we utilize the choice $q_h = \pi^{L^2}p$ to further simplify the representation of the second line in (6.2.29) to be

$$\begin{aligned}b(p, \boldsymbol{\pi}^{\text{div}}\mathbf{w}_h - \mathbf{w}_h) + b(p-q_h, \mathbf{w}_h) - b(r_h, \mathbf{u}-\mathbf{v}_h)&\\ = b(\pi^{L^2}p - q_h, \mathbf{w}_h) - b(p_h - q_h, \mathbf{u}-\mathbf{v}_h)&\\ = 0&\end{aligned}$$

by our choice of $\mathbf{v}_h$. This provides the bound

$$\begin{aligned}\frac{c\mu}{2}\|\mathbf{w}_h\|_1^2 + \frac{1}{2\lambda}\|r_h\|_0^2 \leq 2\mu c&\left(\sum_{T\in\mathcal{T}_h} h_T^{2k}|\mathbf{u}|_{k+1,T}^2\right)^{\frac{1}{2}}\|\mathbf{w}_h\|_1\\ &+ \frac{c\mu}{2}\|\mathbf{u}-\mathbf{v}_h\|_1^2 + \frac{1}{2\lambda}\|p-q_h\|_0^2.\end{aligned} \tag{6.2.30}$$

Of course (6.2.30) provides a bound on $\mathbf{w}_h$ but as it is suboptimal, in view of the λ dependence, we continue by splitting $\mathbf{w}_h = \mathbf{w}_h^0 + \mathbf{w}_h^\perp$.

We first bound $\|\mathbf{w}_h^0\|_1$. Consider $c\mu\|\mathbf{w}_h^0\|_1$ and using that $a(\mathbf{w}_h^\perp, \mathbf{w}_h^0) = 0$, we have, using (6.1.11), (6.2.26), and the choice of $\mathbf{v}_h$ by (6.2.23) that

$$\begin{aligned}
c\mu\|\mathbf{w}_h^0\|_1^2 &\leq a(\mathbf{w}_h^0, \mathbf{w}_h^0) = a(\mathbf{w}_h, \mathbf{w}_h^0) = a(\mathbf{w}_h, \mathbf{w}_h^0) + b(r_h, \mathbf{w}_h^0) \\
&= (f, \boldsymbol{\pi}^{\mathrm{div}} \boldsymbol{w}_h^0 - \boldsymbol{w}_h^0) \\
&\leq \left(-2\mu\nabla\cdot\varepsilon(\mathbf{u}) + \nabla p, \boldsymbol{\pi}^{\mathrm{div}}\mathbf{w}_h^0 - \mathbf{w}_h^0\right) \\
&\leq \left(-2\mu\nabla\cdot\varepsilon(\mathbf{u}), \boldsymbol{\pi}^{\mathrm{div}}\mathbf{w}_h^0 - \mathbf{w}_h^0\right) + \left(\nabla p, \boldsymbol{\pi}^{\mathrm{div}}\mathbf{w}_h^0 - \mathbf{w}_h^0\right) \\
&\leq \left(-2\mu\nabla\cdot\varepsilon(\mathbf{u}), \boldsymbol{\pi}^{\mathrm{div}}\mathbf{w}_h^0\right) - \mu\left(\varepsilon(\mathbf{u}), \varepsilon(\mathbf{w}_h^0)\right) \\
&\leq \mu\left(-2\nabla\cdot\varepsilon(\mathbf{u}), \boldsymbol{\pi}^{\mathrm{div}}\mathbf{w}_h^0\right) - \mu\left(\varepsilon(\mathbf{u}), \varepsilon(\mathbf{w}_h^0)\right).
\end{aligned}$$

Thus, by Lemma 6.6, we conclude

$$c\mu\|\mathbf{w}_h^0\|_1^2 \leq \mu c \sum_{T\in\mathcal{T}_h} h_T^k \|\mathbf{u}\|_{k+1,T}\|\mathbf{w}_h^0\|_{1,T} \leq c\mu h^k \|\mathbf{u}\|_{k+1}\|\mathbf{w}_h^0\|_1$$

and hence

$$\|\mathbf{w}_h^0\|_1 \leq ch^k\|\mathbf{u}\|_{k+1}. \tag{6.2.31}$$

For $\|\mathbf{w}_h^\perp\|_1$, we utilize $\mathbf{w}_h^\perp \in \mathbf{V}_h^\perp$, i.e.,

$$(\nabla\cdot\mathbf{w}_h, q_h) = \left(\nabla\cdot\mathbf{w}_h^\perp, q_h\right) \qquad \forall q_h \in Q_h$$

meaning

$$\pi^{L^2}\nabla\cdot\mathbf{w}_h = \pi^{L^2}\nabla\cdot\mathbf{w}_h^\perp.$$

Using [29, Lemma 3.58], we get with a constant c depending on the inf-sup constant

$$\begin{aligned}
\|\mathbf{w}_h^\perp\|_1 &\leq c\|\pi^{L^2}\left(\nabla\cdot\mathbf{w}_h\right)\|_0 \\
&\leq c\|\pi^{L^2}\nabla\cdot\mathbf{u}_h - \pi^{L^2}\nabla\cdot\mathbf{v}_h\|_0 \\
&\leq c\left\|\frac{p_h}{\lambda} - \pi^{L^2}\nabla\cdot\mathbf{u}\right\|_0
\end{aligned}$$

from the definition of $\mathbf{v}_h$ in (6.2.23). Hence, noting that $\nabla\cdot u = \frac{1}{\lambda}p$, we obtain

$$\|\mathbf{w}_h^\perp\|_1 \leq \frac{c}{\lambda}\|p_h - q_h\|_0 = \frac{c}{\lambda}\|r_h\|_0.$$

We conclude from (6.2.30)

$$\|r_h\|_0^2 \leq c\mu\lambda h^{2k}\|\mathbf{u}\|_{k+1}^2 + c\|p - q_h\|_0^2$$

and thus we obtain the final bound on $\mathbf{w}_h^\perp$

$$\begin{aligned}\|\mathbf{w}_h^\perp\|_1 &\leq \frac{c}{\lambda}\|r_h\|_0 \\ &\leq c\sqrt{\frac{\mu}{\lambda}}h^k\|\mathbf{u}\|_{k+1} + \frac{c}{\lambda}\|p-q_h\|_0.\end{aligned} \tag{6.2.32}$$

Now, we can bound $\|\mathbf{w}_h\|_1$ using (6.2.31) and (6.2.32)

$$\begin{aligned}\|\mathbf{w}_h\|_1 &\leq \|\mathbf{w}_h^0\|_1 + \|\mathbf{w}_h^\perp\|_1 \\ &\leq ch^k\|\mathbf{u}\|_{k+1} + \frac{c}{\lambda}\|r_h\|_0 \\ &\leq ch^k\|\mathbf{u}\|_{k+1} + c\sqrt{\frac{\mu}{\lambda}}h^k\|\mathbf{u}\|_{k+1} + \frac{c}{\lambda}\|p-q_h\|_0 \\ &\leq c\left(1+\sqrt{\frac{\mu}{\lambda}}\right)h^k\|\mathbf{u}\|_{k+1} + \frac{c}{\lambda}\|p-q_h\|_0.\end{aligned} \tag{6.2.33}$$

Finally, we arrive at the desired bound

$$\begin{aligned}\|\mathbf{u}-\mathbf{u}_h\|_1 &\leq \|\mathbf{u}-\mathbf{v}_h\|_1 + \|\mathbf{w}_h\|_1 \\ &\leq c\left(1+\sqrt{\frac{\mu}{\lambda}}\right)h^k\|\mathbf{u}\|_{k+1} + \frac{c}{\lambda}h^k\|p\|_k\end{aligned} \tag{6.2.34}$$

by definition of q_h and Assumption 1. □

6.3 Numerical Results

For our computation, we use DOpElib [24] based on the deal.II [4] finite element library with rectangular meshes. All examples are posed on square domains and the meshes are obtained by bisection. For the computation we considered the inf-sup stable Taylor-Hood element $(\mathcal{Q}_2 \times \mathcal{Q}_1)$, for comparison of our results with [22]. Further, we utilized the inf-sup stable discretization $\mathcal{Q}_2 \times \mathcal{DGP}_1$ (discontinuous P_1 pressure) and its gradient robust modification by interpolation into $\mathcal{BDM}_2$ as discussed in Example 6.3.

First, we present an example for incompressible materials.

Example 6.9. *For the first numerical example, we consider a small variation of Example* 5.1 *in [38], where the displacement and pressure on the domain* $\Omega = (0,1)^2$ *is given as*

$$\mathbf{u}(x,y) = \begin{bmatrix} 200x^2y(1-x)^2(1-y)(1-2y) \\ -200y^2x(1-y)^2(1-x)(1-2x)\end{bmatrix} \tag{6.3.1}$$

$$p(x,y) = -10\left(\left(x-\frac{1}{2}\right)^3 y^2 + (1-x)^3\left(y-\frac{1}{2}\right)^3 + \frac{1}{8}\right). \tag{6.3.2}$$

for the incompressible linear elasticity equation

$$\begin{aligned}-2\mu\nabla\cdot\varepsilon(\mathbf{u}) + \nabla p &= \mathbf{f}, \\ \nabla\cdot\mathbf{u} &= 0\end{aligned} \tag{6.3.3}$$

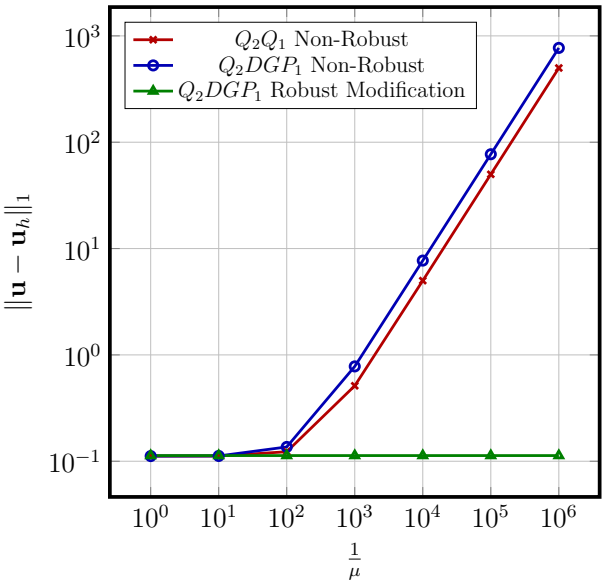

Figure 6.2: Comparing displacement error in H^1 norm vs. $\frac{1}{\mu}$ for Example 6.9 with and without gradient robust modification for 64 square elements

with homogeneous boundary conditions on $\mathbf{u}$ *and thus define* $\mathbf{f}$*, of course the pressure is defined up to a constant only.*

Comparing (6.1.7) with Figure 6.2, we notice that the H^1-norm displacement error without interpolation asymptotically grows linearly w.r.t $\frac{1}{\mu}$ as predicted due to the appearance of the pressure term $\frac{1}{\mu} \inf_{q_h \in Q_h} \|p - q_h\|_0$ in (6.1.7). The error is independent of μ, highlighting the prediction of Theorem 6.5.

For future examples, we consider nearly incompressible materials given by equation (6.0.1).

Example 6.10. *For the second numerical example, we set the right hand side* $f = \nabla\phi; \phi = x^6 + y^6$ *on the domain* $\Omega = (0,1)^2$ *and consider nearly incompressible elasticity, i.e.,*

$$-2\mu \nabla \cdot \varepsilon(\mathbf{u}) - \nabla p = \mathbf{f},$$
$$\nabla \cdot \mathbf{u} - \frac{1}{\lambda} p = 0$$

with homogeneous boundary conditions on $\mathbf{u}$ *as in [22, Example 2].*

From Lemma 6.1, the solution for Example 6.10 in the limiting case ($\lambda = \infty$) is given as $\mathbf{u}^\infty = 0$ and $p^\infty = x^6 + y^6$. From equation (6.2.12), we have the bound for the solution $\mathbf{u}_h^\lambda$ as

$$\|\mathbf{u}^\infty - \mathbf{u}_h^\lambda\|_1 = \|\mathbf{u}_h^\lambda\|_1 \leq \frac{c}{\lambda + \mu} \|\phi\|_0$$

on the discrete function for a gradient robust discretization. For $\mu = 10^{-5}$, we have $\lambda + \mu \approx \lambda, \forall \lambda \geq 1$. Hence, we see a green line with positive slope in Figure 6.3a for the gradient robust method, while the non robust method shows an almost constant

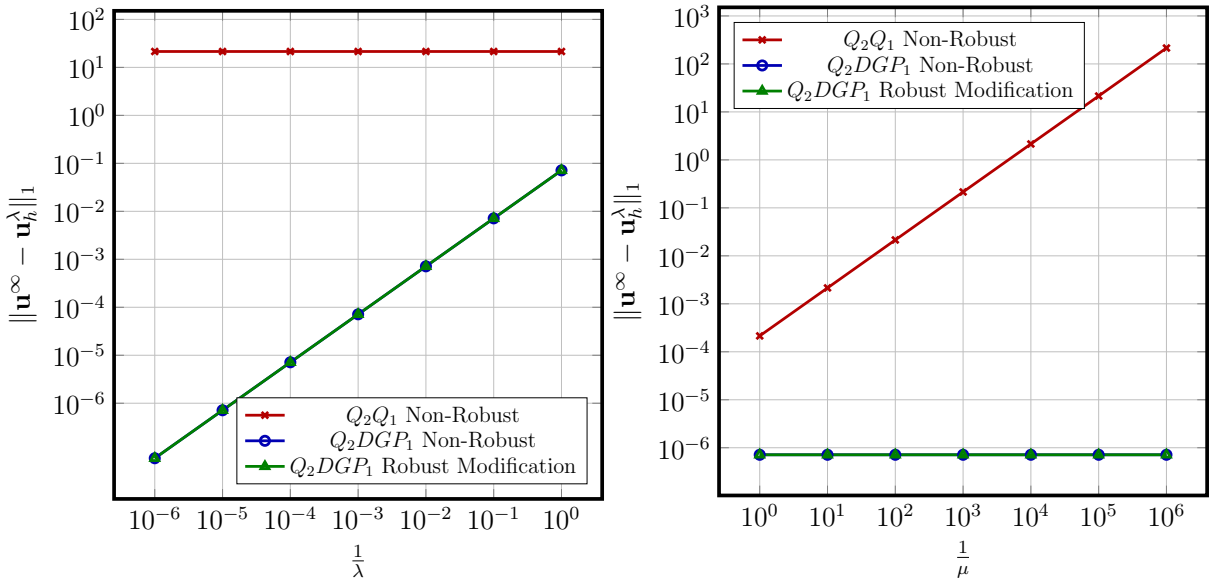

(a) $\|\mathbf{u}^\infty - \mathbf{u}_h^\lambda\|_1$ vs. $\frac{1}{\lambda}$ with $\mu = 10^{-5}$ (b) $\|\mathbf{u}^\infty - \mathbf{u}_h^\lambda\|_1$ vs. $\frac{1}{\mu}$ with $\lambda = 10^5$

Figure 6.3: Comparing displacement error in H^1 norm for Example 6.10 with and without gradient robust modification for 64 square elements

$\|\mathbf{u}_h^\lambda\|_1 \neq 0$. However, for $\lambda = 10^5$ we have $\frac{1}{\lambda+\mu} \approx c(\text{constant})\ \forall 0 < \mu \leq 1$, which is seen in the flat green line in Figure 6.3b.
For non-gradient robust methods, we have

$$\|\mathbf{u}_h^\lambda\|_1 \leq \frac{c}{\mu}\left(\frac{1}{\lambda} + 1\right)\|\phi\|_0$$

from equation (6.1.7). For $\mu = 10^{-5}$, the term $\left(\frac{1}{\lambda} + 1\right) \to 1$ as $\lambda \to \infty$. The same is shown by the flat red line in Figure 6.3a. However, for $\lambda = 10^{-5}$, we have $\|\mathbf{u}_h^\lambda\|_1 \leq \frac{c}{\mu}\|\phi\|_0$. Which is shown by the red line with negative slope in Figure 6.3b.

It should be noted in this example, that the (blue with triangles) line for the non-gradient robust $\mathcal{Q}_2 \times \mathcal{DGP}_1$ method coincides with the (green with dots) line for the gradient robust modification. However, this appears to be due to the particular problem data hiding the non-gradient robustness of the $\mathcal{Q}_2 \times \mathcal{DGP}_1$ discretization. That indeed, the standard $\mathcal{Q}_2 \times \mathcal{DGP}_1$ method is not gradient robust is shown in the following example.

Example 6.11. *For the third numerical example, we consider the right hand side* $f = \nabla\phi; \phi = -\left(10(x-0.5)^3y^2 + (1-x)^3(y-0.5)^3 + 1/8\right)$ *in Example 6.10 while keeping the homogeneous boundary values, and the equation, for* $\mathbf{u}$.

Figure 6.4 shows our previous statement, that Example 6.10 failed to show the missing gradient robustness of the standard $\mathcal{Q}_2 \times \mathcal{DGP}_1$ discretization. Indeed, in this example, both $\mathcal{Q}_2 \times \mathcal{Q}_1$ and $\mathcal{Q}_2 \times \mathcal{DGP}_1$ discretization show the undesirable blowup for $\mu \to 0$ and the constant value as $\lambda \to \infty$, while the gradient robust modification shows the desired convergence.

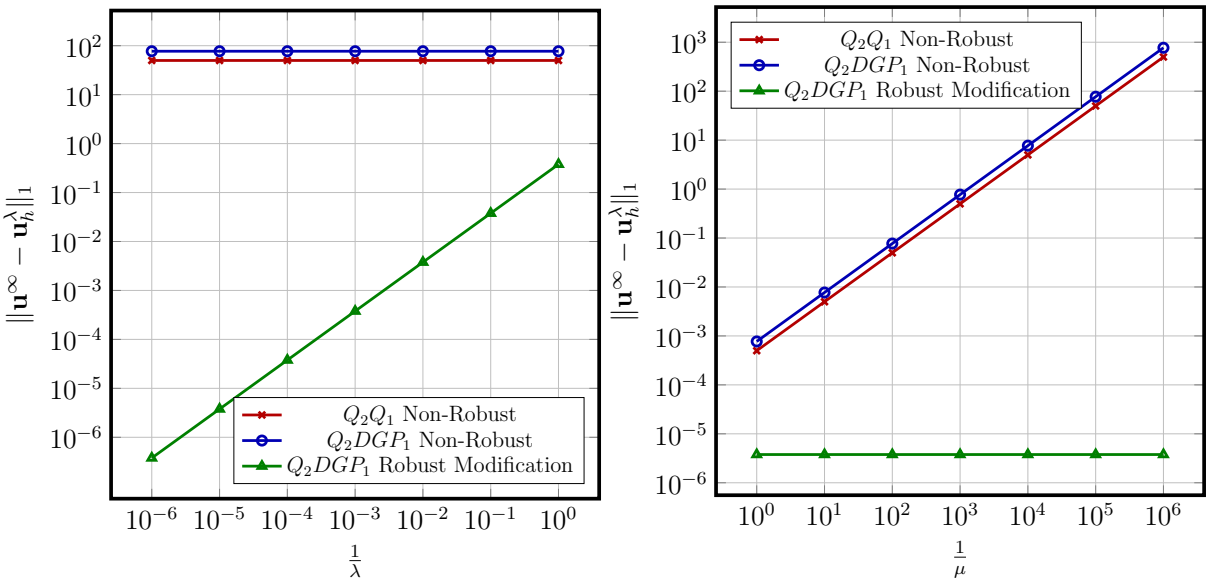

(a) $\|\mathbf{u}^\infty - \mathbf{u}_h\|_1$ vs. $\frac{1}{\lambda}$ with $\mu = 10^{-5}$ (b) $\|\mathbf{u}^\infty - \mathbf{u}_h\|_1$ vs. $\frac{1}{\mu}$ with $\lambda = 10^5$

Figure 6.4: Comparing displacement error in H^1 norm for Example 6.11 with and without gradient robust modification for 64 square elements

Example 6.12. *For the fourth numerical example, we consider, again, the nearly incompressible case with homogeneous boundary conditions on* $\mathbf{u}$*, the values of* $\mathbf{u}^\infty$ *and thus* f *are given as in Example 6.9 and the domain* $\Omega = (0,1)^2$*.*

In this example, for $\lambda = \infty$, the solution $\mathbf{u}^\infty$ is known, i.e., it is given in (6.3.1). We denote the solution, for $\lambda \neq \infty$, as $\left(\mathbf{u}^\lambda, p^\lambda\right)$. We compute the error $\|\mathbf{u}^\infty - \mathbf{u}_h^\lambda\|_1$ in our numerical results, where $\mathbf{u}_h^\lambda$ is the discrete approximated solution for a given value of λ. Since, Theorem 6.8 provides an estimate, for $\|\mathbf{u}^\lambda - \mathbf{u}_h^\lambda\|_1$, we use the triangle inequality to get

$$\begin{aligned} \|\mathbf{u}^\infty - \mathbf{u}_h^\lambda\|_1 &\leq \|\mathbf{u}^\infty - \mathbf{u}^\lambda\|_1 + \|\mathbf{u}^\lambda - \mathbf{u}_h^\lambda\|_1, \\ &\leq \|\mathbf{u}^\infty - \mathbf{u}^\lambda\|_1 + c\left(1 + \sqrt{\frac{\mu}{\lambda}}\right) h^2 \|\mathbf{u}^\lambda\|_3 + \frac{ch^2}{\lambda}\|p^\lambda\|_2. \end{aligned} \tag{6.3.4}$$

Figure 6.5b follows the same pattern as Figure 6.4b. However, there is a slight difference between Figures 6.5a and 6.4a, which can be explained by (6.3.4). In the limit $\lambda \to \infty$ and fixed $\mu = 10^{-5}$, we have $\left(1 + \sqrt{\frac{\mu}{\lambda}}\right) \to 1$ and $\|\mathbf{u}^\infty - \mathbf{u}^\lambda\|_1 \to 0$, and we observe

$$\|\mathbf{u}^\infty - \mathbf{u}_h^\lambda\|_1 \to \|\mathbf{u}^\infty - \mathbf{u}_h^\infty\|_1 \leq ch^2 \|\mathbf{u}^\infty\|_3 \tag{6.3.5}$$

for fixed refinement as it is shown in Figure 6.5a. Figure 6.6a further confirms (6.3.5) as we can see the order $\mathcal{O}(h^2)$ for $\|\mathbf{u}^\infty - \mathbf{u}_h^\lambda\|_1$ for large values of λ. In Figure 6.6b, we observe the convergence $\|\mathbf{u}^\infty - \mathbf{u}_h^\lambda\|_1 \to \|\mathbf{u}^\infty - \mathbf{u}^\lambda\|$ as $h \to 0$ and the decay of the error $\|\mathbf{u}^\infty - \mathbf{u}^\lambda\| \to 0$ as $\lambda \to 0$

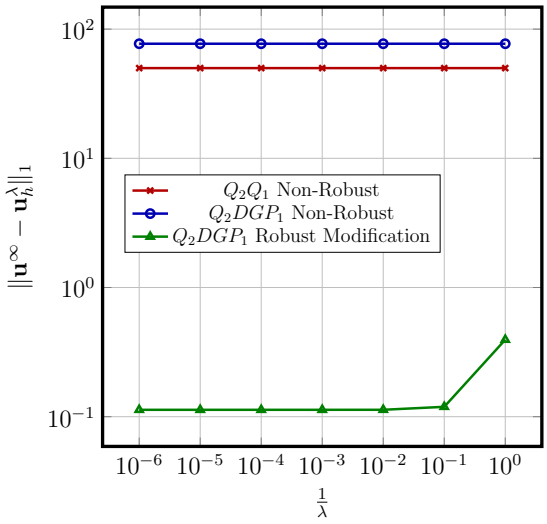

(a) $\|\mathbf{u}^\infty - \mathbf{u}_h^\lambda\|_1$ vs. $\frac{1}{\lambda}$ with $\mu = 10^{-5}$

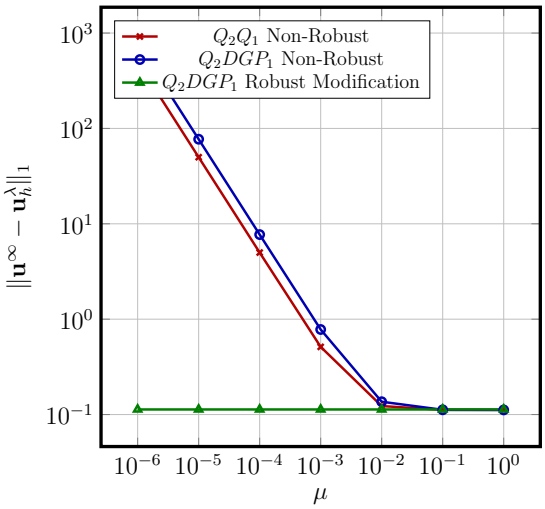

(b) $\|\mathbf{u}^\infty - \mathbf{u}_h^\lambda\|_1$ vs. $\frac{1}{\mu}$ with $\lambda = 10^5$

Figure 6.5: Comparing displacement error in H^1 norm for Example 6.12 with and without gradient robust modification for 64 square elements

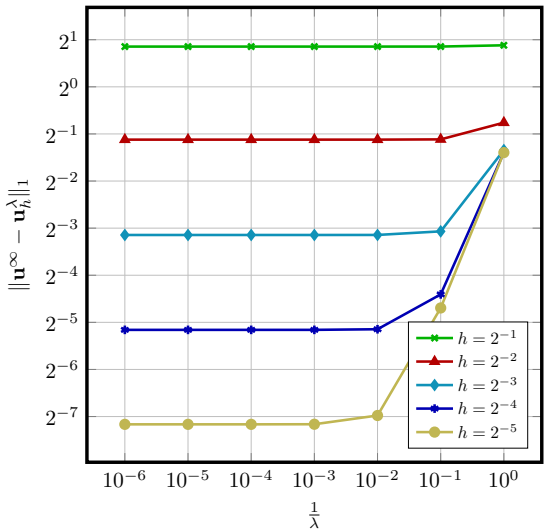

(a) $\|\mathbf{u}^\infty - \mathbf{u}_h^\lambda\|_1$ vs. $\frac{1}{\lambda}$

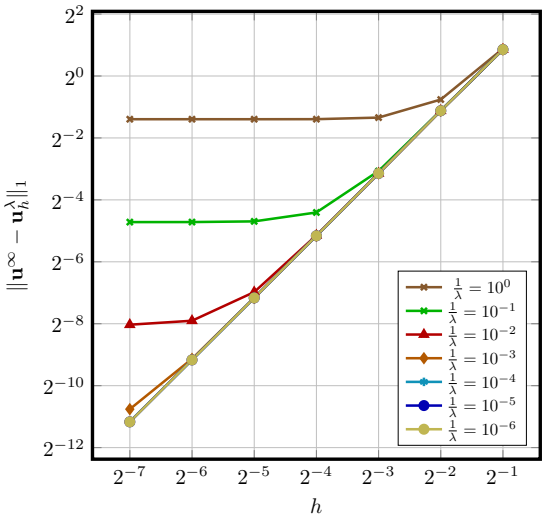

(b) $\|\mathbf{u}^\infty - \mathbf{u}_h^\lambda\|_1$ vs. h

Figure 6.6: Comparing displacement error in H^1 norm for the robust modification of Example 6.12 for $\mu = 10^{-5}$

Example 6.13. *Finally, we would like to compare our results with the thermo-elastic solids example given in [22, Section 6]. The gradient force* $\mathbf{f}$ *is given by a temperature* θ *as*

$$\mathbf{f} = -(2\mu + 3\lambda)\,\alpha\nabla\theta.$$

The material used is a nearly incompressible hard rubber with Young's Modulus $E = 5 \times 10^7[\mathrm{Pa}]$*, Poisson ratio* $\nu = 0.4999$ *and the thermal expansion coefficient* $\alpha = 8\times10^{-5}[1/\mathrm{K}]$*. Hence the Lamé parameters are* $\lambda = 8.332 \times 10^{10}[\mathrm{Pa}]$ *and* $\mu = 1.6667 \times 10^7[\mathrm{Pa}]$*. We take the domain* $\Omega = (0, L)^2$ *with* $L = 0.1[\mathrm{m}]$*. The temperature field is obtained as the solution to the stationary heat equation:*

$$-\nabla \cdot \gamma\nabla\theta = f,$$

where $\gamma = 0.2[\mathrm{W}/(\mathrm{mK})]$ *is the thermal conductivity coefficient and* $f = 4\times\exp(-40r^2)[\mathrm{W}/\mathrm{m}^3]$ *is the heat source, with* $r^2 = (x - 0.5L)^2 + (y - 0.5L)^2$*. Homogeneous Dirichlet boundary conditions are applied on both temperature and displacement. It is important to note that* $\theta \in H^1(\Omega)$ *and thus* $\mathbf{f} \in L^2(\Omega;\mathbb{R}^2)$*. For numerical computation, we additionally solve the temperature equation by a standard* H^1*-conforming finite element discretization. Hence, the finite element spaces now consist of three components, the first two denote the displacement and pressure discretization as before. The third element, always* $\mathcal{Q}_2$*, is used to solve the equation for the temperature* θ*.*

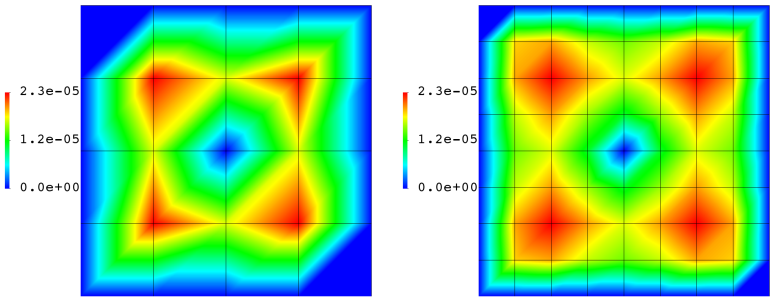

(a) 16 elements (b) 64 elements

Figure 6.7: Displacement $|u| = \sqrt{u_x^2 + u_y^2}$ for different number of elements with $\mathcal{Q}_2 \times \mathcal{DGP}_1 \times \mathcal{Q}_2$ with $\mathcal{BDM}$ Interpolation

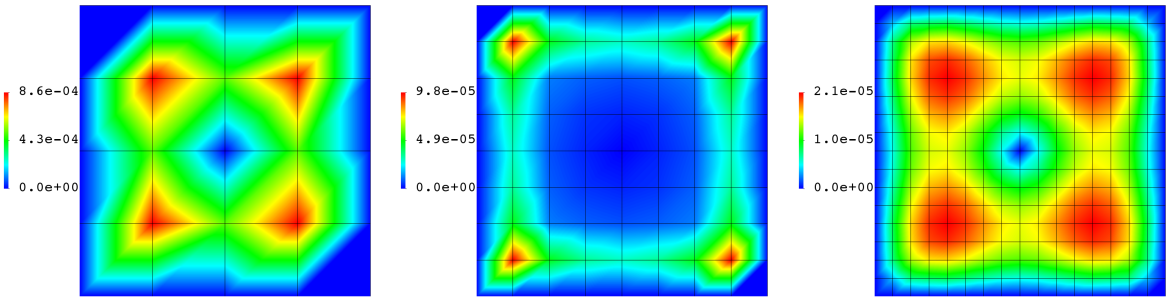

(a) 16 elements (b) 64 elements (c) 256 elements

Figure 6.8: Displacement $|u| = \sqrt{u_x^2 + u_y^2}$ for different number of elements with $\mathcal{Q}_2 \times \mathcal{Q}_1 \times \mathcal{Q}_2$

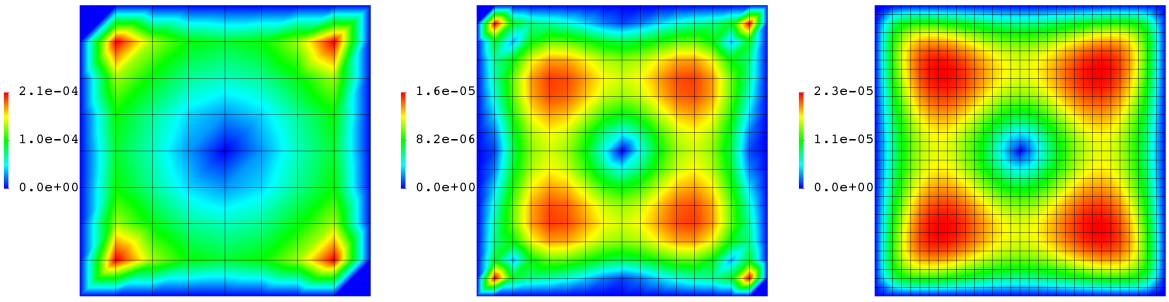

(a) 64 elements (b) 256 elements (c) 1024 elements

Figure 6.9: Displacement $|u| = \sqrt{u_x^2 + u_y^2}$ for different number of elements with $\mathcal{Q}_2 \times \mathcal{DGP}_1 \times \mathcal{Q}_2$

In Figure 6.7, we can see that we achieve a well represented solution for the displacement with only 64 elements using a gradient robust method, and the magnitude is already captured with only 16 elements. In comparison, the non-gradient robust methods require 256 and 1024 elements, respectively, to get a solution of similar shape and magnitude, see Figures 6.8 and 6.9.

The above example and figures show that, using the modified discrete problem (6.1.8) with the interpolation operator, gives us faster convergence of the displacement operator compared to (6.1.6). In the next chapter, we would like to see the effects of the interpolation operator in the phase-field fracture propagation problem.

Chapter 7

Phase-Field Fractures

In this chapter, we present an extension of the work carried out in [8] on pressurized fractures in nearly incompressible solids using an adaptive finite element discretization. We proceed by introducing the notation required for the pressurized fracture problem described in [8], in Section 7.1 and introduce mixed formulation in Section 7.2. In Section 7.3, we discuss the discretization of the problem. In Section 7.4, we provide numerical results and discussions given in [8]. Section 7.4.4, discusses, how can we extend the discussion further, under the effects of an external thermal force similar to Example 6.13 in Chapter 6.

7.1 Notation and Problem

In this section, we introduce notation and describe the problem discussed in [8]. For the sake of better readability, we introduce few already defined notations again. Consider a domain $\Omega \subset \mathbb{R}^2$ with $\mathcal{C} \subset \mathbb{R}$ denoting the fracture and $\widehat{\Omega} \subset \mathbb{R}^2$ is the intact domain. The outer boundary is denoted as $\partial\Omega$ and $\partial_F\widehat{\Omega} \coloneqq \mathcal{C}$ denotes the fracture boundary.

Using a phase-field approach, the one-dimensional fracture C is approximated on the domain $\Omega \in \mathbb{R}^2$ with the help of elliptic (Ambrosio-Tortorelli) functional [1, 2]. This yields an approximate inner fracture boundary $\partial_F\Omega \approx \mathcal{C}$. Variational phase-field fracture starts with an energy functional and the motion of the body under consideration is then determined by the Euler-Lagrange equations, which are obtained by differentiation with respect to the unknowns. The unknown solution variables are vector valued displacement $\mathbf{u}\colon \Omega \to \mathbb{R}^d$ and a scalar valued indicator phase-field function $\varphi\colon \Omega \to [0,1]$. The indicator function $\varphi = 0$ indicates that there is fracture/crack region and $\varphi = 1$ indicates the unbroken material. Any value $\varphi \in (0,1)$ denotes a smooth transition zone dependent on the regularization parameter ϵ. From physics of the underlying problem, we have crack irreversibility condition

$$\varphi \leq \varphi^{n-1}. \tag{7.1.1}$$

Where, φ^{n-1} denote the previous time step solution and φ is the current solution.

7.2 Problem Statement

Given spaces $\mathbf{V} = \mathbf{H}_0^1(\Omega;\mathbb{R}^d)$, $W = H^1(\Omega)$ and the convex set

$$K := K^n = \left\{ w \in W : w \leq \varphi^{n-1} \leq 1 \text{ a.e. on } \Omega \right\} \tag{7.2.1}$$

including the inequality constraint. Note that the latter constraint $\varphi^{n-1} \leq 1$ is provided for convenience, only. The Euler-Lagrange system for pressurized phase-field fracture reads [47]:

Problem 1. *Let $p_g \in W^{1,\infty}(\Omega)$ be given. For the loading steps $n = 1, 2, 3, \ldots, N$: Find vector-valued displacements and a scalar-valued phase-field variable $\{\mathbf{u}, \varphi\} := \{\mathbf{u}^n, \varphi^n\} \in \mathbf{V} \times K$ such that*

$$\Big(g(\varphi)\sigma(\mathbf{u}), e(\mathbf{v})\Big) + \Big(\varphi^2 p_g, \nabla\cdot\mathbf{v}\Big) + \Big(\varphi^2\nabla p_g, \mathbf{v}\Big) = 0 \qquad \forall\, \mathbf{v} \in \mathbf{V}, \tag{7.2.2}$$

and

$$\begin{aligned}(1-\kappa)\,&(\varphi\sigma(\mathbf{u}) : e(\mathbf{u}), \psi - \phi) \\ &+ 2\,(\varphi\, p_g \nabla\cdot\mathbf{u}, \psi - \phi)\, 2\,(\varphi\nabla p_g \cdot \mathbf{u}, \psi - \phi) \\ &+ G_c\left(-\frac{1}{\varepsilon}(1-\varphi, \psi-\phi) + \varepsilon(\nabla\varphi, \nabla(\psi-\varphi))\right) \geq 0 \qquad \forall\, \psi \in K.\end{aligned} \tag{7.2.3}$$

Here,

$$g(\varphi) = \Big((1-\kappa)\,\varphi^2 + \kappa\Big) \tag{7.2.4}$$

is the degradation function with a small regularization parameter κ, G_c is the critical energy release rate, and $\sigma(\mathbf{u})$ is given as

$$\sigma(\mathbf{u}) := 2\mu\, e(\mathbf{u}) + \lambda \mathrm{tr}\, e(\mathbf{u})\mathbf{I}, \tag{7.2.5}$$

from the Hook's law for linear stress-strain relationship of isotropic materials. Where μ and λ denote the Lamé coefficients and $e(\mathbf{u}) = \frac{1}{2}\left(\nabla\mathbf{u} + \nabla\mathbf{u}^T\right)$ is the linearized strain tensor and $\mathbf{I}$ is the identity matrix.

Remark 7.1. *Please note that we used a different notation for the linearized strain tensor than the one used in Chapter 6. We wanted to be consistent with the notation of the regularization parameter ε used in the literature.*

As with Stokes problem in Chapter 4 and Elasticity problem in Chapter 6, we use a mixed form to avoid the volumetric locking phenomenon. Now the stress tensor in the mixed form is given as:

$$\sigma(\mathbf{u}, p) := 2\mu\, e(\mathbf{u}) + p\mathbf{I}, \tag{7.2.6}$$

where, we define the pressure $p \in Q = L_0^2(\Omega)$ as

$$p := \lambda \mathrm{tr}\, e(\mathbf{u}). \tag{7.2.7}$$

Remark 7.2. *The solution variable p is not be confused with the given pressure p_g.*

A mixed form for $p_g = 0$ is given in [43]. Extending that for a non-zero given pressure $p_g \neq 0$, we get

Problem 2. *Let $p_g \in W^{1,\infty}(\Omega)$ be given. For loading steps $n = 1, 2, 3, \ldots, N$: Find vector-valued displacements, a scalar-valued pressure and a scalar-valued phase-field variable $\{\mathbf{u}, p, \varphi\} := \{\mathbf{u}^n, p^n, \varphi^n\} \in \mathbf{V} \times Q \times K$ such that*

$$\Big(g(\varphi)\sigma(\mathbf{u}, p), e(\mathbf{v})\Big) + \Big(\varphi^2 p_g, \nabla\cdot\mathbf{v}\Big) + \Big(\varphi^2\nabla p_g, \mathbf{v}\Big) = 0 \qquad \forall\, \mathbf{v} \in \mathbf{V}, \tag{7.2.8}$$

and

$$(\operatorname{tr} e(\mathbf{u}), q) - \frac{1}{\lambda}(p, q) = 0 \qquad \forall\, q \in Q, \tag{7.2.9}$$

$$\begin{aligned}(1-\kappa)\,&(\varphi\,\sigma(\mathbf{u}, p)\colon e(\mathbf{u}), \psi - \phi)\\ &+ 2\,(\varphi\, p_g \nabla\cdot\mathbf{u}, \psi - \phi)\, 2\,(\varphi\nabla p_g\cdot\mathbf{u}, \psi - \phi)\\ &+ G_c\left(-\frac{1}{\varepsilon}(1-\varphi, \psi-\phi) + \varepsilon(\nabla\varphi, \nabla(\psi - \varphi))\right) \geq 0 \qquad \forall\, \psi \in K.\end{aligned} \tag{7.2.10}$$

Now, we proceed to the discretization of Problem 1 and Problem 2 and also see how we can use the interpolation operator π^{div} and get a modified problem similar to (4.3.23) and (6.1.8) in the next section.

7.3 Discrete formulation

The discretization is similar to the earlier problems with a uniform set of elements $T \in \mathcal{T}_h = \mathcal{T}_h^n$. But to allow adaptive refinement locally, a single hanging node per edge at which degrees of freedom will be eliminated to assert H^1-conformity of the discrete spaces is allowed. The set of nodes q is denoted as N and, we further distinguish the set $N^{\partial\Omega}$ of the nodes at the boundary and the set of interior nodes $N^I = N\backslash N^{\partial\Omega}$. Adhering to the inf-sup condition (3.3.3) and other necessary conditions of Theorem 3.14, we choose the following finite element spaces

$$\begin{aligned} W_h := W_h^n &= \Big\{\mathbf{v}_h \in \mathcal{C}^0(\bar{\Omega})\colon \forall\, T \in \mathcal{T}_h, \mathbf{v}_h|_T \in \mathcal{Q}_1(T)\Big\} \subset W,\\ Q_h := Q_h^n &= \{q_h \in Q\colon \forall\, T \in \mathcal{T}_h, q_h|_T \in \mathcal{P}_1(T)\} \subset Q,\end{aligned} \tag{7.3.1}$$

and we use

$$\mathbf{V}_h := \mathbf{V}_h^n = \Big\{\mathbf{v}_h \in \mathcal{C}^0(\bar{\Omega}; \mathbb{R}^2)\colon \forall\, T \in \mathcal{T}_h, \mathbf{v}_h|_T \in \mathcal{Q}_1(T)^2 \text{ and } \mathbf{v}_h = 0 \text{ on } \partial\Omega\Big\} \subset \mathbf{V} \tag{7.3.2}$$

for Problem 1 and for Problem 2 we use

$$\mathbf{V}_h := \mathbf{V}_h^n = \Big\{\mathbf{v}_h \in \mathcal{C}^0(\bar{\Omega}; \mathbb{R}^2)\colon \forall\, T \in \mathcal{T}_h, \mathbf{v}_h|_T \in \mathcal{Q}_2(T)^2 \text{ and } \mathbf{v}_h = 0 \text{ on } \partial\Omega\Big\} \subset \mathbf{V}. \tag{7.3.3}$$

Using the Nodal Interpolation $\mathcal{N}^n$ from Definition 5.17, where n represents the current time step, we define the discrete feasible set for the phase-field as

$$K_h \coloneqq K_h^n = \left\{ \psi_h \in W_h \colon \psi_h(q) \leq \mathcal{N}^n \left(\varphi_h^{n-1}(q) \right), \qquad \forall\, q \in N \right\}. \tag{7.3.4}$$

The nodal basis functions of the finite element space W_h are denoted by ϕ_h. Now, we define the spatially discretized time step problem.

Problem 3. *Let $p_g \in W^{1,\infty}(\Omega)$ be given. For the loading steps $n = 1, 2, 3, ldots, N$: Find vector-valued displacements and a scalar-valued phase-field variable $\{\mathbf{u}_h, \varphi_h\} \coloneqq \{\mathbf{u}_h^n, \varphi_h^n\} \in \mathbf{V}_h \times K_h$ such that*

$$\left(g(\varphi_h)\sigma(\mathbf{u}_h), e(\mathbf{v}_h) \right) + \left(\varphi_h^2\, p_g, \nabla \cdot \mathbf{v}_h \right) + \left(\phi_h^2 \nabla p_g, \mathbf{v}_h \right) = 0 \qquad \forall\, \mathbf{v}_h \in \mathbf{V}_h, \tag{7.3.5}$$

and

$$\begin{aligned} &(1-\kappa)\left(\varphi_h \sigma(\mathbf{u}_h) \colon e(\mathbf{u}_h), \psi_h - \phi_h\right) \\ &\quad + 2\left(\varphi_h\, p_g \nabla \cdot \mathbf{u}_h, \psi_h - \varphi_h\right) + 2\left(\varphi_h \nabla p_g \cdot \mathbf{u}_h, \psi_h - \varphi_h\right), \\ &\quad + G_c \left(-\frac{1}{\varepsilon}\left(1 - \varphi_h, \psi_h - \varphi_h\right) + \varepsilon \left(\nabla \varphi_h, \nabla\left(\psi_h - \varphi_h\right)\right)\right) \geq 0 \qquad \forall\, \psi_h \in K_h. \end{aligned} \tag{7.3.6}$$

Now, we proceed to discretize the mixed form Problem 2 as

Problem 4. *Let $p_g \in W^{1,\infty}(\Omega)$ be given. For the loading steps $n = 1, 2, 3, \ldots, N$: Find vector-valued displacements, a scalar-valued pressure and a scalar-valued phase-field variables $\{\mathbf{u}_h, p_h, \varphi_h\} \coloneqq \{\mathbf{u}_h^n, p_h^n, \varphi_h^n\} \in \mathbf{V}_h \times Q_h \times K_h$ such that*

$$\left(g(\varphi_h)\sigma(\mathbf{u}_h, p_h), e(\mathbf{v}_h) \right) + \left(\varphi_h^2\, p_g, \nabla \cdot \mathbf{v}_h \right) + \left(\phi_h^2 \nabla p_g, \mathbf{v}_h \right) = 0 \qquad \forall\, \mathbf{v}_h \in \mathbf{V}_h, \tag{7.3.7}$$

and

$$\left(\operatorname{tr} e(\mathbf{u}_h), q_h \right) - \frac{1}{\lambda}(p_h, q_h) = 0 \qquad \forall\, q_h \in Q_h, \tag{7.3.8}$$

and

$$\begin{aligned} &(1-\kappa)\left(\varphi_h \sigma(\mathbf{u}_h, p_h) \colon e(\mathbf{u}_h), \psi_h - \phi_h\right) \\ &\quad + 2\left(\varphi_h\, p_g \nabla \cdot \mathbf{u}_h, \psi_h - \varphi_h\right) + 2\left(\varphi_h \nabla p_g \cdot \mathbf{u}_h, \psi_h - \varphi_h\right), \\ &\quad + G_c \left(-\frac{1}{\varepsilon}\left(1 - \varphi_h, \psi_h - \varphi_h\right) + \varepsilon \left(\nabla \varphi_h, \nabla\left(\psi_h - \varphi_h\right)\right)\right) \geq 0 \qquad \forall\, \psi_h \in K_h. \end{aligned} \tag{7.3.9}$$

Similar to the previous chapters, we provide a modified version of the above problem using the interpolation operator π^{div}. Now, as mentioned in Section 7.3, we used the finite element pair $\mathcal{Q}_2 \times \mathcal{P}_1$ in [8]. So we have to use the Raviart-Thomas element of order 1; $(\mathcal{RT}_1)$ for the H^{div} conforming space. Hence, the interpolation operator is given as $\pi^{\text{rt}} \colon \mathbf{V}_h \to \widehat{\mathbf{V}}_h$, where

$$\widehat{\mathbf{V}}_h \coloneqq \left\{ \mathbf{v}_h \in \mathcal{C}^0\left(\bar{\Omega}; \mathbb{R}^2\right) : \forall\, T \in \mathcal{T}_h, \mathbf{v}_h|_T \in \mathcal{RT}_1(T) \right\} \tag{7.3.10}$$

The modified problem is given as

Problem 5. *Let $p_g \in W^{1,\infty}(\Omega)$ be given. For the loading steps $n = 1, 2, 3, \ldots, N$: Find vector-valued displacements, a scalar-valued pressure, and a scalar-valued phase-field variable $\{\mathbf{u}_h, p_h, \varphi_h\} : \{\mathbf{u}_h^n, p_h^n, \varphi_h^n\} \in \mathbf{V}_h \times Q_h \times K_h$ such that*

$$\begin{aligned}\Big(g(\varphi_h)\sigma(\mathbf{u}_h, p_h), e(\mathbf{v}_h)\Big) + \Big(\varphi_h^2\, p_g, \nabla\cdot \pi^{\mathrm{rt}}\mathbf{v}_h\Big) \\ + \Big(\phi_h^2 \nabla p_g, \pi^{\mathrm{rt}}\mathbf{v}_h\Big) = 0 \qquad \forall\, \mathbf{v}_h \in \mathbf{V}_h,\end{aligned} \tag{7.3.11}$$

and

$$(\operatorname{tr} e(\mathbf{u}_h), q_h) - \frac{1}{\lambda}(p_h, q_h) = 0 \qquad \forall\, q_h \in Q_h, \tag{7.3.12}$$

and

$$\begin{aligned}&(1-\kappa)\,(\varphi_h \sigma(\mathbf{u}_h, p_h) \colon e(\mathbf{u}_h), \psi_h - \phi_h) \\ &\quad + 2\,(\varphi_h\, p_g \nabla\cdot \mathbf{u}_h, \psi_h - \varphi_h) + 2\,(\varphi_h \nabla p_g \cdot \mathbf{u}_h, \psi_h - \varphi_h)\,, \\ &\quad + G_c\left(-\frac{1}{\varepsilon}\,(1-\varphi_h, \psi_h - \varphi_h) + \varepsilon\,(\nabla\varphi_h, \nabla\,(\psi_h - \varphi_h))\right) \geq 0 \qquad \forall\, \psi_h \in K_h.\end{aligned} \tag{7.3.13}$$

In order to calculate the divergence of the interpolated term $(\nabla\cdot \pi^{\mathrm{rt}}\mathbf{v}_h)$, we use the `FEValuesInterpolated.gradient` function from (5.4.9) and calculate the divergence as a trace of the gradient tensor. For calculating the interpolation term $\pi^{\mathrm{rt}}\mathbf{v}_h$, we use `FEValuesInterpolated.values` from (5.4.8).

7.4 Numerical Tests

In this section, we describe the setting of the numerical examples discussed in [8], which are motivated by the theoretical calculations of Sneddon [55] and Sneddon and Lowengrub [54].

7.4.1 Setup

Following [51], where $\nu = 0.2$ is discussed, a two-dimensional domain $\Omega = [-10, 10]^2$ as seen in Figure 7.1. The initial crack length is defined as $l_0 = 2.0$ and width is $2d$. The crack domain $\Omega_c = [-1, 1] \times [-d, d] \subset \Omega$. As discussed earlier, the phase-field function φ describes the crack domain, i.e., $\varphi = 0$ in Ω_c and $\varphi = 1$ in $\Omega \backslash \Omega_c$. The thickness $2d$ corresponds to $2h\sqrt{2}$, where h is the diameter(maximum length inside) of the cell T. For the numerical testing, we use $\varphi_h^0 = \mathcal{N}^0\,(\varphi_h^0)$.

We consider homogeneous boundary conditions for displacement and Neumann condition (traction free condition) for phase-field, i.e., $\epsilon\partial_n\varphi = 0$ on $\partial\Omega$. For all tests in this section, the crack bandwidth ϵ is set as $\epsilon = 4\sqrt{2}d$, the regularization parameter κ is determined sufficiently small with $\kappa = 10^{-8}$. The fracture toughness of the observed material is G_c and the Young's modulus $E = 1.0$. All the numerical tests are based on the three configurations derived from Sneddon's setup [51].

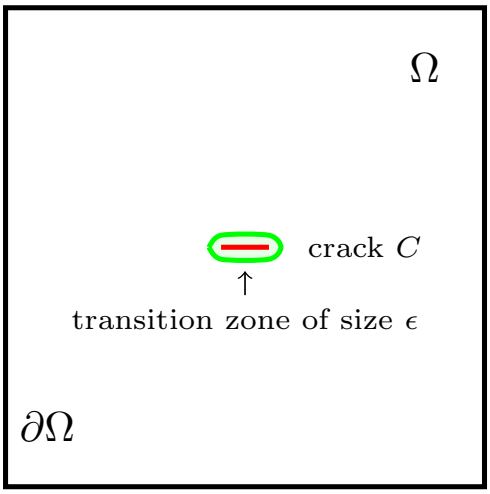

Figure 7.1: 2D domain Ω with Dirichlet boundaries on $\partial\Omega$, an initial crack $\mathcal{C}$ of length $2l_0$ and width ϵ, where the phase-field function φ is defined.

7.4.2 Examples

Example 7.3. *Constant given pressure $p_g = 10^{-3}$ and $\nu = 0.2$ to $\nu = 0.5$ using Problem 3 and compare it to Problem 4.*

Example 7.4. *Constant given pressure $p_g = 10^{-3}, \nu = 0.2$ to $\nu = 0.5$ and a compressible layer around the finite domain as well as in the prescribed fracture using Problem 3 and compare it to Problem 4.*

Example 7.5. *Non-constant pressure $p_g, \nu = 0.5$ and a compressible layer around the finite domain as well as in the prescribed fracture using Problem 4 and compare it to Problem 5.*

7.4.3 Observations

For all examples described, the following quantities of interest are calculated:

- Total crack volume (TCV);
- Bulk energy E_b;
- Crack energy E_c.

For TCV, manufactured reference values can be computed for an infinite domain from the formulae presented in [54][Section 2.4]. Numerical values on the cut-off domain in Figure 7.1 for $\nu = 0.2$ can be found in [51]. Numerically, the total crack volume can be computed by using

$$\mathrm{TCV} = \int_\Omega \mathbf{u}(x,y) \cdot \nabla\varphi(x,y)\ \mathrm{d}(x,y). \tag{7.4.1}$$

As a second quantity of interest, the bulk energy E_b is defined as

$$E_b := \int_\Omega \frac{g(\phi)}{2}\sigma : e(\mathbf{u})\mathrm{d}x, \tag{7.4.2}$$

where $\sigma := \sigma(\mathbf{u})$ for Problem 3 and $\sigma := \sigma(\mathbf{u}, p)$ for Problem 4 and 5. As third quantity of interest, the crack energy is computed via

$$E_c := \frac{G_c}{2}\int_\Omega \left(\frac{(\varphi-1)^2}{\epsilon} + \epsilon|\nabla\varphi|^2\right)\,\mathrm{d}x. \tag{7.4.3}$$

As we focus on the gradient robust methods using interpolation operator in this thesis, we are interested in Example 7.5, where the comparison is done between Problem 4 and the modified, Problem 5. Building on Figure 7.1, we construct a domain $[-20, 20]^2$ which contains the previously define domain $[-10, 10]^2$. The surrounding layer of width 10 is defined as a compressible material with $\nu = 0.2$. All other parameters, namely, E, G_c, κ and Ω_c are same as defined in Section 7.4.1. The same compressible layer is used inside the prescribed fracture on the set $[-1, 1] \times [-d, d]$.

We use a non-constant given pressure p_g is given as

$$p_g = f(x)g(y) \tag{7.4.4}$$

where,

$$f(x) = \begin{cases} 0.001 & 1 \le x < 2, \\ -0.002\,x^2(x-1.5) & 0 \le x < 1, \\ 0.002\,(x-3)^2(x-1.5) & 2 \le x < 3, \\ 0 & \text{otherwise}, \end{cases}$$

$$g(y) = \begin{cases} 1 & |y| < 0.5, \\ 2(|y|-1.5)^2|y| & 0.5 \le |y| < 1.5, \\ 0 & \text{otherwise}. \end{cases}$$

When we compare the quantities of interest, i.e., TCV, E_c, and E_b for Problem 4 and Problem 5, we observe that the results are almost similar up to 5 decimal points [8]. This can be explained by the choice of the pressure p_g. The pressure chosen in (7.4.4) is relatively simple and the jump in the pressure on the prescribed fracture is aligned with the mesh and no difficulty in the pressure approximation.

The thermal example considered in Example 6.13, showed that a well represented solution can be obtained with fewer number of elements in case of gradient-robust methods, compared to the non-gradient-robust version of the Elasticity problem. In the next section, we would like to apply the same external force under similar conditions to Example 7.5 and see if we can observe changes with and without the interpolation operator.

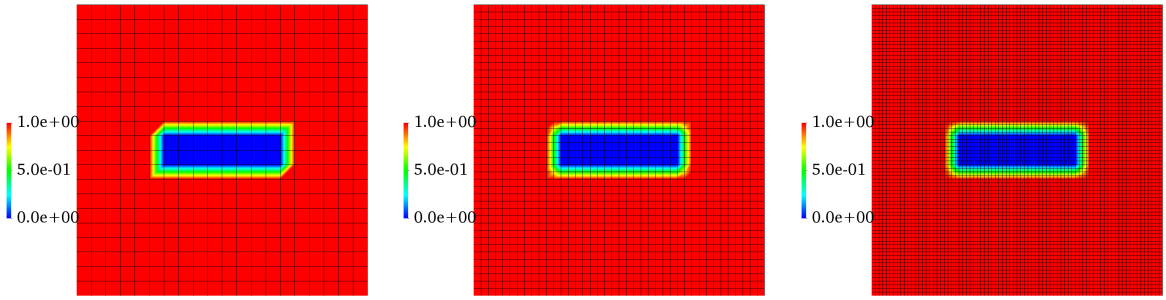

(a) 400 elements (b) 1600 elements (c) 6400 elements

Figure 7.2: Initial setup of the domain, $\varphi = 0$ for fracture and $\varphi = 1$ for no crack for various meshes

7.4.4 External Thermal force

Since the given pressure p_g used in Example 7.5 did not give any observable change between Problems 4 and 5 (see [8, Table 5]), we remove the given pressure p_g entirely and introduce an external gradient force $\mathbf{f}$ which is given by a temperature θ, similar to what we did in Example 6.13 as

$$\mathbf{f} = -(2\mu + 3\lambda)\,\alpha\nabla\theta,$$

where, the temperature field is obtained as the solution to the stationary heat equation:

$$-\nabla\cdot\gamma\nabla\theta = f.$$

The following table shows the list of all values used in this example.

Parameter		Value
Young's Modulus	E	5×10^7[Pa]
Poison ratio	ν	0.4999
Lamé Parameter	λ	8.332×10^{10}[Pa]
Lamé Parameter	μ	1.6667×10^7[Pa]
Thermal conductivity coefficient	γ	0.2[W/mK]
Thermal expansion coefficient	α	8×10^{-5}[1/K]

We consider the domain $\Omega = [-2.5, 2.5]^2$ with a fracture of length $2cm$ and width $1cm$ centered at the origin, which can be seen in Figure 7.2. As described earlier, phase-field function $\varphi = 0$ refers to the material with crack and $\varphi = 1$ refers to no crack on the material. We use a smooth bilinear transformation for the phase-field φ to go from 0 to 1.

Unlike Example 6.13, we cannot put the external thermal force at the origin due to the

fracture, so we move the thermal force to four edges of the domain as

$$\begin{aligned} f =& 4t^2 \exp\left\{-40\left((x-2.5)^2+(y-2.5)^2\right)\right\}+ \\ & 4t^2 \exp\left\{-40\left((x-2.5)^2+(y+2.5)^2\right)\right\}+ \\ & 4t^2 \exp\left\{-40\left((x+2.5)^2+(y-2.5)^2\right)\right\}+ \\ & 4t^2 \exp\left\{-40\left((x+2.5)^2+(y+2.5)^2\right)\right\}. \end{aligned} \tag{7.4.5}$$

We define the discrete temperature space T_h as

$$T_h \coloneqq T_h^n = \left\{\tau_h \in \mathcal{C}^0(\bar{\Omega})\colon \forall\, T \in \mathcal{T}_h, \tau_h|_T \in \mathcal{Q}_2(T) \text{ and } \tau_h = 0 \text{ on } \partial\Omega\right\} \tag{7.4.6}$$

The mixed problem for the external thermal force f is given as

Problem 6. *Let $f \in \mathbf{L}^2(\Omega)$ be given. For the loading steps $n = 1, 2, 3, \ldots, N$: Find vector-valued displacements, a scalar-valued pressure and a scalar-valued phase-field variables $\{\mathbf{u}_h, p_h, \varphi_h, \tau_h\} \coloneqq \{\mathbf{u}_h^n, p_h^n, \varphi_h^n, \tau_h^n\} \in \mathbf{V}_h \times Q_h \times K_h \times T_h$ such that*

$$\begin{aligned} \Big(g(\varphi_h)\sigma(\mathbf{u}_h, p_h), e(\mathbf{v}_h)\Big) &+ (2\mu + 3\lambda)\,\alpha\,(\nabla\tau_h, \mathbf{v}_h) \\ &+\gamma\,(\nabla\tau_h, \nabla\tau_h) \qquad\qquad = f, \quad \forall\, \tau_h \in T_h, \forall\, \mathbf{v}_h \in \mathbf{V}_h, \end{aligned} \tag{7.4.7}$$

and

$$(\operatorname{tr} e(\mathbf{u}_h), q_h) - \frac{1}{\lambda}(p_h, q_h) = 0 \qquad \forall\, q_h \in Q_h, \tag{7.4.8}$$

and

$$\begin{aligned} (1-\kappa)\,&(\varphi_h \sigma(\mathbf{u}_h, p_h)\colon e(\mathbf{u}_h), \psi_h - \phi_h) \\ &+ 2\,(\varphi_h\, p_g \nabla\cdot \mathbf{u}_h, \psi_h - \varphi_h) + 2\,(\varphi_h \nabla p_g \cdot \mathbf{u}_h, \psi_h - \varphi_h)\,, \\ &+ G_c\left(-\frac{1}{\varepsilon}\,(1-\varphi_h, \psi_h - \varphi_h) + \varepsilon\,(\nabla\varphi_h, \nabla\,(\psi_h - \varphi_h))\right) \geq 0 \qquad \forall\, \psi_h \in K_h. \end{aligned} \tag{7.4.9}$$

The modified interpolated version of the above problem is given as

Problem 7. *Let $p_g \in W^{1,\infty}(\Omega)$ be given. For the loading steps $n = 1, 2, 3, \ldots, N$: Find vector-valued displacements, a scalar-valued pressure, and a scalar-valued phase-field variables $\{\mathbf{u}_h, p_h, \varphi_h, \tau_h\} \coloneqq \{\mathbf{u}_h^n, p_h^n, \varphi_h^n, \tau_h^n\} \in \mathbf{V}_h \times Q_h \times K_h \times T_h$ such that*

$$\begin{aligned} \Big(g(\varphi_h)\sigma(\mathbf{u}_h, p_h), e(\mathbf{v}_h)\Big) &+ (2\mu + 3\lambda)\,\alpha\left(\nabla\tau_h, \pi^{\mathrm{bdm}}\,\mathbf{v}_h\right) \\ &+\gamma\,(\nabla\tau_h, \nabla\tau_h) \qquad\qquad = f, \quad \forall\, \tau_h \in T_h, \forall\, \mathbf{v}_h \in \mathbf{V}_h, \end{aligned} \tag{7.4.10}$$

and

$$(\operatorname{tr} e(\mathbf{u}_h), q_h) - \frac{1}{\lambda}(p_h, q_h) = 0 \qquad \forall\, q_h \in Q_h, \tag{7.4.11}$$

and

$$\begin{aligned} (1-\kappa)\,&(\varphi_h \sigma(\mathbf{u}_h, p_h)\colon e(\mathbf{u}_h), \psi_h - \phi_h) \\ &+ 2\,(\varphi_h\, p_g \nabla\cdot \mathbf{u}_h, \psi_h - \varphi_h) + 2\,(\varphi_h \nabla p_g \cdot \mathbf{u}_h, \psi_h - \varphi_h)\,, \\ &+ G_c\left(-\frac{1}{\varepsilon}\,(1-\varphi_h, \psi_h - \varphi_h) + \varepsilon\,(\nabla\varphi_h, \nabla\,(\psi_h - \varphi_h))\right) \geq 0 \qquad \forall\, \psi_h \in K_h. \end{aligned} \tag{7.4.12}$$

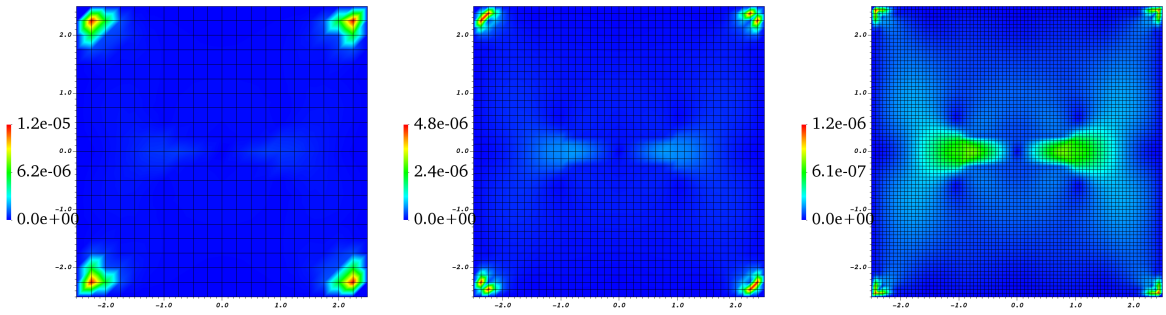

(a) 400 elements (b) 1600 elements (c) 6400 elements

Figure 7.3: Displacement vector for various meshes with $\mathcal{Q}_2 \times \mathcal{DGP}_1 \times \mathcal{Q}_2$ for Problem 6 at time $t = 0.33$ seconds

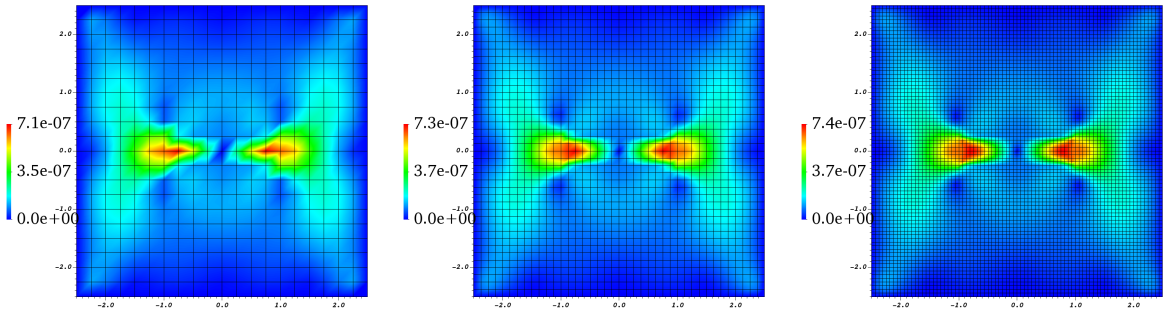

(a) 400 elements (b) 1600 elements (c) 6400 elements

Figure 7.4: Displacement vector for various meshes with $\mathcal{Q}_2 \times \mathcal{DGP}_1 \times \mathcal{Q}_2$ for Problem 7 at time $t = 0.33$ seconds

We use Homogeneous Dirichlet boundary conditions for both temperature and displacement. Furthermore, it is important to note that $\theta \in H^1(\Omega)$ and thus $\mathbf{f} \in \mathbf{L}^2(\Omega; \mathbb{R}^d)$. Similar to Example 6.13, we solve the temperature equation numerically by a standard H^1- conforming finite element discretization using the space $\mathcal{Q}_2$ (see (7.4.6)). We use the same setup for both Problems 6 and 7. We also change the pressure finite element space Q_h to $\mathcal{DGQ}_1$ and use the $\mathcal{BDM}_2$ space instead of $\mathcal{RT}_1$ to be consistent with the numerical simulations used in Example 6.13.

In Figure 7.4, we can see that we have achieved a well represented solution for the displacement vector with only 400 elements using Problem 5. The magnitude is captured with 1600 elements. In comparison, even with 6400 elements, we can observe that a well represented solution or magnitude, is very far from what was obtained when using Problem 4, as shown in Figure 7.3.

From Tables 7.1, 7.2 and 7.3, we observe that the difference in the values for TCV and bulk energy E_b for all three time steps, $t = 0.33$, $t = 0.66$ and $t = 1$ between 1600 and 6400

	$t = 0.333$ seconds		$t = 0.666$ seconds		$t = 1$ second	
	Problem 6	Problem 7	Problem 6	Problem 7	Problem 6	Problem 7
TCV	-2.22555×10^{-7}	-2.56719×10^{-7}	7.76821×10^{-7}	-9.48268×10^{-7}	-8.37626×10^{-5}	-1.95683×10^{-6}
E_b	3.30868×10^{-2}	2.56991×10^{-3}	2.49472×10^{-1}	4.92219×10^{-2}	-1.70555×10	2.07536×10^{-1}
E_c	4.04412	4.043	4.19369	4.04416	2.44036×10	4.06779

Table 7.1: Values of quantities of interest given for Problem 6 and 7 for 400 elements

	$t = 0.333$ seconds		$t = 0.666$ seconds		$t = 1$ second	
	Problem 6	Problem 7	Problem 6	Problem 7	Problem 6	Problem 7
TCV	-3.12872×10^{-7}	-3.42527×10^{-7}	3.20657×10^{-7}	-1.28599×10^{-6}	6.26908×10^{-6}	-2.60384×10^{-6}
E_b	2.90055×10^{-2}	4.95787×10^{-3}	4.5927×10^{-2}	8.20492×10^{-2}	-5.78296	3.20263×10^{-1}
E_c	4.03704	4.03546	4.24409	4.03841	7.8537	4.0985

Table 7.2: Values of quantities of interest given for Problem 6 and 7 for 1600 elements

	$t = 0.333$ seconds		$t = 0.666$ seconds		$t = 1$ second	
	Problem 6	Problem 7	Problem 6	Problem 7	Problem 6	Problem 7
TCV	-3.54157×10^{-7}	-3.55814×10^{-7}	-1.33274×10^{-6}	-1.3715×10^{-6}	-2.41516×10^{-6}	-2.79791×10^{-6}
E_b	8.0492×10^{-3}	5.4281×10^{-3}	1.09163×10^{-1}	8.26011×10^{-2}	2.98415×10^{-1}	3.25712×10^{-1}
E_c	4.35277	4.35273	4.36436	4.35632	4.53817	4.42821

Table 7.3: Values of quantities of interest given for Problem 6 and 7 for 6400 elements

elements, is much less for gradient-robust Problem 7, compared to non-gradient-robust Problem 6. This indicates that, with the use of gradient-robust method, we are closer to the actual value with 1600 elements, compared to non-gradient-robust Problem 6.

Regarding fracture propagation, in Figures 7.5, we see that, a well represented solution is given only with 400 elements. Whereas, in Figure 7.6, it takes up to 6400 elements for the same.

In the next chapter, we give an overview and conclude the thesis.

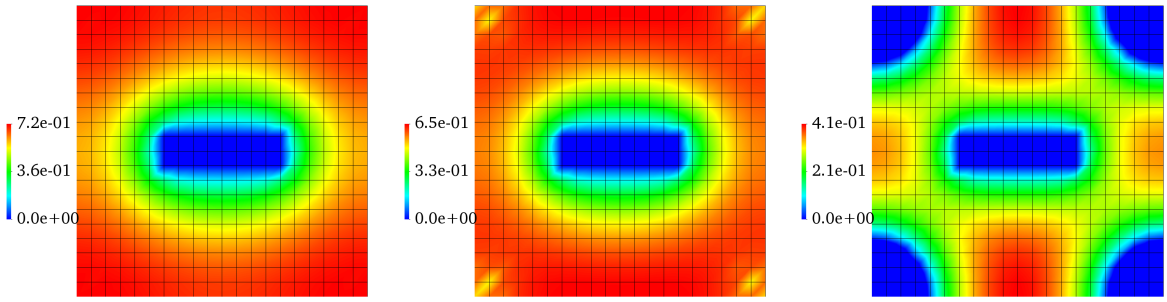

(a) $t = 0.33$ seconds, 400 elements

(b) $t = 0.667$ seconds, 400 elements

(c) $t = 1$ second, 400 elements

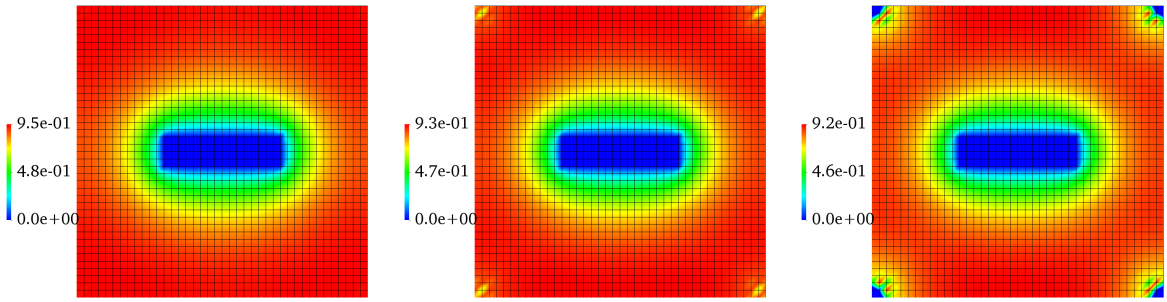

(d) $t = 0.33$ seconds, 1600 elements

(e) $t = 0.667$ seconds, 1600 elements

(f) $t = 1$ second, 1600 elements

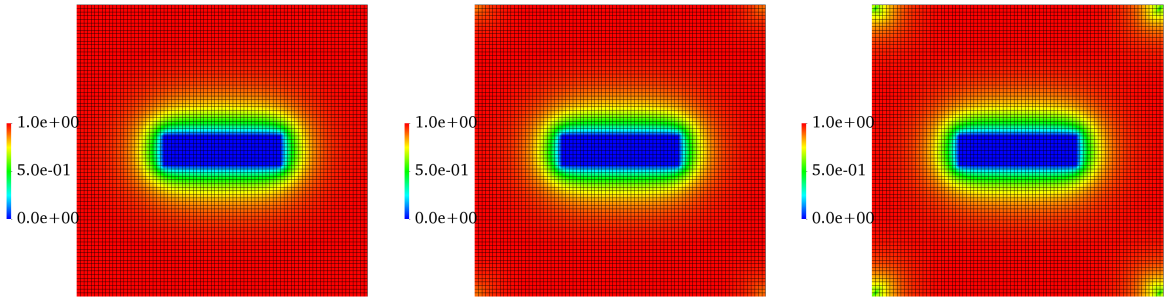

(g) $t = 0.33$ seconds, 6400 elements

(h) $t = 0.667$ seconds, 6400 elements

(i) $t = 1$ second, 6400 elements

Figure 7.5: Fracture propagation with $\mathcal{Q}_2 \times \mathcal{DGP}_1 \times \mathcal{Q}_2$ for Problem 6

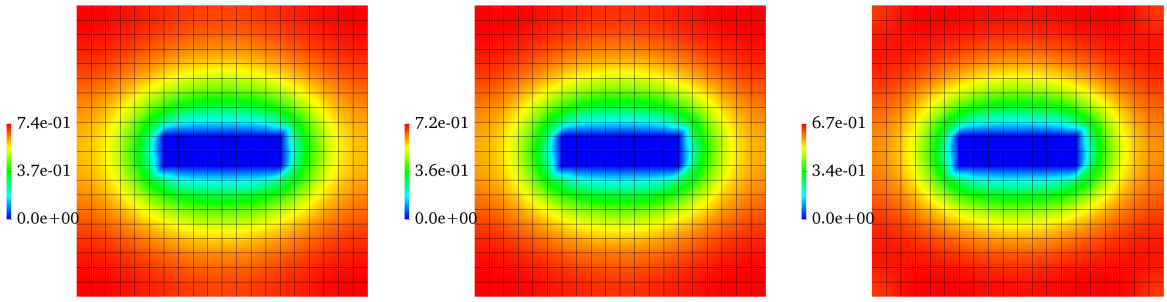

(a) $t = 0.33$ seconds, 400 elements

(b) $t = 0.667$ seconds, 400 elements

(c) $t = 1$ second, 400 elements

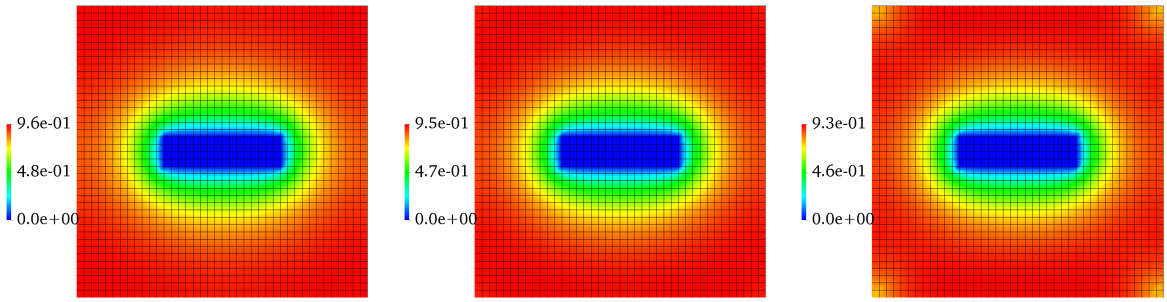

(d) $t = 0.33$ seconds, 1600 elements

(e) $t = 0.667$ seconds, 1600 elements

(f) $t = 1$ second, 1600 elements

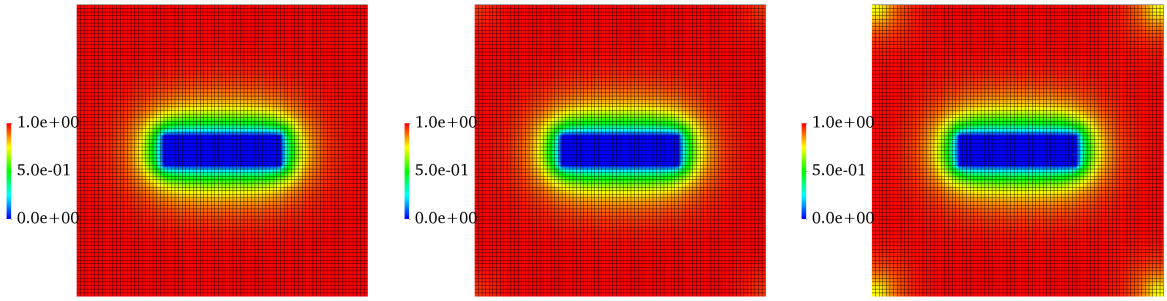

(g) $t = 0.33$ seconds, 6400 elements

(h) $t = 0.667$ seconds, 6400 elements

(i) $t = 1$ second, 6400 elements

Figure 7.6: Fracture propagation with $\mathcal{Q}_2 \times \mathcal{DGP}_1 \times \mathcal{Q}_2$ for Problem 7

Chapter 8

Conclusion

Gradient dependency of the vector valued solution is a common problem when solving saddle point problems numerically. In this thesis, we consider one of the solutions to that problem proposed by Linke in [38] for stationary Stokes equation. In Chapter 5, we have given a brief introduction on constructing finite dimensional subspaces of $\mathbf{H}^{\text{div}}(\Omega;\mathbb{R}^d)$ space, such as Raviart-Thomas and Brezzi-Douglas-Marini finite element spaces. An implementation of the `FEValuesInterpolated` class in `DOpElib` library was given in Section 5.4. After testing the correctness of the class in Section 5.5, we have extended the variational crime by Linke to linear elastic incompressible and nearly incompressible materials in Chapter 6.

After laying out necessary assumptions on how to choose the appropriate $\mathbf{H}^{\text{div}}(\Omega;\mathbb{R}^d)$ subspace for a given inf-sup stable finite element in Section 6.1.3, a detailed error analysis for both incompressible and nearly incompressible materials was conducted in Section 6.2. In order to validate the error estimates, several numerical tests were conducted. In the final numerical example, an external thermal force was applied to a rubber like nearly incompressible material. We show in Section 6.3, that a well represented solution and magnitude is achieved for the displacement vector with fewer elements, when using gradient-robust method.

In Section 7.2, we have stated different versions of the phase-field fracture problems as given in [8]. As mentioned Chapter 6, the standard mixed form of the problem given in Problem 4, though solves the issue of volume locking, it doesn't make the displacement vector pressure-robust. In order to rectify that, we have applied the interpolation operator and used a modified version in Problem 5. In Section 7.4, we have seen that the quantities of interest TCV, E_b and E_c show similar results for both Problems 4 and 5. To solve this issue, we have used the external thermal force used in Example 6.13 instead of the given pressure p_g. In Section 7.4.4, for the external thermal example, we show that we reach a well represented solution for the displacement vector with fewer elements for Problem 7 when compared to Problem 6.

Bibliography

[1] L. Ambrosio and V. M. Tortorelli, *Approximation of functional depending on jumps by elliptic functional via t-convergence*, Communications on Pure and Applied Mathematics **43** (1990), no. 8, 999–1036.

[2] ———, *On the approximation of free discontinuity problems*, Bollettino dell'Unione Matematica Italiana **6** (1992), no. 1, 105–123.

[3] T. Apel and V. Kempf, *Pressure-robust error estimate of optimal order for the Stokes equations: domains with re-entrant edges and anisotropic mesh grading*, Calcolo **58** (2021), no. 2, 15.

[4] D. Arndt, W. Bangerth, B. Blais, M. Fehling, R. Gassmöller, T. Heister, L. Heltai, U. Köcher, M. Kronbichler, M. Maier, P. Munch, J. P. Pelteret, Sebastian Proell, K. Simon, B. Turcksin, D. Wells, and J. Zhang, *The `deal.II` library, version 9.3*, Journal of Numerical Mathematics **29** (2021), no. 3, 171–186.

[5] D. Arndt, W. Bangerth, D. Davydov, T. Heister, L. Heltai, M. Kronbichler, M. Maier, J. P. Pelteret, B. Turcksin, and D. Wells, *The deal.II finite element library: Design, features, and insights*, Computers & Mathematics with Applications **81** (2021), 407–422, Development and Application of Open-source Software for Problems with Numerical PDEs.

[6] M. Artina, M. Fornasier, S. Micheletti, and S. Perotto, *Anisotropic mesh adaptation for crack detection in brittle materials*, SIAM Journal on Scientific Computing **37** (2015), no. 4, B633–B659.

[7] W. Bangerth, R. Hartmann, and G. Kanschat, *Deal.II—A general-purpose object-oriented finite element library*, ACM Transactions on Mathematical Software **33** (2007), no. 4, 24/1–24/27.

[8] S. Basava, K. Mang, M. Walloth, T. Wick, and W. Wollner, *Adaptive and pressure-robust discretization of incompressible pressure-driven phase-field fracture*, pp. 191–215, Springer International Publishing, Cham, 2022.

[9] S. Basava and W. Wollner, *Gradient robust mixed methods for nearly incompressible elasticity*, Journal of Scientific Computing **95** (2023), no. 3, 93.

[10] D. Boffi, F. Brezzi, and M. Fortin, *Mixed finite element methods and applications*, Springer Series in Computational Mathematics, vol. 44, Springer, Heidelberg, 2013. MR 3097958

[11] B. Bourdin, G. A. Francfort, and J. J. Marigo, *Numerical experiments in revisited brittle fracture*, Journal of the Mechanics and Physics of Solids **48** (2000), no. 4, 797–826.

[12] D. Braess, *Finite elements*, third ed., Cambridge University Press, Cambridge, 2007, Theory, fast solvers, and applications in elasticity theory, Translated from the German by Larry L. Schumaker. MR 2322235

[13] S. C. Brenner and L. R. Scott, *The mathematical theory of finite element methods*, third ed., Texts in Applied Mathematics, vol. 15, Springer, New York, 2008. MR 2373954

[14] H. Brezis, *Functional analysis, Sobolev spaces and partial differential equations*, Universitext, Springer, New York, 2011. MR 2759829

[15] F. Brezzi and M. Fortin, *Mixed and hybrid finite element methods*, 1 ed., vol. 15, Springer New York, NY, 2012.

[16] S. Burke, C. Ortner, and E. Süli, *An adaptive finite element approximation of a variational model of brittle fracture*, SIAM Journal on Numerical Analysis **48** (2010), no. 3, 980–1012.

[17] ———, *An Adaptive finite element approximation of a generalized Ambrosio–Tortorelli functional*, Mathematical Models and Methods in Applied Sciences **23** (2013), no. 09, 1663–1697.

[18] C. Chukwudozie, B. Bourdin, and K. Yoshioka, *A variational phase-field model for hydraulic fracturing in porous media*, Computer Methods in Applied Mechanics and Engineering **347** (2019), 957–982.

[19] R. G. Durán, *Mixed finite element methods*, pp. 1–44, Springer Berlin Heidelberg, Berlin, Heidelberg, 2008.

[20] H. Elman, D. Silvester, and A. Wathen, *Finite elements and fast iterative solvers: with applications in incompressible fluid dynamics*, Oxford University Press, 06 2014.

[21] G. A. Francfort and J. J. Marigo, *Revisiting brittle fracture as an energy minimization problem*, Journal of the Mechanics and Physics of Solids **46** (1998), no. 8, 1319–1342.

[22] G. Fu, C. Lehrenfeld, A. Linke, and T. Streckenbach, *Locking-free and gradient-robust $H(div)$-conforming HDG methods for linear elasticity*, Journal of Scientific Computing **86** (2021), no. 3, 39.

[23] V. Girault and P.A. Raviart, *Finite element methods for Navier-Stokes equations*, Springer Series in Computational Mathematics, vol. 5, Springer Berlin, Heidelberg, 1986, Theory and Algorithms.

[24] C. Goll, T. Wick, and W. Wollner, *DOpelib: Differential equations and optimization environment; A goal oriented software library for solving pdes and optimization problems with pdes*, Archive of Numerical Software **5** (2017), no. 2.

[25] Y. Heider, S. Reiche, P. Siebert, and B. Markert, *Modeling of hydraulic fracturing using a porous-media phase-field approach with reference to experimental data*, Engineering Fracture Mechanics **202** (2018), 116–134.

[26] T. Heister, M. F. Wheeler, and T. Wick, *A primal-dual active set method and predictor-corrector mesh adaptivity for computing fracture propagation using a phase-field approach*, Computer Methods in Applied Mechanics and Engineering **290** (2015), 466–495.

[27] G. A. Holzapfel, *Nonlinear solid mechanics: A continuum approach for engineering science*, Meccanica **37** (2002), no. 4, 489–490.

[28] G. A. Holzapfel, R. Eberlein, P. Wriggers, and H. W. Weizsäcker, *Large strain analysis of soft biological membranes: Formulation and finite element analysis*, Computer Methods in Applied Mechanics and Engineering **132** (1996), no. 1, 45–61.

[29] V. John, *Finite element methods for incompressible flow problems*, Springer Series in Computational Mathematics, vol. 51, Springer, Cham, 2016. MR 3561143

[30] G. Kanschat, *Mixed finite element methods*, (2017).

[31] R. Krause, A. Veeser, and M. Walloth, *An efficient and reliable residual-type a posteriori error estimator for the signorini problem*, Numerische Mathematik **130** (2015), no. 1, 151–197.

[32] C. Kreuzer, R. Verfürth, and P. Zanotti, *Quasi-optimal and pressure robust discretizations of the stokes equations by moment and divergence-preserving operators*, Computational Methods in Applied Mathematics **21** (2021), no. 2, 423–443.

[33] A. Kubo and Y. Umeno, *Velocity mode transition of dynamic crack propagation in hyperviscoelastic materials: A continuum model study*, Scientific Reports **7** (2017), no. 1, 42305.

[34] W. Layton, *Introduction to the numerical analysis of incompressible viscous flows*, Society for Industrial and Applied Mathematics, Philadelphia, PA, 2008.

[35] P. L. Lederer, A. Linke, C. Merdon, and J. Schöberl, *Divergence-free Reconstruction Operators for Pressure-Robust Stokes Discretizations with Continuous Pressure Finite E lements*, SIAM Journal on Numerical Analysis **55** (2017), no. 3, 1291–1314.

[36] P. L. Lederer and S. Rhebergen, *A pressure-robust embedded discontinuous galerkin method for the S tokes problem by reconstruction operators*, SIAM Journal on Numerical Analysis **58** (2020), no. 5, 2915–2933. MR 4161756

[37] S. Lee, M. F. Wheeler, and T. Wick, *Pressure and fluid-driven fracture propagation in porous media using an adaptive finite element phase field model*, Computer Methods in Applied Mechanics and Engineering **305** (2016), 111–132.

[38] A. Linke, *On the role of the Helmholtz decomposition in mixed methods for incompressible flows and a new variational crime*, Computer Methods in Applied Mechanics and Engineering **268** (2014), 782–800.

[39] A. Linke, G. Matthies, and L. Tobiska, *Robust arbitrary order mixed finite element methods for the incompressible Stokes equations with pressure independent velocity errors*, ESAIM: M2AN **50** (2016), no. 1, 289–309.

[40] A. Linke, C. Merdon, and W. Wollner, *Optimal L^2 velocity error estimate for a modified pressure-robust Crouzeix–Raviart Stokes element*, IMA Journal of Numerical Analysis **37** (2017), no. 1, 354–374. MR 3614889

[41] K. Mang, M. Walloth, T. Wick, and W. Wollner, *Mesh adaptivity for quasi-static phase-field fractures based on a residual-type a posteriori error estimator*, GAMM-Mitteilungen **43** (2020), no. 1, e202000003.

[42] ———, *Adaptive numerical simulation of a phase-field fracture model in mixed form tested on an L-shaped specimen with high poisson ratios*, Numerical Mathematics and Advanced Applications ENUMATH 2019 (Cham) (Fred J. Vermolen and Cornelis Vuik, eds.), Springer International Publishing, 2021, pp. 1185–1193.

[43] K. Mang, T. Wick, and W. Wollner, *A phase-field model for fractures in nearly incompressible solids*, Computational Mechanics **65** (2020), no. 1, 61–78.

[44] G. Matthies and L. Tobiska, *The inf-sup condition for the mapped Q_k-P^{disc}_{k-1} element in arbitrary space dimensions*, Computing **69** (2002), no. 2, 119–139.

[45] C. Miehe, S. Mauthe, and S. Teichtmeister, *Minimization principles for the coupled problem of Darcy–B iot-type fluid transport in porous media linked to phase field modeling of fracture*, Journal of the Mechanics and Physics of Solids **82** (2015), 186–217.

[46] A. Mikelić, M. F. Wheeler, and T. Wick, *Phase-field modeling through iterative splitting of hydraulic fractures in a poroelastic medium*, GEM - International Journal on Geomathematics **10** (2019), no. 1, 2.

[47] ———, *Phase-field modeling through iterative splitting of hydraulic fractures in a poroelastic medium*, GEM - International Journal on Geomathematics **10** (2019), no. 1, 2–33.

[48] A. Mikelić, M. F Wheeler, and T. Wick, *A quasi-static phase-field approach to pressurized fractures*, Nonlinearity **28** (2015), no. 5, 1371.

[49] N. Noii, F. Aldakheel, T. Wick, and P. Wriggers, *An adaptive global–local approach*

for phase-field modeling of anisotropic brittle fracture, Computer Methods in Applied Mechanics and Engineering **361** (2020), 112744.

[50] D. Di Pietro and A. Ern, *Mathematical aspects of discontinuous galerkin methods*, vol. 69, Springer Berlin, Heidelberg, 01 2012.

[51] J. Schröder, T. Wick, S. Reese, P. Wriggers, R. Müller, S. Kollmannsberger, M. K ästner, A. Schwarz, M. Igelbüscher, N. Viebahn, H. R. Bayat, S. Wulfinghoff, K. Mang, E. Rank, T. Bog, D. D'Angella, M. Elhaddad, P. Hennig, A. Düster, W. Garhuom, S. Hubrich, M. Walloth, W. Wollner, C. Kuhn, and T. Heister, *A selection of benchmark problems in solid mechanics and applied mathematics*, Archives of Computational Methods in Engineering **28** (2021), no. 2, 713–751.

[52] J. Schröder, P. Neff, and D. Balzani, *A variational approach for materially stable anisotropic hyperelasticity*, International Journal of Solids and Structures **42** (2005), no. 15, 4352–4371.

[53] D. Silvester, H. Elman, D. Kay, and A. Wathen, *Efficient preconditioning of the linearized Navier–Stokes equations for incompressible flow*, Journal of Computational and Applied Mathematics **128** (2001), no. 1, 261–279, Numerical Analysis 2000. Vol. VII: Partial Differential Equations.

[54] I. N. Sneddon and M. Lowengrub, *Crack problems in the classical theory of elasticity*, SIAM series in applied mathematics, John Wiley & Sons, Inc., Philadelphia, April 1969.

[55] I. N. Sneddon and N. F. Mott, *The distribution of stress in the neighbourhood of a crack in an elastic solid*, Proceedings of the Royal Society of London. Series A. Mathematical and Physical Sciences **187** (1946), no. 1009, 229–260.

[56] H. Sohr, *The Navier-Stokes equations: An elementary functional analytic approach*, 1 ed., Birkhäuser advanced texts, Birkhäuser Verlag, 2001.

[57] R. L. Taylor, *Isogeometric analysis of nearly incompressible solids*, International Journal for Numerical Methods in Engineering **87** (2011), no. 1-5, 273–288.

[58] M. Walloth, *Residual-type A posteriori estimators for a singularly perturbed reaction-diffusion variational inequality – reliability, efficiency and robustness*, arXiv: Numerical Analysis (2018).

[59] _____, *Residual-type a posteriori error estimator for a quasi-static Signorini contact problem*, IMA Journal of Numerical Analysis **40** (2019), no. 3, 1937–1971.

[60] M. F. Wheeler, T. Wick, and S. Lee, *IPACS: Integrated phase-field advanced crack propagation simulator. An adaptive, parallel, physics-based-discretization phase-field framework for fracture propagation in porous media*, Computer Methods in Applied Mechanics and Engineering **367** (2020), 113124.

[61] M. F. Wheeler, T. Wick, and W. Wollner, *An augmented-lagrangian method for the phase-field approach for pressurized fractures*, Computer Methods in Applied Mechanics and Engineering **271** (2014), 69–85.

[62] T. Wick, *Goal functional evaluations for phase-field fracture using PU-based DWR mesh adaptivity*, Computational Mechanics **57** (2016), no. 6, 1017–1035.